SURFACE AND DEEP WATER CIRCULATION IN LATE CRETACEOUS NORTH ATLANTIC GREENHOUSE OCEAN

A Dissertation presented to the Faculty of the Graduate School
University of Missouri

In Partial Fulfillment
Of the Requirements for the Degree

Doctor of Philosophy

---

by
CAROLINA ISAZA LONDOÑO

Dr. Kenneth G. MacLeod, Dissertation Supervisor

JULY 2009

The undersigned, appointed by the Dean of the Graduate School, have examined the dissertation entitled

SURFACE AND DEEP WATER CIRCULATION IN THE LATE CRETACEOUS NORTH ATLANTIC GREENHOUSE OCEAN

presented by Carolina Isaza Londoño

a candidate for the degree of doctor of philosophy

and hereby certify that in their opinion it is worthy of acceptance.

Professor Kenneth G. MacLeod

Professor Gerald Summers

Professor Cheryl Kelley

Professor Mitchell Schulte

Professor Raymond Ethington

A mi familia
Por motivarme a seguir adelante.

A Lolo y Lita (mis abuelos):
Por su perseverancia, ejemplo y enseñanzas.

A mi madre Ruth,
Por todos los sacrificios que has hecho en tu vida para sacarnos a Felipe y a mi adelante.

A mi hermano Felipe,
Tu amor y apoyo icondicional me recuerdan cada instante que no estoy sola y que he sido grandemente bendecida por tenerte a mi lado.

A Scott,
Simplemente, te amo.

……..Be one with the thesis.
Plato

ACKNOWLEDGEMENTS

The Ph.D. has been a long and arduous but extraordinary journey, one that I had never dreamed would happen. It would not have been possible without the help of many people along the way. I am deeply thankful to my advisor Dr. Ken MacLeod for taking a chance on me eight years ago. Thank you for pushing me to achieve more than I thought I could. Thank you for your encouragement, advice, mentoring and research support during my master's and doctoral studies. But more importantly, thank you for welcoming me into your family. Knowing that you, Meera, and the kids are going to be part of my life forever makes it all worth it.

I also want to thank my committee members Dr. Kelley, Dr. Schulte, Dr. Ethington, and Dr. Summers. Each of you have been patient, flexible, thoughtful, and insightful. Also, I would like to thank Dr. Brian Huber at the Smithsonian Institution and Dr. Ellen Martin at the University of Florida for their collaborations during my research. Thanks to the faculty and staff of the Geology department as I have been the luckiest person to find good friends in all of you. During this journey I had the chance to meet many students. The understanding of what we were going through made us closer and at the end, good friendships were made that still remain.

I would wholeheartedly like to thank my family in Colombia as it would have been impossible to obtain my research career without your support and encouragement. This journey started in Colombia twenty-five years ago when my grandfather gave me complete access to his library and taught me that education is the foundation of a strong

life. Finally, my best friend, my fiancé, the love of my life, Scott, you understood better than anybody what I was going through because you were on the same PhD path and you always put my needs first. Your unconditional love and support kept us going and I cannot wait to start our new journey and spend the rest of our lives together.

TABLE OF CONTENTS

LIST OF FIGURES

SURFACE AND DEEP WATER CIRCULATION IN LATE CRETACEOUS NORTH ATLANTIC GREENHOUSE OCEAN

Carolina Isaza Londoño

Dr. Kenneth G. MacLeod, Dissertation Supervisor

ABSTRACT

Paleoclimatic data show that patterns in the natural climate system of the Earth have changed dramatically many times in the past. These climate changes have been closely linked to changes in the ocean and its biogeochemical cycles. In this sense, past signatures of climate change, and research during greenhouse periods allows us to assess these signatures to factors such as warming/cooling, and sea level change. Among past warm climates, the Cretaceous is an excellent interval to study that is widely agreed to be a time of high atmospheric CO_2 levels and warm temperatures.

Late Cretaceous, greenhouse conditions started to wane after the Cenomanian and a long term cooling trend is observed up to the end of the Cretaceous. This cooling trend was included by a significant event in the Maastrichtian that is marked by several paleobiological and paleoceanographic perturbations. Significant climate differences among ocean basins during the Maastrichtian are observed around the same time. Notably, North Atlantic basin shows a 3 million years warming trend of approximately 6°C whereas the other basins showed cooling. To explain these Maastrichtian events, changes in the intermediate and/or deep water sources have been invoked. Details vary

among study sites with primary differences residing in source regions for intermediate and deep waters as well as cause and effects relationships. .

This research attempts to address these questions by trying to constrain evolution of Maastrichtian surface to deep ocean circulation in the North Atlantic. First to investigate the unusual surface warming trend observed in the subtropical North Atlantic we analyzed planktonic foraminifera $\delta^{13}C$ and $\delta^{18}O$ isotopes signatures, foraminifera species assemblages, and their correlation to Milankovitch cyclic variation during the Maastrichtian. Results, demonstrate the evolution and development of a well-established western boundary current through out the Maastrichtian, that had migrated laterally long and short time scales.

Second, we concentrated on the Nd isotopic record at Demerara Rise in the tropical North Atlantic and previous implications on deep/intermediate water formation at low latitudes during the Maastrichtian. Results showed that between the early Maastrichtian and mid Danian, $\varepsilon_{Nd(t)}$ values of fish debris from three sites on Demerara Rise shift by ~6 units from -17 to -11. The shift that begins in the Maastrichtian, is gradual within the sites, is diachronous among the sites, and provides the most direct evidence yet presented for reorganization of ocean circulation patterns during the Maastrichtian.

Finally, we took a multiregional approach that will allows us to begin tracking deepwater circulation in the North Atlantic basin through the Late Cretaceous (with an emphasis on the Maastrichtian) from bathyal to abyssal depths. Results indicate that during the Late Cretaceous the North Atlantic exhibits different $\varepsilon_{Nd(t)}$ signatures at

different latitudes indicating the presence of multiple water masses whose distribution change through time. Nonetheless, sometime between the Maastrichtian and the Danian, converge on values of ~- 11 indicating an homogenization of the deep water source after the Cretaceous.

CHAPTER 1

INTRODUCTION

Some of the most important earth science questions of our time relate to understanding how human activities may be modifying current and future climates. Increasing levels of CO_2 in the atmosphere over the past century are thought to be a cause for global warming (Hansen et al, 2008; IPCC, 2008) and the geologic record of greenhouse times provides a critical perspective on how the Earth system (atmosphere, biosphere, and hydrosphere) might respond (Royer et al, 2007).

In the modern time, climate in many regions is strongly influenced by oceanic deep and/or surface water circulation, and one of the most important aspects of the global ocean system is the transport of excess radiative heat absorbed in the tropics to high latitudes (Macdonald et al, 2001). Deep water formation today is dominated by cooling and salinitization in high latitude surface waters (D'Hondt and Arthur, 2002; Marshall and Plumb, 2006). The main sources of deep water are the North Atlantic (North Atlantic Deep Water NADW) and the Southern Ocean (Antarctic Bottom water AABW). NADW transports cold water southward at depth towards the Antarctic circumpolar current; this process is compensated by northward transport of heat from the south in surface and shallow waters. This Atlantic overturning cell is a dynamic element of the oceanic thermohaline circulation (THC). Moreover, sea-air interaction plays an important role in surface currents dynamics and heat transport. For instance, the cold

Humboldt Current off South America and the warm Gulf Stream in the North Atlantic both effectively exchange heat between low and high latitudes (Marshall and Plumb, 2006).

Paleoclimatic data show that patterns in the natural climate system of the Earth have changed dramatically many times in the past (Hodell et al, 1985; Sarnthein, 1994; MacLeod and Huber, 1996; Barrera et al, 1997; Erbacher et al, 2001; Pearson, 2001; Kravtsov and Dewar, 2003; Nisancioglu et al, 2003; Scher and Martin, 2006; Gutiérrez et al, 2008; Wagner et al, 2008; Ishizaki et al, 2009). These climate changes have been closely linked to changes in the ocean and its biogeochemical cycles (Sarmiento et al, 1998; Joos et al, 1999; Bopp et al, 2001; D'Hondt and Arthur, 2002; Behrenfeld et al, 2006). Past signatures of climate change, and research during greenhouse periods allow us to assess these signatures to factors such as warming/cooling, and sea level change. Therefore, understanding greenhouse climate patterns on a local and regional scale may hold the key to improve our understanding of climate variability and biotic responses in modern time.

Among past warm climates the Cretaceous is an excellent interval to study. It was a greenhouse period with a relatively complete, accessible, and well-preserved stratigraphic record. It is also widely agreed to be a time of high atmospheric CO_2 levels and warm temperatures (Jenkyns, 1994; Huber et al, 2002; MacLeod et al, 2005; Royer, 2006). Substantial evidence for warmth includes $\delta^{18}O$-based bathyal temperatures reaching 20°C in the subtropical North Atlantic (Norris and Wilson, 1998; Huber et al, 1999), upper ocean isotopic paleotemperatures of 22-28°C at southern high latitude sites

(Huber et al, 1995), tropical sea surface temperatures of 33 to 34°C (Norris et al, 2002), and fauna intolerant of freezing conditions discovered at 71°N (Tarduno et al, 1998).

Conditions however, were not continuously hot during this interval. A Progressive warming starting in the Aptian (Huber et al, 2002) reached peak conditions during the Mid-Cretaceous (Cenomanian/Turonian boundary) (Clarke and Jenkyns, 1999; Forster et al, 2007) when globally average surface temperatures were up to 14°C higher than today (Tarduno et al, 1998; Wilson et al, 2002; Forster et al, 2007). Associated with this peak, a significant $\delta^{13}C$ excursion related to widespread deposition of organic carbon rich sediments (black shales) and labeled OAE2 (oceanic anoxic even 2) is observed (Schlanger, 1976; Jenkyns, 1980; Arthur et al, 1988; Kuypers et al, 2002). Despite the warming, several cooling trends have been reported during this interval. Ando et al (2009), reported a cooling episode during Mid Cenomanian Event 1, represented by a $\delta^{18}O$ positive excursion in benthic foraminifera that the authors associated with changes in the deep water source. Furthermore, glaciations have even been invoked during the Mid Cenomanian Event (MCE) and the Maastrichtian (Stoll and Schrag, 2000; Miller et al, 2003; Miller et al, 2005). Greenhouse conditions started to wane after the Cenomanian and a long term cooling trend is observed up to the end of the Cretaceous (Huber et al, 1995; Pucéat et al, 2003; Voigt et al, 2004; Forster et al, 2007; Bornemann et al, 2008).

Despite agreement on broad trends, there is uncertainty as to how much warming or cooling occurred in the Late Cretaceous, especially in the tropics. Based on $\delta^{18}O$ analyses of planktonic foraminifers D'Hondt and Arthur (1996) proposed that the

Maastrichtian was characterized by cool tropical sea surface temperatures (SSTs) (20°-21°C). However, Wilson and Opdyke (1996) measured $\delta^{18}O$ values on rudist aragonite and magnesian calcite cements recovered from Pacific guyots and concluded that tropical SSTs in the same interval were extremely warm (between 27° and 32°C). More recent studies in pristine planktonic foraminifera (Pearson, 2001) suggest Maastrichtian tropical temperatures of up to 32°, and Bice et al (2006) reported that the temperature of the Atlantic equatorial region (Demarara Rise) may have been as warm as 42°C in the late Turonian.

Furthermore, the Late Cretaceous cooling trend from the late Campanian-Maastrichtian (85-65 Ma) was punctuated by a significant event in the Maastrichtian that is marked by several paleobiological and paleoceanographic perturbations, such as the extinction among inoceramid bivalve (Kauffman, 1986; MacLeod, 1994; MacLeod and Huber, 1996) and rudist bivalves (Johnson et al, 1996; Johnson, 2002; Steuber et al, 2002). Significant climate differences among ocean basins during the Maastrichtian are observed around the same time. Notably, the North Atlantic basin shows a 3 million year warming trend of approximately 6°C whereas other basins (South Atlantic, Pacific, and Indian Ocean) showed cooling (MacLeod et al, 2005; Isaza-Londoño et al, 2006).

To explain these Maastrichtian events, changes in the intermediate and/or deep water sources have been invoked (MacLeod and Huber, 1996; Barrera et al, 1997; Frank and Arthur, 1999). Details vary among studies with primary differences residing in the proposed source regions for intermediate and deep waters as well as cause and effect relationships. However, all models agree that there was a significant Maastrichtian

reorganization in ocean circulation. Potential regional controls that could cause this reorganization can be projected from the present time but the appropriateness of the extrapolations are difficult to evaluate for Cretaceous greenhouse interval. In order to discriminate among alternatives we need a better control on temporal and spatial changes from surface to deep/intermediate processes and sources for deep water formation during greenhouse intervals.

This research attempts to address these questions by trying to constrain the evolution of Maastrichtian surface to deep ocean circulation in the North Atlantic. The North Atlantic is targeted because it was a growing basin (geographically and bathymetrically) with connections to the Tethys, South Atlantic, and Pacific Oceans. Further, previous studies have suggested that changing circulation in this basin may have controlled the timing and nature of global climate change for the Maastrichtian (MacLeod and Huber, 1996; Frank and Arthur, 1999; Poulsen et al, 2003; MacLeod et al, 2005; Isaza-Londoño et al, 2006).

This dissertation is divided into three studies (chapters 2-4) that address circulation at surface, intermediate, and deep-water depths. Chapter 2 considers surface water gradients between two closely spaced sites in the subtropical North Atlantic at the end of the Maastrichtian (MacLeod et al, 2005; Isaza-Londoño et al, 2006). We will test whether variations in runoff and/or upwelling or migrations of surface water masses are responsible for temperature and foraminifera assemblages cyclic variations (MacLeod et al, 2001; Watkins and Self-Trail, 2005). In order to do so, we analyzed planktonic foraminifera species assemblages and foraminifera $\delta^{13}C$ and $\delta^{18}O$ isotope signatures, and

their correlation to Milankovitch cyclic variation. Foraminifera population dynamics from this study demonstrate the evolution and development of a well established western boundary current throughout the Maastrichtian that migrated laterally over both long and short time scales.

Chapter three concentrates on the Nd isotopic record at Demerara Rise in the tropical North Atlantic and its implication for deep/intermediate water formation at low latitudes during the Maastrichtian. MacLeod et al (2008) reported extremely low $\varepsilon_{Nd(t)}$ (~ -16) values for the Demerara Rise throughout most of the Cretaceous compared to other basins in the same period. They proposed that the values observed are the signature of a distinct bottom water mass they called "Demerara bottom water mass" (DBWM) indicative of regional (low latitude) sinking of surface waters. These low $\varepsilon_{Nd(t)}$ isotopic values were associated with black shales but continued into Campanian and Maastrichtian chalks suggesting that the source of the DBWM was constant for most of the Late Cretaceous. On the other hand, low-resolution data from Bourbon (2008) showed a shift to values of -11 by the middle Paleocene, but at only one site and with five million year resolution. The objective of chapter three was to acquire a high-resolution record from multiple sites for the Maastrichtian in the Demerara Rise that will document the timing and pattern of the shift in time and depth. Results show that $\varepsilon_{Nd(t)}$ values of fish debris from three sites on Demerara Rise shift by ~6 units from -17 to -11 between the early Maastrichtian and mid Danian. The shift begins in the Maastrichtian is gradual within the sites, is diachronous among the sites, and provides the most direct evidence yet presented for reorganization of ocean circulation patterns during the Maastrichtian.

Finally, in chapter four, we took a multiregional approach that allow us to begin tracking deep water circulation from bathyal to abyssal depths in the North Atlantic basin through the Late Cretaceous (with an emphasis on the Maastrichtian). First, by extending the Demerara transect to true deep depths in the Cape Verde Basin, we can test the evolution of the DBWM and the significance of low latitude deep-water formation during the Maastrichtian. Second, by studying a similar depth transect in the Subtropical North Atlantic from the Blake Nose (bathyal) to the Bermuda Rise (abyssal), we can provide new insights and a more complete view of deep-water circulation patterns and test hypotheses regarding deep-water sources and patterns. Results indicate that the Late Cretaceous North Atlantic exhibits different $\varepsilon_{Nd(t)}$ signatures at different latitudes indicating the presence of multiple water masses whose distribution changes through time. Nonetheless, sometime between the Maastrichtian and the Danian, they converge on values of ~-11 indicating homogenization of the deep water source after the Cretaceous.

1.1. SCIENTIFIC BACKGROUND

These studies employ paleontological and several geochemical techniques to infer paleoceanographic conditions and circulation patterns. Within each chapter is a brief description of the techniques used. Below we provide a more expanded and general background of these methods.

1.1.1. DEEP CIRCULATION AND NEODYMIUM ISOTOPES

The most commonly applied geochemical proxies to reconstruct past deep water

circulation have been the stable carbon isotope composition ($\delta^{13}C$) given in per mil (Curry and Lohmann, 1983; Curry et al, 1988; Woodruff and Savin, 1989; Ravelo and Andreasen, 2000) and the Cd/Ca ratio (Boyle, 1988) in benthic foraminifera. In general the oceanic record of $\delta^{13}C$ in planktonic and benthic foraminifera at any site always reflects at least three components: 1) the $\delta^{13}C$ values of total dissolved carbonate in the oceans; 2) the local primary productivity; 3) the global pattern of deep-sea circulation (Rohling and Cooke, 1999). Carbon moves through oceanic reservoirs as inorganic and organic carbon, and the biological pump is key in this process. During primary productivity, ^{12}C preferentially goes into organic matter, and then is released in the deep water as this organic matter is remineralized. As this bottom water circulates, progressive addition of remineralized organic carbon causes bottom water $\delta^{13}C$ to decrease. Thus, gradients in $\delta^{13}C$ values within a water mass can indicate flow patterns (Frank, 2002). However, these water masses all start out in equilibrium with the atmosphere, meaning they start with about the same $\delta^{13}C$ value. Further, they evolve in the same direction as they move though the ocean. So determining flow without prior knowledge of the distribution of water masses is difficult. Also, nonconservative effects of temperature, nutrient availability, and variability in carbonate ion concentration are potentially confounding factors (Broecker and Peng, 1982; Spero et al, 1997; Frank, 2002).

A second technique that uses Cd/Ca from benthic foraminifera was developed in parallel with the carbon isotope method. Cadmium concentrations in seawater follow a nutrient-like (phosphate, nitrate) distribution. Benthic foraminifera incorporate cadmium

and calcium into their shells in proportion to their abundance in seawater, which allows for the reconstruction of deep-water cadmium (and thus macronutrient) gradients (Frank, 2002). This knowledge could allow the distinction between low-nutrient (such as NADW) and high-nutrient deep waters (such as in the North Pacific) in the past. However, it is difficult to make quantitative estimates of mixing between water masses on the basis of Cd/Ca or $\delta^{13}C$ data because neither of the two proxies may exclusively mirror the nutrient content of ambient deep water (Frank, 2002). For Cd/Ca, problems also arise from thermodynamic effects (Boyle, 1988; Frank, 2002). Consequently, applying these methods requires a large set of data that not only follows the flow path across significant distances, but also samples different depths so you know inferences are being made from data representing the same water mass.

Recent studies have demonstrated that neodymium (Nd) isotopes are a powerful proxy for past water mass structure and mixing that could help constrain major circulation changes in the past without the complications of $\delta^{13}C$ and Ca/Cd. The residence time of Nd in the ocean is about ~600-1000 years (Tachikawa et al, 1999), which is shorter than the total mixing time of the oceans (~1500 years) (Broecker et al, 1960). Because of this Nd isotopes can be used to track deep water masses (Stille and Shields, 1997). However, Nd is considered a quasi-conservative element because the signal of the water masses can be altered by weathering inputs within the basin (Frank, 2002). Even so, Nd provides a more direct means of tracking water masses than $\delta^{13}C$ or Ca/Cd in benthic foraminifera. In addition, because the isotopic distinction associates with mass aging among water masses is large relative to measurement uncertainty or

changes, records of Nd isotopes can be used to infer source regions of contemporary bottom waters and connections between seaways, as well as mixing of water masses (Piepgras and Wasserburg, 1982, 1987; Piepgras and Jacobsen, 1988; Albaréde et al, 1997; Jeandel et al, 1998; Goldstein and Hemming, 2004).

To determine the Nd values of seawater in the past, we need to find a physical archive that incorporates the seawater signature and that is not altered by burial or diagenesis, and it also must be datable. Archives for Nd include, ferromanganese (Fe-Mn) oxide crusts and nodules, biogenic phosphates, and Fe-Mn coatings (Thomas, 2005). Early studies showed that as inorganic host of Nd, Fe-Mn crusts and nodules were an effective archive, and they are still widely used. However, their slow growth makes dating them very hard, limiting temporal resolution, and their rarity limits geographic coverage (Martin, 2000). In general, they provide good record of long term trends of ocean circulation.

In contrast, phosphates, especially apatite in the form of conodonts and fossil fish teeth, have proven to be useful archives of Nd isotopes for higher resolution paleoceanographic studies (Elderfield and Pagett, 1986; Martin and Scher, 2004; MacLeod et al, 2008). The Nd is incorporated into teeth and other fish debris (bioapatite) from bottom waters during early diagenesis at the seafloor (Elderfield and Pagget, 1986; Martin and Scher, 2004) and this value is relatively insensitive to later diagenetic alteration (Martin and Sher, 2004). Unlike crusts, teeth can be dated easily using biostratigraphy, orbital cyclostratigraphy, chemostratigraphy and paleomagnetism applied to sediments in which they occur. For this reason, relatively high resolution records can

be produced.

Samarium (Sm) and neodymium are closely related rare earth elements. ^{143}Nd is a radiogenic daughter product of ^{147}Sm produced by alpha decay with a half-life of approximately 106 billion years. Sm is relatively concentrated in the crust and Nd is relatively concentrated in the mantle (Stille et al, 1992). Both Sm and Nd occur as trace constituents in seawater. The Sm/Nd ratio of sea water is about 0.20, which is about the same as that of average crustal rock or of average suspended loads (Stille et al, 1992). The $^{143}Nd/^{144}Nd$ ratio is measured in a sample and commonly reported as ε_{Nd}. This expression allows small, but significant, variations in the isotopic ratio to be reported in whole numbers relative to a bulk Earth value (DePaolo and Wasserburg, 1976). Nd isotopic measures in sea water have shown that major oceanic basins differ in their Nd compositions (Piepgras et al, 1979; Piepgras and Wasserburg, 1980, 1982) and these differences (within and/or among the basins) reflect the changes in the isotopic compositions of the Nd sources (Stille et al, 1992). High ε_{Nd} values (more radiogenic) in general reflect contributions from younger rocks (mantle derived basaltic, volcanic, and juvenile crust), while low ε_{Nd} values (less radiogenic) result from the contribution of old continental blocks (cratons).

The reference values of $^{143}Nd/^{144}Nd$ are those that would be found in a reservoir that has a Sm/Nd ratio equal to that of the average chondritic reservoir meteorite for all time (DePaolo, 1988). This standard reservoir is referred as CHUR (Chondritic Uniform Reservoir) and its $^{143}Nd/^{144}Nd$ ratio at any time (T) into the past is given by:

$$\left(\frac{^{143}Nd}{^{144}Nd}\right)_{CHUR(T)} = \left(\frac{^{143}Nd}{^{144}Nd}\right)_{CHUR(0)} - \left(\frac{^{147}Sm}{^{144}Nd}\right)_{CHUR(0)} \left(e^{\lambda T} - 1\right)$$

where λ is the half life (6.54×10^{-12} y^{-1}) of ^{147}Sm and $^{143}Nd/^{144}Nd_{CHUR(0)}$ and $^{147}Sm/^{144}Nd_{CHUR(0)}$ are the values of CHUR today (0.512638 and 0.1967 respectively) (De Paolo and Wasserburg, 1976). The $^{143}Nd/^{144}Nd$ ratio of any rock sample at T=0 is represented by the parameter $\varepsilon_{Nd(0)}$ defined as:

$$\varepsilon_{Nd(0)} = \left[\frac{\left(^{143}Nd/_{144}Nd\right)_{Sample(0)}}{\left(^{143}Nd/_{144}Nd\right)_{CHUR(0)}} - 1\right] \times 10^4$$

where the $\varepsilon_{Nd(0)}$ of any sample refers to the $^{143}Nd/^{144}Nd$ measured in the laboratory. Similarly, the $^{143}Nd/^{144}Nd$ ratio of any rock sample at time T is represented by the parameter $\varepsilon_{Nd(t)}$ defined as:

$$\varepsilon_{Nd(T)} = \left[\frac{\left(^{143}Nd/_{144}Nd\right)_{Sample(T)}}{\left(^{143}Nd/_{144}Nd\right)_{CHUR(T)}} - 1\right] \times 10^4$$

where $\varepsilon_{Nd(T)}$ indicates the deviation of the $^{143}Nd/^{144}Nd$ value of the sample from that of CHUR in units of parts in 10^4. To calculate $\varepsilon_{Nd(T)}$ we need to know the $^{143}Nd/^{144}Nd$ ratio of the sample at time T which is calculated by:

$$\left(\frac{^{143}Nd}{^{144}Nd}\right)_{Sample(T)} = \left(\frac{^{143}Nd}{^{144}Nd}\right)_{Sample(0)} - \left(\frac{^{147}Sm}{^{144}Nd}\right)_{Sample(0)} \left(e^{\lambda T} - 1\right)$$

where (0) indicates the laboratory measured value of present time.

The $^{147}Sm/^{144}Nd_{Sample(0)}$ varies depending on the material analyzed. For this research the material was fish debris on whose small variations among the different basins were observed. When $\varepsilon_{Nd(t)}$ was calculated, the $^{147}Sm/^{144}Nd_{Sample(0)}$ used was 0.125 for fish from Demerara Rise and Blake Nose, 0.147 for fish from Bermuda Rise, and 0.130 for fish from Cape Verde.

1.1.2. $\delta^{18}O$ Values In Foraminifera

Analyzing the oxygen isotopic composition of carbonate in microorganisms allows us to deduce the temperature at which the calcite was precipitated. The empirically determined temperature equation that is used most often in work with deep sea carbonates is:

$$t^oC = 16.9 - 4.2\ (\delta_c - \delta_w) + 0.13\ (\delta_c - \delta_w)^2 \text{ (modified by Craig 1965).}$$

in which t^oC is the temperature in degrees Celsius, δ_c is the oxygen isotopic composition of calcite compared with the PDB standard, and δ_w the oxygen isotopic composition of the water from which it was precipitated compared to the Standard Mean Ocean Water (SMOW).

However, we can use this method to determine the temperature at which calcite was precipitated only if we know the isotopic composition of the water in which the calcite formed. This value is not easy to determine because $\delta^{18}O$ values are related to salinity, and because the isotopic composition of oxygen in the ocean as a whole depends on the amount of water stored in the continents in the form of glaciers. Nonetheless, by knowing the present ocean mean $\delta^{18}O$ and calculating the effect of maximum glaciations,

we can make reasonable assumptions about $\delta^{18}O$ seawater values for the geologic past. For this study we assume that the Maastrichtian was an ice free interval where the δ_w is -1‰ (Shackleton, 1965).

The combination of oxygen isotopes values stored in the tests of planktonic and benthic foraminifera allows the determination of temperatures in surface and deep waters. Furthermore, planktonic species live at different depths (thus at different temperatures) in the water column. Isotopic signals of different species within one sample differ according to their depth-habitat and these differences allow us to get a close look at the water column structure.

1.1.3. $\delta^{13}C$ Values In Planktonic Foraminifera

Carbon exists in two main reservoirs: organic matter and sedimentary carbonates. In the modern ocean, the distribution of ^{13}C is mainly controlled by the biological pump. CO_2 from the atmosphere dissolves into the ocean and this inorganic carbon can be converted into organic matter by photosynthesis (Rohling and Cooke, 1999). Marine foraminifera shells serve as an archive for inorganic carbon throughout the geologic record. Carbon isotopes are fractionated during photosynthesis where ^{12}C is preferentially incorporated into photosynthate. This fractionation shifts the $\delta^{13}C$ value of organic matter toward lower (relatively ^{12}C enriched) values compared to that of inorganic carbon (Goodney et al, 1980) and leaves the residual inorganic pool with higher $\delta^{13}C$ values. The organic matter sinks and is remineralized resulting in a gradient in dissolved inorganic carbon from high value at the surface to low values at depth. As a result, local

increases in productivity are reflected as increases in this gradient and vice versa. Net global increases or decreases in carbon burial on the other hand, result in a shift of all reservoirs towards higher (or lower) $\delta^{13}C$ values. Complications that result in $\delta^{13}C$ foraminiferal disequilibrium can include 1) utilization of metabolic CO_2 during shell formation, 2) photosynthetic activity of symbionts, 3) growth rate, and 4) variation in carbonate ion concentrations in ambient waters (Spero, 1987; Spero and Deniro, 1987; Spero, 1993, 1996; Spero and Lea, 1996; Spero, 1997; Spero et al, 1997). Still the basic pattern of foraminiferal $\delta^{13}C$ variation with water column depth facilitates the reconstruction of fossil foraminiferal depth habitats based on the relative stable isotope offsets between species in an assemblage and enable us to track changes in the water column structure (Pearson et al, 1997; Spero, 1998; Sexton et al, 2006a; Sexton et al, 2006b).

1.1.4. FORAMINIFERA ASSEMBLAGES

Planktonic foraminifera live under a variety of environmental conditions in the upper ocean, and they reflect environmental parameters such as water temperature, salinity, food availability, and water mass structure in their assemblages and individual tests (Abramovich et al, 2003; Coxall et al, 2007). Depth distributions of Cretaceous planktonic foraminifera are belived to have been similar to modern analogs, where large/heavy ornamented morphotypes inhabit “deeper” waters while small, globular, less ornamented morphotypes inhabit surface waters (Kucera, 1997; Fraile et al, 2008). In addition, given that foraminifera are relatively abundant and have short reproductive cycles (~20 days) (Bijma et al, 1990) foraminifera are a primary contributors of biogenic

calcite to ocean marine sediments (Spero, 1998). All of these factors combined makes planktonic foraminifera an ideal tool for reconstructing paleoenviroments. Nonetheless, the isotope record often contradicts the expected paleoecological signal. Therefore, a better approach (used in this research) combines multiple proxies (assemblages and isotopic signatures) to better understand the depth habitat of Maastrichtian foraminifera and their variation in response to changes in ocean circulation or water stratification.

REFERENCES

Abramovich, S., Keller, G., Stüben, D., and Berner, Z., 2003. Characterization of late Campanian and Maastrichtian planktonic foraminiferal depth habitats and vital activities based on stable isotopes: Palaeogeography, Palaeoclimatology, Palaeoecology, v. 202, p. 1-29.

Albaréde, F., Goldstein, S.L., and Dautel, D., 1997. The neodymium isotopic composition of manganese nodules from the Southern and Indian oceans, the global oceanic neodymium budget, and their bearing on deep ocean circulation: Geochimica et Cosmochimica Acta, v. 61, p. 1277-1291.

Ando, A., Huber, B.T., MacLeod, K.G., Ohta, T., and Khim, B.-K., 2009. Blake Nose stable isotopic evidence against the mid-Cenomanian glaciation hypothesis: Geology, v. 37, p. 451-454.

Arsouze, T., Dutay, J.C., Kageyama, M., Lacan, F., Alkama, R., Marti, O., and Jeandel, C., 2008. A modeling sensitivity study of the influence of the Atlantic meridional overturning circulation on neodymium isotopic composition at the last glacial maximum: Climate of the Past, v. 4, p. 191-203.

Arthur, M.A., Dean, W.E., and Pratt, L.M., 1988. Geochemical and climatic effects of increased marine organic carbon burial at the Cenomanian/Turonian boundary: Nature, v. 335, p. 714-717.

Barrera, E., Savin, S.M., Thomas, E., and Jones, C.E., 1997. Evidence for thermohaline-circulation reversals controlled by sea-level change in the latest Cretaceous: Geology, v. 25, p. 715-718.

Behrenfeld, M.J., O'Malley, R.T., Siegel, D.A., McClain, C.R., Sarmiento, J.L., Feldman, G.C., Milligan, A.J., et al., 2006. Climate-driven trends in contemporary ocean productivity: Nature, v. 444, p. 752-755.

Bice, K.L., Birgel, D., Meyers, P.A., Dahl, K.A., Hinrichs, K.U., and Norris, R.D., 2006. A multiple proxy and model study of Cretaceous upper ocean temperatures and atmospheric CO_2 concentrations: Paleoceanography, v. 21, p. PA2002, doi:10.1029/2005PA001203.

Bijma, J., Erez, J., and Hemleben, C., 1990. Lunar and semi-lunar reproductive cycles in some spinose planktonic foraminifers: Journal of Foraminiferal Research, v. 20, p. 117-127.

Bopp, L., Monfray, P., Aumont, O., Dufresne, J.L., Le Treut, H., Madec, G., Terray, L., and Orr, J.C., 2001. Potential impact of climate change on marine export production: Global Biogeochemical Cycles, v. 15, p. 81-99.

Bornemann, A., Norris, R.D., Friedrich, O., Beckmann, B., Schouten, S., Damst√©, J.S.S., Vogel, J., Hofmann, P., and Wagner, T., 2008. Isotopic evidence for glaciation during the Cretaceous supergreenhouse: Science, v. 319, p. 189-192.

Bourbon, É., 2008. Nd isotopes throughout the North Atlantic in the Late Cretaceous and across the Oceanic Anoxic event 2. M.S Thesis. University of Florida.

Boyle, E.A., 1988. Cadmium: chemical tracer of deepwater paleoceanography: Paleoceanography, v. 3, p. 471-489.

Broecker, W.S., Gerard, R., Ewing, M., and Heezen, B.C., 1960. Natural radiocarbon in the Atlantic Ocean: J. Geophys. Res., v. 65, p. 2903-2931.

Broecker, W.S., and Peng, T.H., 1982. Tracers in the sea: Lamont-Doherty Geological Observatory, p. 690.

Clarke, L.J., and Jenkyns, H.C., 1999. New oxygen isotope evidence for long-term Cretaceous climatic change in the Southern Hemisphere: Geology, v. 27, p. 699-702.

Coxall, H.K., Wilson, P.A., Pearson, P.N., and Sexton, P.E., 2007. Iterative evolution of digitate planktonic foraminifera: Paleobiology, v. 33, p. 495-516.

Craig, H., 1965. The measurement of oxygen isotope paleotemperature/stable isotopes in oceanographic studies and paleotemperature: The Measurement of Oxygen Isotope Paleotemperatures in Stable Isotopes in Oceanographic Studies and Paleotemperatures, p. 1-24

Curry, W.B., and Lohmann, G.P., 1983. Reduced advection into Atlantic Ocean deep eastern basins during last glaciation maximum: Nature, v. 306, p. 577-580.

Curry, W.B., Duplessy, J.C., Labeyrie, L.D., and Shackleton, N.J., 1988. Changes in the distribution of $\delta^{13}C$ of deep water and ΣCO_2 between the last glaciation and the Holocene: Paleoceanography, v. 3, p. 317-341.

D'Hondt, S., and Arthur, M.A., 1996. Late Cretaceous oceans and the cool tropic paradox: Science, v. 271, p. 1838-1841.

D'Hondt, S., and Arthur, M.A., 2002. Deep water in the late Maastrichtian ocean: Paleoceanography, v. 17, p. 8-1-8-11.

DePaolo, D.J., and Wasserburg, G.J., 1976. Nd isotopic variations and petrogenetic models: Geophysical Research Letters, v. 3, p. 249-252.

DePaolo, D.J., 1988. Neodymium isotope geochemistry: Springer, Berlin Heidelberg New York.

Elderfield, H., and Pagett, R., 1986. Rare earth elements in ichthyoliths: Variations with redox conditions and depositional environment: Science of the Total Environment, v. 49, p. 175-197.

Erbacher, J., Huber, B.T., Norris, R.D., and Markey, M., 2001. Increased thermohaline stratification as a possible cause for an ocean anoxic event in the Cretaceous period: Nature, v. 409, p. 325-327.

Forster, A., Schouten, S., Moriya, K., Wilson, P.A., Sinninghe, D., and Jaap, S., 2007. Tropical warming and intermittent cooling during the Cenomanian/Turonian oceanic anoxic event 2: Sea surface temperature records from the equatorial Atlantic: Paleoceanography, v. 22. PA1219.

Fraile, I., Schulz, M., Mulitza, S., and Kucera, M., 2008. Predicting the global distribution of planktonic foraminifera using a dynamic ecosystem model: Biogeosciences, v. 5, p. 891-911.

Frank, M., 2002. Radiogenic isotopes: Tracers of past ocean circulation and erosional input: Rev. Geophys., v. 40. 1001.

Frank, T.D., and Arthur, M.A., 1999, Tectonic forcings of Maastrichtian ocean-climate evolution, *in* Arthur, M.A., ed., Paleoceanography, Volume 14: United States, American Geophysical Union : Washington, DC, United States, p. 103.

Goldstein, S.L., and Hemming, S.R., 2004. Long-lived isotopic tracers in oceanography, paleoceanography, and ice-sheet dynamics: Treatise on Geochemistry: The Oceans and Marine Geochemistry, v. 6, p. 453-489.

Goodney, D.E., Margolis, S.V., Dudley, W.C., Kroopnick, P., and Williams, D.F., 1980. Oxygen and carbon isotopes of Recent calcareous nannofossils as paleoceanographic indicators: Marine Micropaleontology, v. 5, p. 31-42.

Gutiérrez, D., Sifeddine, A., Field, D.B., Ortlieb, L., Vargas, G., Chávez, F., Velazco, F., et al., 2008. Rapid reorganization in ocean biogeochemistry off Peru towards the end of the Little Ice Age: Biogeosciences Discussions, v. 5, p. 3919-3943.

Hansen, J., Makiko, S., Kharecha, P., Beerling, D., Berner, R.A., Masson-Delmotte, V., Pagani, M., et al., 2008. Target Atmospheric CO_2: Where Should Humanity Aim?: The Open Atmospheric Science Journal, p. 217-231.

Hodell, D.A., Williams, D.F., and Kennett, J.P., 1985. Late Pliocene reorganization of deep vertical water-mass structure in the western South Atlantic: faunal and isotopic evidence: Geological Society of America Bulletin, v. 96, p. 495-503.

Huber, B.T., Hodell, D.A., and Hamilton, C.P., 1995. Middle-late Cretaceous climate of the southern high latitudes: stable isotopic evidence for minimal equator-to-pole thermal gradients: Geological Society of America Bulletin, v. 107, p. 1164-1191.

Huber, B.T., Leckie, R.M., Norris, R.D., Bralower, T.J., and CoBabe, E., 1999. Foraminiferal assemblage and stable isotopic change across the Cenomanian-Turonian boundary in the Subtropical North Atlantic: Journal of Foraminiferal Research, v. 29, p. 392-417.

Huber, B.T., Norris, R.D., and MacLeod, K.G., 2002. Deep-sea paleotemperature record of extreme warmth during the Cretaceous: Geology, v. 30, p. 123-126.

IPCC, 2008. Climate Change 2007: The Physical Science Basis: Contribution of Working Group I to the Fourth Assessment Report of the Intergovernmental Panel on Climate Change [Solomon, S., D. Qin, M. Manning, Z. Chen, M. Marquis, K.B. Averyt, M. Tignor and H.L. Miller (eds.)]. Cambridge University Press, Cambridge, United Kingdom and New York, NY, USA, 996 pp.

Isaza-Londoño, C., MacLeod, K.G., and Huber, B.T., 2006. Maastrichtian North Atlantic warming, increasing stratification, and foraminiferal paleobiology at three timescales: Paleoceanography, v. 21. PA1012.

Ishizaki, Y., Ohkushi, K., Ito, T., and Kawahata, H., 2009. Abrupt changes of intermediate-water oxygen in the northwestern Pacific during the last 27 kyr: Geo-Marine Letters, v. 29, p. 125-131.

IPCC, 2008. Climate Change 2007: The Physical Science Basis: Contribution of Working Group I to the Fourth Assessment Report of the Intergovernmental Panel on Climate Change [Solomon, S., D. Qin, M. Manning, Z. Chen, M. Marquis, K.B.

Averyt, M. Tignor and H.L. Miller (eds.)]. Cambridge University Press, Cambridge, United Kingdom and New York, NY, USA, 996 pp.

Jeandel, C., Thouron, D., and Fieux, M., 1998. Concentrations and isotopic compositions of neodymium in the eastern Indian Ocean and Indonesian straits: Geochimica et Cosmochimica Acta, v. 62, p. 2597-2607.

Jenkyns, H.C., 1980. Cretaceous anoxic events: from continents to oceans: Journal of the Geological Society, v. 137, p. 171-188.

Jenkyns, H.C., Gale, A.S. and Corfield, R.M, 1994. Carbon- and oxygen-isotope stratigraphy of the English Chalk and Italian Scaglia and its palaeoclimatic significance: Geology Magazine, v. 131, p. 1-34.

Johnson, C.C., Barron, E.J., Kauffman, E.G., Arthur, M.A., Fawcett, P.J., and Yasuda, M.K., 1996. Middle cretaceous reef collapse linked to ocean heat transport: Geology, v. 24, p. 376-380.

Johnson, C.C., 2002. The rise and fall of Rudist reefs: Reefs of the dinosaur era were dominated not by corals but by odd mollusks, which died off at the end of the cretaceous from causes yet to be discovered: American Scientist, v. 90, p. 148-153.

Joos, F., Plattner, G.K., and Stocker, T.F., 1999. Global warming and marine carbon cycle feedbacks on future atmospheric CO_2: Science, v. 284, p. 464-467.

Kauffman, E.G., 1986. High-resolution event stratigraphy: regional and global Cretaceous bio-events: Global bio-events. Proc. 1st meeting of the IGCP Project 216, p. 279-335.

Kravtsov, S., and Dewar, W.K., 2003. On the role of thermohaline advection and sea ice in glacial transitions: Journal of Geophysical Research C: Oceans, v. 108, p. 34-1.

Kucera, M., 1997, Quantitative studies of morphological evolution and biogeographic patterns in Cretaceous and Tertiary Foraminifera, Publ. - Earth Sciences Centre, Volume A26: Sweden, Goteborg University, Earth Sciences Centre : Goteborg, Sweden.

Kuypers, M., Pancost, R.D., Nijenhuis, I.A., and Sinninghe Damsté, J.S., 2002. Enhanced productivity led to increased organic carbon burial in the euxinic North Atlantic basin during the late Cenomanian oceanic anoxic event: Paleoceanography, v. 17, p. 3-1.

Macdonald, A.M., Baringer, M.O., and Ganachaud, A., 2001. Heat transport and climate: Encyclopedia of Ocean Sciences, v. 2, p. 1195-1206.

MacLeod, K.G., 1994. Bioturbation, inoceramid extinction, and mid-Maastrichtian ecological change: Geology, v. 22, p. 139-142.

MacLeod, K.G., and Huber, B.T., 1996. Reorganization of deep ocean circulation accompanying a late Cretaceous extinction event: Nature, v. 380, p. 422-425.

MacLeod, K.G., Kucera, M., Huber, B.T., Pletsch, T., and Röhl, U., 2001. Maastrichtian foraminiferal and paleoceanographic changes on Milankovitch timescales: Paleoceanography, v. 16, p. 133-154.

MacLeod, K.G., Huber, B.T., and Isaza-Londoño, C., 2005. North Atlantic warming during global cooling at the end of the Cretaceous: Geology, v. 33, p. 437-440.

MacLeod, K.G., Martin, E.E., and Blair, S.W., 2008. Nd isotopic excursion across Cretaceous ocean anoxic event 2 (Cenomanian-Turonian) in the tropical North Atlantic: Geology, v. 36, p. 811-814.

Marshall, J., and Plumb, A., 2006. Circulation of the Atmosphere and Ocean: an introductory text: Massachusetts Institute of Technology.

Martin, E.E., 2000, Fossil fish teeth as proxies for seawater Sr and Nd isotopes, *in* Haley, B.A., ed., Geochimica et Cosmochimica Acta, Volume 64: International, Pergamon : Oxford, International, p. 835.

Martin, E.E., and Scher, H.D., 2004. Preservation of seawater Sr and Nd isotopes in fossil fish teeth: bad news and good news: Earth and Planetary Science Letters, v. 220, p. 25-39.

Miller, K.G., Sugarman, P.J., Browning, J.V., Kominz, M.A., Hernández, J.C., Olsson, R.K., Wright, J.D., Feigenson, M.D., and Van Sickel, W., 2003. Late Cretaceous chronology of large, rapid sea-level changes: Glacioeustasy during the greenhouse world: Geology, v. 31, p. 585-588.

Miller, K.G., Wright, J.D., and Browning, J.V., 2005. Visions of ice sheets in a greenhouse world: Marine Geology, v. 217, p. 215-231.

Nisancioglu, K.H., Raymo, M.E., and Stone, P.H., 2003. Reorganization of Miocene deep water circulation in response to the shoaling of the Central American Seaway: Paleoceanography, v. 18, p. 6-1.

Norris, R.D., and Wilson, P.A., 1998. Low-latitude sea-surface temperatures for the mid-Cretaceous and the evolution of planktic foraminifera: Geology, v. 26, p. 823-826.

Norris, R.D., Bice, K.L., Magno, E.A., and Wilson, P.A., 2002. Jiggling the tropical thermostat in the Cretaceous hothouse: Geology, v. 30, p. 299-302.

Pearson, P.N., Shackleton, N.J., and Hall, M.A., 1997. Stable isotopic evidence for the sympatric divergence of Globigerinoides trilobus and Orbulina universa (planktonic foraminifera): Journal of the Geological Society, v. 154, p. 295-302.

Pearson, P.N., 2001, Warm tropical sea surface temperatures in the Late Cretaceous and Eocene epochs, *in* Ditchfield, P.W., Singano, J., Harcourt-Brown, K.G., Nicholas, C.J., Olsson, R.K., Shackleton, N.J., and Hall, M.A., eds., Nature London, Volume 413: United Kingdom, Macmillan Journals : London, United Kingdom, p. 481.

Piepgras, D.J., Wasserburg, G.J., and Dasch, E.J., 1979. The isotopic composition of Nd in different ocean masses: Earth and Planetary Science Letters, v. 45, p. 223-236.

Piepgras, D.J., and Wasserburg, G.J., 1980. Neodymium isotopic variations in seawater: Earth and Planetary Science Letters, v. 50, p. 128-138.

—, 1982. Isotopic composition of neodymium in waters from the Drake Passage: Science, v. 217, p. 207-214.

—, 1987. Rare earth element transport in the western North Atlantic inferred from Nd isotopic observations: Geochimica et Cosmochimica Acta, v. 51, p. 1257-1271.

Piepgras, D.J., and Jacobsen, S.B., 1988. The isotopic composition of neodymium in the North Pacific: Geochimica et Cosmochimica Acta, v. 52, p. 1373-1381.

Poulsen, C.J., Gendaszek, A.S., and Jacob, R.L., 2003. Did the rifting of the Atlantic Ocean cause the Cretaceous thermal maximum?: Geology, v. 31, p. 115-118.

Pucéat, E., Lécuyer, C., Sheppard, S.M.F., Dromart, G., Reboulet, S., and Grandjean, P., 2003. Thermal evolution of Cretaceous Tethyan marine waters inferred from oxygen isotope composition of fish tooth enamels: Paleoceanography, v. 18, p. 7-1.

Ravelo, A.C., and Andreasen, D.H., 2000. Enhanced circulation during a warm period: Geophysical Research Letters, v. 27, p. 1001-1004.

Rohling, E.J., and Cooke, S., 1999. Stable oxygen and carbon isotopes in foraminiferal carbonate shells: Modern Foraminifera, p. 239-258.

Royer, D.L., 2006. CO2-forced climate thresholds during the Phanerozoic: Geochimica et Cosmochimica Acta, v. 70, p. 5665-5675.

Royer, D.L., Berner, R.A., and Park, J., 2007. Climate sensitivity constrained by CO_2 concentrations over the past 420 million years: Nature, v. 446, p. 530-532.

Sarmiento, J.L., Hughes, T.M.C., Stouffer, R.J., and Manabe, S., 1998. Simulated response of the ocean carbon cycle to anthropogenic climate warming: Nature, v. 393, p. 245-249.

Sarnthein, M., 1994. Changes in east Atlantic deepwater circulation over the last 30 000 years: eight time slice reconstructions: Paleoceanography, v. 9, p. 209-267.

Scher, H.D., and Martin, E.E., 2006. Timing and climatic consequences of the opening of drake passage: Science, v. 312, p. 428-430.

Schlanger, S.O., 1976. Cretaceous oceanic anoxic events; causes and consequences, *in* Jenkyns, H.C., ed., Geologie en Mijnbouw, Volume 55: Netherlands, De Bussy Ellerman Harms : Amsterdam, Netherlands, p. 179.

Sexton, P.F., Wilson, P.A., and Pearson, P.N., 2006. Palaeoecology of late middle Eocene planktic foraminifera and evolutionary implications: Marine Micropaleontology, v. 60, p. 1-16.

Shackleton, N.J., 1965. The high-precision isotopic analysis of oxygen and carbon in carbon dioxide: Journal of Scientific Instruments, v. 42, p. 689-692.

Spero, H.J., 1987, The effect of irradiance and temperature on stable isotope incorporation and shell morphology in a symbiont-bearing planktonic foraminifera, *in* Williams, D.F., ed., Eos, Transactions, American Geophysical Union, Volume 68: United States, American Geophysical Union : Washington, DC, United States, p. 1714.

Spero, H.J., and Deniro, M.J., 1987. The influence of symbiont photosynthesis on the $\delta^{18}O$ and $\delta^{13}C$ values of planktonic foraminiferal shell calcite: Symbiosis, v. 4, p. 213-228.

Spero, H.J., 1993, Intraspecific stable isotope variability in the planktic foraminifera *Globigerinoides sacculifer*; results from laboratory experiments, *in* Lea, D.W., ed., Marine Micropaleontology, Volume 22: Netherlands, Elsevier : Amsterdam, Netherlands, p. 221.

—, 1996, Experimental determination of stable isotope variability in *Globigerina bulloides*; implications for paleoceanographic reconstructions, *in* Lea, D.W., ed., Marine Micropaleontology, Volume 28: Netherlands, Elsevier : Amsterdam, Netherlands, p. 231.

Spero, H.J., and Lea, D.W., 1996. Experimental determination of stable isotope variability in *Globigerina bulloides*: Implications for paleoceanographic reconstructions: Marine Micropaleontology, v. 28, p. 231-246.

Spero, H.J., 1997, Effect of seawater carbonate concentration on foraminiferal carbon and oxygen isotopes, *in* Bijma, J., Lea, D.W., and Bemis, B.E., eds., Nature London, Volume 390: United Kingdom, Macmillan Journals : London, United Kingdom, p. 497.

Spero, H.J., Bijma, J., Lea, D.W., and Bernis, B.E., 1997. Effect of seawater carbonate concentration on foraminiferal carbon and oxygen isotopes: Nature, v. 390, p. 497-500.

Spero, H.J., 1998, Extracting surface ocean carbonate chemistry from the planktonic Foraminifera carbon isotope record, *in* Lea, D.W., and Bijma, J., eds., Eos, Transactions, American Geophysical Union, Volume 79: United States, American Geophysical Union : Washington, DC, United States, p. 444.

Steuber, T., Mitchell, S.F., Buhl, D., Gunter, G., and Kasper, H.U., 2002. Catastrophic extinction of Caribbean rudist bivalves at the Cretaceous-Tertiary boundary: Geology, v. 30, p. 999-1002.

Stille, P., Chaudhuri, S., Kharaka, Y.K., and Clauer, N., 1992. Neodymium, strontium, oxygen and hydrogen isotope compositions of waters in present and past oceans: Isotopic Signatures and Sedimentary Rocks, p. 389-410.

Stille, P., and Shields, G.A., 1997. Radiogenic isotope geochemistry of sedimentary and aquatic systems: Lecture Notes in Earth Science, v. 68.

Stoll, H.M., and Schrag, D.P., 2000. High-resolution stable isotope records from the upper cretaceous rocks of Italy and Spain: Glacial episodes in a greenshouse planet?: Bulletin of the Geological Society of America, v. 112, p. 308-319.

Tachikawa, K., Jeandel, C., and Roy-Barman, M., 1999. A new approach to the Nd residence time in the ocean: The role of atmospheric inputs: Earth and Planetary Science Letters, v. 170, p. 433-446.

Tarduno, J.A., Brinkman, D.B., Renne, P.R., Cottrell, R.D., Scher, H., and Castillo, P., 1998. Evidence for extreme climatic warmth from Late Cretaceous arctic vertebrates: Science, v. 282, p. 2241-2244.

Thomas, D.J., 2005, Reconstructing ancient deep-sea circulation patterns using the Nd isotopic composition of fossil fish debris, Special Paper - Geological Society of America, Volume 395: United States, Geological Society of America (GSA) : Boulder, CO, United States, p. 1.

Voigt, S., Gale, A.S., and Flügel, S., 2004. Midlatitude shelf seas in the Cenomanian-Turonian greenhouse world: Temperature evolution and North Atlantic circulation: Paleoceanography, v. 19, p. 1-17.

Wilson, P.A., and Opdyke, B.N., 1996. Equatorial sea-surface temperatures for the Maastrichtian revealed through remarkable preservation of metastable carbonate: Geology, v. 24, p. 555-558

Wagner, T., Herrle, J.O., Damsté, J.S., Schouten, S., Stüsser, I., and Hofmann, P., 2008. Rapid warming and salinity changes of Cretaceous surface waters in the subtropical north Atlantic: Geology, v. 36, p. 203-206.

Watkins, D.K., and Self-Trail, J.M., 2005. Calcareous nannofossil evidence for the existence of the Gulf Stream during the late Maastrichtian: Paleoceanography, v. 20, p. 1-9.

Woodruff, F., and Savin, S.M., 1989. Miocene deepwater oceanography: Paleoceanography, v. 4, p. 87-140.

CHAPTER 2

FORAMINIFERAL ASSEMBLAGE EVIDENCE FOR A WESTERN BOUNDARY CURRENT WITH SECULAR VARIATION AND SHORT TIME SCALE LATERAL MIGRATION DURING THE MAASTRICHTIAN (BLAKE NOSE, WESTERN NORTH ATLANTIC)

ABSTRACT

Maastrichtian foraminiferal assemblages at two Ocean Drilling Program (ODP) sites separated by ~ 40 km on Blake Nose (western North Atlantic) show similar temporal trends with consistent differences between correlative samples. Both sites show decreasing fine fraction $\delta^{18}O$ values upsection consistent with warming through the Maastrichtian. Also, at both sites the genera *Globotruncana* and *Heterohelix* dominate all assemblages (25%-70%). However, while their relative proportion change through time, in correlative samples *Globotruncana* spp. are more abundant and *Heterohelix* spp. are less abundant in the offshore, deeper Site (1050) than in the more inshore, shallower Site (1052). A number of other taxa show consistently higher relative abundances in either the nearshore (e.g., *Archeoglobigerina* spp.) or offshore (*Rugoglobigerina* spp.) site. Finally, both sites also exhibit short-term (decimeter to meter scale) variation that range from dramatic red-green color cycles in portions of Hole 1050C to subtle light-dark alteration in Hole 1052E that are paralleled by stable isotopic and foraminiferal changes. Combined with previously documented onshore-offshore trends among nannofossil taxa, these observations both confirm the presence of a well defined water mass boundary

(consistent with a well developed western boundary current) throughout the Maastrichtian North Atlantic and also allow its position to be mapped on long (million year) time scales and short (thousand years) time scales.

2.1. INTRODUCTION

Increasing levels of CO_2 in the atmosphere over the past century are believe have caused global warming, and the geologic record of greenhouse times provides a critical perspective on how the Earth system (atmosphere, biosphere, and hydrosphere) might respond to continued increases in atmospheric CO_2 levels. The ocean's role in distributing heat is an important part of the equation. In modern oceans, surface circulation is not symmetric about the center of ocean basins. Trade winds and the Coriolis effect result in relatively narrow, poleward flowing western boundary currents (e.g. the North Atlantic Gulf Stream) that are important engines for transporting tropical warmth poleward and separating water masses. What is poorly constrained is how western boundary currents behaved during greenhouse climates characterized by global warmth and reduced latitudinal thermal gradients.

Among past warm climates, the Maastrichtian (65.5-71.3 Ma) is an excellent interval to study because it has a relatively complete, accessible, and well-preserved stratigraphic record. Previous studies have documented several paleoceanographic (e.g, different temperatures among ocean basin, and changes in water column structure) and paleobiological changes (e.g, inoceramid bivalve extinction, rudist bivalves extinction, and diversity and abundance changes among planktic and benthic foraminifera) through the age (Johnson et al, 1996; Johnson and Kauffman, 1996; Kauffman and Hart, 1996;

MacLeod and Huber, 1996; Huber et al, 2002; Johnson, 2002; Steuber et al, 2002; Isaza-Londoño et al, 2006). The Maastrichtian was an interval bracketed by extremely warm climates earlier in the Late Cretaceous and in the Early Eocene (Barrera et al, 1987; Frank and Arthur, 1999; MacLeod and Huber, 2001). Even though the Maastrichtian exhibited typical greenhouse features, it has been recognized as a time of global cooling (Douglas and Savin, 1978; Boersma, 1981; Barrera et al, 1987; MacLeod and Huber, 2001; MacLeod et al, 2005) with pCO_2 levels two to three times higher than preindustrial values (Berner, 1994; Upchurch Jr, 1998; Berner and Kothavala, 2001). This estimate is within the ranges reported by the intergovernmental Panel on Climate Change (IPCC, 2008) of expected carbon dioxide concentrations by 2100.

This study addresses samples from two sites on Blake Nose in the subtropical North Atlantic (figure 2.1) for which two alternative models have been proposed to explain microfossil distribution and isotopic trends. The first model (regional forcing model) invokes changes in continental runoff and or/upwelling intensity (MacLeod et al, 2001), whereas the second model (local control model) invokes an onshore-offshore gradient and the development of a proto-Gulf Stream (Watkins and Self-Trail, 2005). By parallel examination of stable isotopic signals and abundance patterns in planktonic foraminifera throughout the Maastrichtian, we empirically evaluated these models and thus provide constraints on surface circulation in the region. If the observed patterns resulted from regional changes, then variation in planktonic foraminifera realm should show similar variations at both sites. On the other hand, if the observed patterns reflect the position of a site relative to the position of a water mass boundary, then the sites might exhibit different patterns with steep gradient between them.

2.2. AREA OF STUDY

Ocean Drilling Program (ODP) Leg 171b Holes 1050C (offshore) and 1052E (onshore) are located on the crest of Blake Nose (figure 2.1) which is a gently sloping topographic high that extends eastward from the Blake Plateau (MacLeod and Huber, 2001). The distance between the two sites is approximately 40 km. Modern water depths along Blake Nose range from 1000 m to 2700 m water depth. The sedimentary record at Blake Nose consists of Eocene carbonate ooze and chalk that overlies Paleocene claystone as well as Maastrichtian and upper Campanian chalk (Norris et al, 2001).

During Maastrichtian time Blake Nose was located at the northwestern boundary of the Tethys Seaway at a paleolatitude of ~30ºN. The Maastrichtian in the Blake Nose is represented by 75 m (Site 1050) and 185 m (Site 1052) sections that consist mostly of gray nannofossil ooze or chalk containing abundant well preserved foraminifera (Norris et al, 1998). Slumping locally disturbs the Maastrichtian sequence at both sites. These slumps have been attributed to a large-magnitude earthquake produced by the Chicxulub impact (Klaus et al, 2000; Norris et al, 2000). However, $^{87}Sr/^{86}Sr$ results and sedimentological observations (MacLeod et al, 2003) suggest that pelagic deposition punctuated by gravity flows during the Maastrichtian better explain the record at Blake Nose. The latter interpretation is supported an integrated bio-, magneto-, and chemostratigraphic study, which also provides the age models used in this study (Huber et al, 2008).

Site 1050 contains the most complete Campanian-Maastrichtian record at the Blake Nose, with a sedimentation rate of ~18m/m.y for most of the interval (Huber et al,

2008). At the offshore Site 1052, sedimentation rates during the Maastrichtian vary from 38 m/m.y (late Maastrichtian) to 50 m/m.y. (early Maastrichtian) (Huber et al, 2008). Major slumps occur during the early Maastrichtian at both sites and strontium analysis in Site 1052 suggested that the slumped material includes material older than the subjacent hemipelagic interval (MacLeod et al, 2003). These slumps add uncertainty to the age model. For example, Sr-based dates for the youngest sediment below the late Campanian/early Maastrichtian slump at Site 1052E would be 0.5 m.y. older than those ages estimated biostratigraphically, whereas the early Maastrichtian slump (470 meter below sea floor mbsf) in Hole 1050C could be up to 0.5 to 1.0 m.y. younger than those estimated from fossils (Huber et al, 2008). These complications notwithstanding, the Maastrichtian biostratigraphic sequence is still relatively complete and observations can be tied with confidence to relative age estimates.

During this research, high resolution Maastrichtian samples were examined from three roughly correlative levels at Sites 1050 and 1052. Biostratigraphically these sections are located within the *Abathomphalus mayaroensis* zone (late Maastrichtian: Hole 1050C section 13R-5 and Hole 1052E section 21R), near the top of the *Racemiguembelina fructicosa* zone (mid Maastrichtian: Hole 1050C section 16R-2 (after Macleod et al, 2001) and Hole 1052E section 26R), and in the top of the *Gansserina gansseri* zone (Hole 1050C section 18R-2 and Hole 1052E section 29R).

Sites 1050 and 1052 both show centimeter to meter-thick rhythmic alterations in color (chroma and hue according to Munsell scale) and magnetic susceptibility that likely represent ~20 Kyr Milankovitch precessional cycle but are variably expressed. They are

generally stronger at Site 1050 than Site 1052 (MacLeod et al, 2001). In section 1050C-16R-2, all three variables show high amplitude cyclic variations and the color sediments varies between red and green (figure 2.2). Detailed analysis of this section (MacLeod et al, 2001) suggests that the color (degree of saturation and hue) may reflect $\%CaCO_3$, and that magnetic susceptibility varies as a function of terrigenous input. Section 1050C-13R-5 exhibits moderate cyclicity in chroma, while changes in hue and magnetic susceptibility are minor (figure 2.2). Similarly, section 1050C-18R-2 presents moderate chroma cyclicity but values are more saturated than in 1050C-13R-5. However, opposite to patterns observed in sections 1050C-16R-2 and 1050C-13R-5 the small variation in hue in section 1050C-18R-2 shows redder hues associated with intervals of less saturated colors (figure 2.2).

Site 1052 represents half the paleodepth (Site 1052: middle bathyal (600m – 1000m); Site 1050: lower bathyal (1000m – 2000m)), and about twice the sedimentation rate of Site 1050 (Norris et al, 1998) implying more shoreward conditions with greater terrigenous input than Site 1050. Where present, cycles are less evident in Hole 1052E than in Hole 1050C, but chroma still shows significant variation that allows inferences about possible cyclic intervals. No significant change is observed in the magnetic susceptibility in any of the Hole 1052E sections, and moderate hue variability is only observed on the lowest section (1052E-29R) (figure 2.3). In addition, hue shows a trend toward green shades upsection through the Maastrichtian in Hole 1052E.

2.3. PREVIOUS WORK

Even though the Cretaceous/Tertiary (K/T) boundary has been the center of attention for most of Maastrichtian studies, recent research has recognized the importance of paleoceanographic and climatic changes several millions years before the boundary. Important differences among the climatic signatures of the ocean basins and significant coeval variations in the paleoceanographic and paleobiological record during this period have been observed. Extinction of deep-sea inoceramid bivalves (Kauffman, 1986; MacLeod, 1994; MacLeod and Huber, 1996) and tropical rudist bivalves (Johnson et al, 1996; Johnson and Kauffman, 1996, 2001; Steuber et al, 2002) occurred during the mid Maastrichtian at the same time as geochemical shifts in deep-sea biogenic carbonates and a possible cooling of surface waters (MacLeod and Huber, 1996; MacLeod and Bergen, 2004; Frank et al, 2005). Diverse data from Southern and Pacific Oceans support the idea of widespread cooling during the Maastrichtian (Barrera and Savin, 1999; Frank and Arthur, 1999; Francis and Poole, 2002; MacLeod and Bergen, 2004). However, at the same time, several lines of evidence (leaf physiognomy, foraminifera stable isotopes, and bulk carbonate isotopes) show warming in the North Atlantic and Tethys (Corfield and Norris, 1996; Barrera and Savin, 1999; Frank and Arthur, 1999; Isaza-Londoño et al, 2006).

Superimposed on the long-term Maastrichtian trends, the subtropical North Atlantic exhibits short term geochemical and paleobiological changes. In order to explain these variations two different models (MacLeod et al, 2001) have been developed. A regional forcing model was constructed based on high amplitude cycles

observed on the Blake Nose Hole 1050C core-section 16R-2 by MacLeod et al (2001), where correlative changes among foraminiferal populations, stable isotopic values of foraminifera, relative abundance of different minerals, and elemental abundances were observed (figure 2.4). The authors suggested that lighter colored (green) intervals were apparently deposited during times of relatively high productivity and relatively cool temperatures and contain higher relative abundances of *Heterohelix* spp. and *Globigerinelloides* spp. On the other hand, darker intervals (red) seemed to represent deposition during warm/low productivity intervals and contain high relative abundances of *Globotruncana* spp. and *Pseudoguembelina* spp. In order to explain the variations the authors invoked regional changes in continental runoff and/or upwelling intensity.

Addressing geographic trends, Watkins and Self-Trail (2005) analyzed upper Maastrichtian calcareous nannofossil assemblages from continental/onshore sites (eight cores in the South Carolina coastal plain) and ocean/offshore sites (Blake Nose Holes 1050C and 1052E and mid Atlantic ridge deep sea drilling project (DSDP) site 10). Based on correlation and principal component analysis applied to the data set, and temperature index derived from published paleobiogeographic information, they found a strong separation of the samples into onshore and offshore sets, with the latter inferred to represent significantly warmer temperatures. They proposed the presence of a local, stable proto-Gulf Stream during the Maastrichtian as a plausible explanation for their results.

It is clear that the Maastrichtian exhibited differences among sites and through time. The models (regional/local) invoked though, have quite different implications for

North Atlantic oceanography. Therefore, testing the models during this greenhouse interval could be important for our understanding of greenhouse oceans. If the regional forcing model is correct, temporal variability should be expressed in similar ways in both sites. In contrast, if the local model is correct, then the occurrence of a western boundary current (WBC) will generate a temperature contrast in the subtropical North Atlantic similar to what we see in the modern Gulf Stream. Therefore, conditions and foraminifera assemblages at each site will be strongly influenced by their position relative to the WBC and steep gradients might exist between sites.

2.4. MATERIALS AND METHODS

High resolution samples representing a portion of the early, middle and late Maastrichtian at Holes 1050C and 1052E were examined for this project. We analyzed 162 samples for stable isotopes (fine fraction, and individual species) and foraminifera abundances (appendix 1). Coring gaps and sedimentological complications (e.g. slumps) prevent precise correlation among individual samples or suites of samples (e.g. Huber et al, 2008), yet this uncertainty does not compromise our ability to compare patterns within and between sites. Sample spacing and size was based on identification of possible peak intervals from visual analysis of the correlation between chroma and magnetic susceptibility.

Bulk samples were dried (50°C), weighed, and disaggregated using kerosene and a mild soap solution before being washed on a 63 μm sieve (after MacLeod and Orr, 1993). The wash water with the < 63 μm fraction was collected and allowed to settle before being decanted. The coarse fraction (> 63 μm) was sonicated in distilled water and

methanol to remove any adhering fine particles and then decanted. All separates were dried (<50°C) and weighed.

Foraminifera abundances were counted for a total of 65 samples. For each sample the >63μm fraction was dried and sieved on a 125 μm screen (sometimes this residue was sonicated and dried again in order to acquire better sample quality). This fraction was divided using a sediment microsplitter until a separate containing approximately 300 to 500 foraminifera remained. The sample was spread on a gridded picking tray and all individuals were counted and glued to a micropaleontological slide as an archive. Counts from Hole 1050C section 16R-2 are from MacLeod et al (2001).

The < 63 μm fraction from 162 samples were analyzed for $\delta^{18}O$ and $\delta^{13}C$ stable isotopes. In addition, foraminifera from 21 samples in Hole 1050C section 13R-5 were selected for species specific isotope analysis. Because isotopic signatures of planktonic forams can vary as a function of size, a consistent size interval was picked, and different numbers of individuals per species were analyzed for each taxon. Planktics: *Globigerinelloides subcarinatus* and *Heterohelix globulosa* (~15 individuals per sample); *Rugoglobigerina rugosa* and *Pseudoguembelina palpebra* (3 individuals per sample); Benthics: *Gavellinella beccariformis* and *Nutalloides truempyi* (3-5 individuals per sample).

Samples for isotope analysis were reacted with three drops of 100% phosphoric acid at 70ºC in a Kiel III carbonate device. The $\delta^{13}C$ and $\delta^{18}O$ values of the resultant CO_2 were measured online in a Thermo Finnegan Delta Plus mass spectrometer in the Biogeochemistry Isotope Laboratory at the University of Missouri, Columbia. Results

are expressed in δ-notation relative to the Vienna Pee Dee Belemnite standard (V-PDB). The mass spectrometer was calibrated for each run based on the average of multiple analyses of NBS-19 standard. The precision of the instrument for this study was <0.03‰ and <0.05‰ for $\delta^{13}C$ and $\delta^{18}O$ values, respectively (1σ, standard deviation).

2.5. RESULTS

2.5.1. STABLE ISOTOPES

Approximately 189 species-specific isotope analyses were conducted on section 13R-5 Hole 1050C (appendix 1). Relative to previous results from section 16R-2 in Hole 1050C (figure 2.4) both the color and isotopic variability are greatly subdued in Hole 1050C-13R-5. However, sediment color and isotopic values generally seem to co-vary. Benthic and planktic foraminifera show relatively small cyclic variation for $\delta^{13}C$ and $\delta^{18}O$ values. Cyclicity within the $\delta^{18}O$ values is more evident for *G. subcarinatus*, *H. globulosa* and *R. rugosa*, while benthic foraminifera and *P. palpebra* show no apparent cyclicity. Lighter color (shifts to the right in the color bar) intervals are associated with higher $\delta^{18}O$ values (relatively cool time), while darker color (shifts to the left in the color bar) intervals are associated with lower $\delta^{18}O$ values (times of relative warmth). The difference in $\delta^{18}O$ of almost ~0.7‰ in *G. subcarinatus* suggests temperature changes across the cycles of up to 3°C (figure 2.5).

In general, low variability in $\delta^{13}C$ values characterizes all the samples. *P. palpebra* shows quite high variability in $\delta^{13}C$ values, while subtle cyclicity is observed on the fine fraction and the rest of the foraminifera species. The *P. palpebra* results likely reflect

high variability between individuals that is not averaged out due to the small number of individuals per analysis (figure 2.5).

At the other four intervals studied (Hole 1050C-18R, Hole 1052E-21R, Hole 1052E-26R, and Hole 1052E-29R), only fine fraction isotopic data have been generated. With the exception of the highest interval in Hole 1052E (core 21R), $\delta^{18}O$ values seem to track variability in chroma (figure 2.6, 2.7). Variability in each Hole (1050C and 1052E) and within each section (Hole 1050C-13R-5, Hole 1050C-18R-2, Hole 1052E-21R, Hole 1052E-26R, and Hole 1052E-29R) is proportional to the amplitude of the color cycles. Variability on Hole 1050C's sections is generally about 0.7‰, and variability on Hole 1052E's sections about 0.3‰. In both Hole 1050C and Hole 1052E there is a long-term $\delta^{18}O$ negative shift throughout the Maastrichtian (figure 2.6, 2.7). However, there is a consistent offset in $\delta^{18}O$ values between sites, with signatures in the onshore Hole (1052E) ~0.25‰ lower than in correlative samples in Hole 1050C. Carbon isotopes values of the fine sediments are similar at both sites and maintain a general value of about 2.25‰ throughout the Maastrichtian (figure 2.6, 2.7).

2.5.2. FORAMINIFERA ABUNDANCES

Approximately 16500 planktic individuals distributed among forty-nine species were identified (appendix 1). Faunal abundance at both sites is dominated by species of *Heterohelix* and *Globotruncana*. A number of other taxa show consistently higher relative abundances in either the nearshore site (e.g., *Archeoglobigerina* spp.) or offshore site (*Rugoglobigerina* spp). In addition, changes in distribution and percentages are observed between sites and through the sections (figure 2.6, and figure 2.7).

Cyclic changes in foraminifera abundances associated with chroma variability are observed in all sections in Hole 1050C (figure 2.6). For the most part, *Heterohelix* spp. peak abundances are associated with lighter colored intervals which, by analogy to core 16R-2 in Hole 1050C (MacLeod et al, 2001) represent relative carbonate rich intervals. *Globotruncana* spp. are more prominent on the darker intervals, presumably less carbonate rich intervals. Unlike results in site 1050, none of the sections in Hole 1052E show any apparent cyclicity within the faunal abundances (figure 2.7).

Differences through time in the relative abundances of the dominant species are also observed in Hole 1050C. Section 18R-2 (early Maastrichtian) assemblage is strongly dominated by *Globotruncana* spp. (averaging 70%), followed by *Heterohelix* spp. (15%), and the remaining 15% is distributed among the rest of the taxa (figure 2.6, appendix 1). Species abundances from MacLeod and Huber (2001) show that *Heterohelix* spp. make up approximately 40% of the population in the mid Maastrichtian samples (16R-2), followed by *Globotruncana* spp. with a 25% (figure 2.6). Faunal abundance in late Maastrichtian samples (13R-5) is co-dominated by *Globotruncana* (35%) and *Heterohelix* (35%) with the remaining 30% of the population represented by a number of relatively evenly distributed taxa (figure 2.6) including a number of taxa whose first appearance in the region occurs during the late Maastrichtian (MacLeod et al, 2001).

Results from Hole 1052E show a long trend through time towards increasing dominance by *Heterohelix* spp.. Faunal abundance in the early Maastrichtian section (29R) is comprised of ~45% *Globotruncana* spp., followed by ~30% of *Heterohelix* spp., and 9% of *Archeoglobigerina* (figure 2.7). The mid Maastrichtian section (26R) is

dominated by *Heterohelix* spp. making up 40% of the population, followed by *Globotruncana* spp. with 25% and *Archeoglobigerina* spp. with 7% (figure 2.7). Finally, late Maastrichtian population percentages in section 21R are 55% and 25% for *Heterohelix* spp. and *Globotruncana* spp., respectively. Deviations in these percentages are observed throughout but no apparent cyclicity is observed (figure 2.7).

2.6. DISCUSSION

Through parallel examination of planktonic foraminifera assemblages data from the studied intervals in the Maastrichtian ODP Sites1050 and 1052, we can empirically test the regional climate model (MacLeod et al, 2001) and the local water mass model (Watkins and Self-Trail, 2005). If the cyclicity observed in 1050C is the result of regional forcing, foraminifera assemblages in Hole 1052E should change more or less in parallel to what is observed in Hole 1050C. On the other hand, if the local water mass model is correct the position of a western boundary current (WBC) should be evident in the foraminifera distribution when comparing sites. Assuming that an ecological gradient is generated by the WBC that acts in similar ways to the modern Gulf Stream, then the onshore Hole (1052E) should present faunal characteristics typical of the green/cooler intervals (after MacLeod et al, 2001) including dominance by *Heterohelix* spp. On the contrary, the offshore Hole (1050C) should exhibit faunal characteristic typical of the red/warmer intervals and show higher relative abundance of *Globotruncana* spp.

Results for early Maastrichtian samples show clear differences between the sites. Offshore section 1050C-18R-2 is strongly dominated by *Globotruncana* spp. and exhibits relatively weak cyclicity associated with chroma (figure 2.6). By comparison,

foraminifera populations in onshore section 1052E-29-R is slightly dominated by *Globotruncana* spp. followed by *Heterohelix* spp. Note, though, that in this interval *Globotruncana* spp. reach their highest abundance in Hole 1052E samples studied. Further, this interval is the only interval at Site 1052 that shows any suggestion of cyclic variations in relative abundances (figure 2.7), and stable isotopes results show that *Globotruncana* spp. are more abundant in the potentially warmer and dark part of the cycles. Under the regional-forcing model, these conditions would represent a time of generally warmer waters and little upwelling, but the steep faunal gradient between the sites is difficult to explain. Under the local control model, both sites show *Globotruncana* spp. (an hypothesized offshore indicator) has relatively high abundance. Therefore, during deposition of these samples the position of the WBC would be close to or inboard of the onshore site.

Mid Maastrichtian section 16R-2 from Hole 1050C was studied in detail by MacLeod et al (2001) where a high degree of cyclicity is observed in the foraminifera populations and isotopic data (figure 2.4). The corresponding section (1052E-26R) in the onshore site shows possible cyclicity in chroma; but no significant variability is observed within the foraminifera population or fine fraction isotopic values. Comparing the mid-Maastrichtian sites shows higher relative abundances of *Heterohelix* spp. in most samples than in the early Maastrichtian intervals. Cyclicity is only prominent in the offshore site. Whereas the average increase in *Heterohelix* spp. relative abundances is similar between the sites, lack of cyclicity in Hole 1052E paired with dramatic cyclicity in Hole 1050C is inconsistent with the regional forcing model. Under the local control model the differences among the sites would be explained by having the WBC close to the offshore

site, with the strong cyclicity in section 1050C-16R-2 explained by short term migrations across the position of Site 1050.

In the late Maastrichtian samples, *Globotruncana* spp. again are more abundant in the offshore site than the onshore site, whereas *Heterohelix* spp. reach their highest relative abundance in the late Maastrichtian sample suite at Site 1052. Cyclicity is again observed only in the offshore section 1050C-13R-5. The abundances of *Heterohelix* spp. and *Globotruncana* spp. and the $\delta^{18}O$ values of several planktic foraminifera show cyclic variations that track dark-light color cycles in the section (figure 2.5). However, the magnitude of these variations is lower in core-section 1050C-13R-5 (low amplitude color cycles) than in core-section 1050C-16R-2 (high amplitude cycles). As expected, *Heterohelix* spp. are relatively abundant in the light intervals and *Globotruncana* spp. are relatively abundant in the dark intervals. In addition, $\delta^{18}O$ values of *G. subcarinatus*, *H. globulosa* and *R. rugosa* all suggest that paleotemperatures were relatively cool in the light color intervals and relatively warm in the darker intervals, confirming paleoecological observations from MacLeod et al (2001). As above, though the differences between sites do not match simple predictions of the regional forcing model, but can be explained by the local control model if the WBC was between the two sites.

Given the small horizontal distance separating the two sites (~40 Km), they show remarkable and consistent differences including steep faunal gradients throughout the ~6 million years of the Maastrichtian interval. Specifically, in correlative samples, *Globotruncana* spp. are consistently more abundant in the offshore than the onshore site whereas *Heterohelix* spp. are more abundant at the onshore site. Cyclicity is always more

strongly expressed in the offshore site. All combined, these observations favor a local control model where the contemporary position of a WBC explains well most aspects of the data set with short time lateral migration controlling the cyclicity.

During the early Maastrichtian, we suggest that this WBC was located towards the onshore Site (1052) (figure 2.8) and variation in the abundances of *Globotruncana* spp. and *Heterohelix* spp. are explained by short time-scale lateral migrations of the current. In contrast, Site 1050 was always on the ocean side of the WBC explaining during this same time, which explains the dominance of *Globotruncana* spp. (figure 2.8). During the mid-Maastrichtian, the WBC was apparently close to Site 1050 (figure 2.8), and dramatic cyclicity is explained by a sharp WBC with short time-scale lateral migration of the water mass boundary across Site 1050. When Site 1050 was on the ocean side of the boundary, the sediment deposited was characteristic of the red cycles (warm/high abundance of *Globotruncana* spp.). When this water mass boundary migrates oceanward, Site 1050 was on the continent side and green cycles (cooler/high abundance of *Heterohelix* spp.) were deposited. There is no correlative cyclicity at Site 1052 because it was on the onshore side of the boundary (figure 2.8). Finally for the late Maastrichtian, the western boundary current would have been located between the two sites explaining not only the lower magnitude of cyclicity and the lack of difference in the abundance between *Globotruncana* spp. or *Heterohelix* spp. at the offshore Site 1050 but also the high dominance of *Heterohelix* spp. in onshore samples from Site 1052 (figure 2.8).

What is not explained entirely by the local control model are trends throughout the Maastrichtian. For example, the degree of dominance by *Heterohelix* spp. on the proposed shoreward side of the water mass boundary varies through time. In addition, a number of new taxa first appear in the late Maastrichtian (MacLeod et al, 2001) (appendix 1). Based on differences among isotopic signatures of fine sediments and on species specific planktonic foraminifera isotope data from Site 1050C sections 13R-5 and 16R-2, we inferred a long term warming trend evidenced by a negative excursion of approximately 1.5‰ on $\delta^{18}O$ values at site 1050C that correspond to an increase of temperature of ~6°C over the Maastrichtian (MacLeod et al, 2005., Isaza-Londoño et al, 2006). We believe these changes reflect long-term evolution of global climate and North Atlantic circulation patterns (Chapter 3, and Chapter 4). Yet, throughout the Maastrichtian a strong gradient existed between Sites 1052 and 1050 supporting the presence of a relatively sharp water mass boundary.

2.7. CONCLUSIONS

Foraminifera population dynamics from this study demonstrate the evolution and development of a well established WBC throughout the Maastrichtian. In addition, this current migrated laterally both on long and short term scales. The presence of a WBC provides a new line of evidence that can be added to the numerous intriguing observations for the North Atlantic ocean during the Maastrichtian and raises questions regarding ocean circulation during the Late Cretaceous. Given the importance of the modern Gulf Stream in the North Atlantic Ocean, findings from this research establishing evidence of a similar feature, a WBC, back in the Maastrichtian and constraining such

surface circulation patterns are key to improving our understanding of the climate dynamics during greenhouse intervals.

REFERENCES

Barrera, E., Huber, B.T., Savin, S.M., and Webb, P.N., 1987. Antarctic marine temperatures: late Campanian through early Paleocene: Paleoceanography, v. 2, p. 21-47.

Barrera, E., and Savin, S.M., 1999. Evolution of late Campanian-Maastrichtian marine climates and oceans: Evolution of the Cretaceous Ocean-Climate System, v. 332, p. 245-282.

Berner, R.A., 1994. GEOCARB II: a revised model of atmospheric CO_2 over Phanerozoic time: American Journal of Science, v. 294, p. 56-91.

Berner, R.A., and Kothavala, Z., 2001. Geocarb III: A Revised Model of Atmospheric CO_2 over Phanerozoic Time: Am J Sci, v. 301, p. 182-204.

Boersma, A., 1981, Oxygen- and carbon-isotope variations and planktonic-foraminifer depth habitats, Late Cretaceous to Paleocene, central Pacific, Deep Sea Drilling Project sites 463 and 465, *in* Shackleton, N.J., ed., Initial Reports of the Deep Sea Drilling Project, Volume 62: United States, Texas A & M University, Ocean Drilling Program : College Station, TX, United States, p. 513.

Corfield, R.M., and Norris, R.D., 1996, Deep water circulation in the Paleocene Ocean, Geological Society Special Publication, p. 443-456

Douglas, R.G., and Savin, S.M., 1978. Oxygen isotopic evidence for the depth stratification of tertiary and cretaceous planktic foraminifera: Marine Micropaleontology, v. 3, p. 175-196.

Francis, J.E., and Poole, I., 2002. Cretaceous and early Tertiary climates of Antarctica: Evidence from fossil wood: Palaeogeography, Palaeoclimatology, Palaeoecology, v. 182, p. 47-64.

Frank, T.D., and Arthur, M.A., 1999, Tectonic forcings of Maastrichtian ocean-climate evolution, *in* Arthur, M.A., ed., Paleoceanography, Volume 14: United States, American Geophysical Union : Washington, DC, United States, p. 103.

Frank, T.D., Brown, P.R., Jones, K., Lees, J.A., Thomas, D.J., Leckie, R.M., and Arthur, M.A., 2005. The Maastrichtian record from Shatsky Rise (northwest Pacific): A tropical perspective on global ecological and oceanographic changes: Paleoceanography, v. 20, p. 1-14.

Huber, B.T., Norris, R.D., and MacLeod, K.G., 2002. Deep-sea paleotemperature record of extreme warmth during the Cretaceous: Geology, v. 30, p. 123-126.

Huber, B.T., MacLeod, K.G., and Tur, N.A., 2008. Chronostratigraphic Framework For Upper Campanian-Maastrichtian Sediments On The Blake Nose (Subtropical North Atlantic): Journal of Foraminiferal Research, v. 38, p. 162-182.

IPCC, 2008. Climate Change 2007: The Physical Science Basis: Contribution of Working Group I to the Fourth Assessment Report of the Intergovernmental Panel on Climate Change [Solomon, S., D. Qin, M. Manning, Z. Chen, M. Marquis, K.B. Averyt, M. Tignor and H.L. Miller (eds.)]. Cambridge University Press, Cambridge, United Kingdom and New York, NY, USA, 996 pp.

Isaza-Londoño, C., MacLeod, K.G., and Huber, B.T., 2006. Maastrichtian North Atlantic warming, increasing stratification, and foraminiferal paleobiology at three timescales: Paleoceanography, 21, PA1012, doi:10.1029/2004PA001130.

Johnson, C.C., Barron, E.J., Kauffman, E.G., Arthur, M.A., Fawcett, P.J., and Yasuda, M.K., 1996. Middle cretaceous reef collapse linked to ocean heat transport: Geology, v. 24, p. 376-380.

Johnson, C.C., and Kauffman, E.G., 1996. Maastrichtian extinction patterns of Caribbean province rudistids: Cretaceous-Tertiary Mass Extinctions: Biotic and Environmental Changes, p. 231-273.

—, 2001. Cretaceous evolution of reef ecosystems; a regional synthesis of the caribbean tropics: Topics in Geobiology, v. 17, p. 311-349.

Johnson, C.C., 2002. The rise and fall of rudist reefs: Reefs of the dinosaur era were dominated not by corals but by odd mollusks, which died off at the end of the cretaceous from causes yet to be discovered: American Scientist, v. 90, p. 148-153.

Kauffman, E.G., 1986. High-resolution event stratigraphy: regional and global Cretaceous bio-events: Global bio-events. Proc. 1st meeting of the IGCP Project 216, p. 279-335.

Kauffman, E.G., and Hart, M.B., 1996. Cretaceous bio-events: Global Events and Event Stratigraphy in the Phanerozoic, p. 285-312.

Klaus, A., Norris, R.D., Kroon, D., and Smit, J., 2000. Impact-induced mass wasting at the K-T boundary: Blake Nose, western North Atlantic: Geology, v. 28, p. 319-322.

MacLeod, K.G., and Orr, W.N., 1993. The Taphonomy of Maastrichtian Inoceramids in the Basque Region of France and Spain and the Pattern of their Decline and Disappearance: Paleobiology, v. 19, p. 235-250.

MacLeod, K.G., 1994. Bioturbation, inoceramid extinction, and mid-Maastrichtian ecological change: Geology, v. 22, p. 139-142.

MacLeod, K.G., and Huber, B.T., 1996. Reorganization of deep ocean circulation accompanying a late Cretaceous extinction event: Nature, v. 380, p. 422-425.

—, 2001. The Maastrichtian record at Blake Nose (western North Atlantic) and implications for global palaeoceanographic and biotic changes: Geological Society Special Publication, p. 111-130.

MacLeod, K.G., Kucera, M., Huber, B.T., Pletsch, T., and Röhl, U., 2001. Maastrichtian foraminiferal and paleoceanographic changes on Milankovitch timescales: Paleoceanography, v. 16, p. 133-154.

MacLeod, K.G., Fullagar, P.D., and Huber, B.T., 2003. $^{87}Sr/^{86}Sr$ test of the degree of impact-induced slope failure in the Maastrichtian of the western North Atlantic: Geology, v. 31, p. 311-314.

MacLeod, K.G., and Bergen, J.A., 2004. Apparent cooling in the tropical Pacific during the Maastrichtian and diagenetic artifacts in Late Cretaceous stable isotopic trends in bulk carbonate from Ontong Java plateau: Proceedings of the Ocean Drilling Program, v. 192, p. 1-15.

MacLeod, K.G., Huber, B.T., and Isaza-Londoño, C., 2005. North Atlantic warming during global cooling at the end of the Cretaceous: Geology, v. 33, p. 437-440.

Norris, R.D., Kroon, D., Klaus, A., et al., 1998. Proceedings of the Ocean drilling program, initial reports, 171B, Ocean Drilling program, College Station, TX.

Norris, R.D., Firth, J., Blusztajn, J.S., and Rivizza, G., 2000. Mass failure of the North Atlantic margin triggered by the cretaceous-Paleogene bolide impact: Geology, v. 28, p. 1119-1122.

Norris, R.D., Kroon, D., and Klaus, A., 2001. Introduction: Cretaceous-Paleogene Climatic Evolution of the Western North Atlantic. Results from ODP Leg 171B, Blake Nose: Proceedings of the Ocean Drilling Program, p. 1-10.

Steuber, T., Mitchell, S.F., Buhl, D., Gunter, G., and Kasper, H.U., 2002. Catastrophic extinction of Caribbean rudist bivalves at the Cretaceous-Tertiary boundary: Geology, v. 30, p. 999-1002.

Upchurch Jr, G.R., 1998. Vegetation-atmosphere interactions and their role in global warming during the latest Cretaceous: Philosophical Transactions of the Royal Society B: Biological Sciences, v. 353, p. 97-112.

Watkins, D.K., and Self-Trail, J.M., 2005. Calcareous nannofossil evidence for the existence of the Gulf Stream during the late Maastrichtian: Paleoceanography, v. 20, p. 1-9.

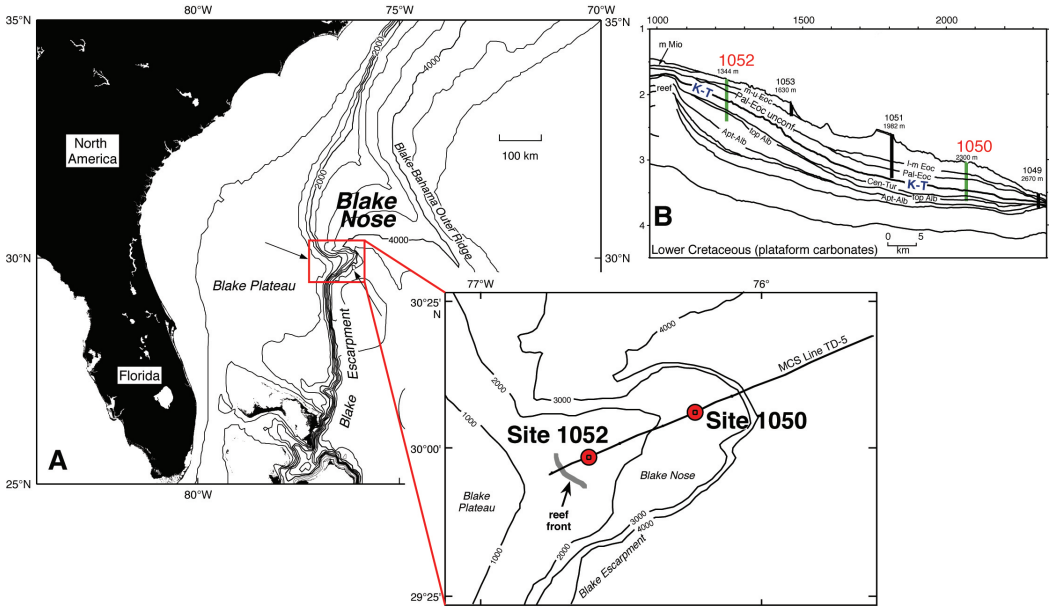

Figure 2.1. A) Location of Blake Nose with position relative to southeastern North America. Inset shows the seismic line with the drilling site (bathymetry is in meters) B) Schematic interpretation of MCS Line TD-5 showing major reflectors, their interpreted ages, and locations of Leg 171B sites. (Modified from Norris et al, 1998)

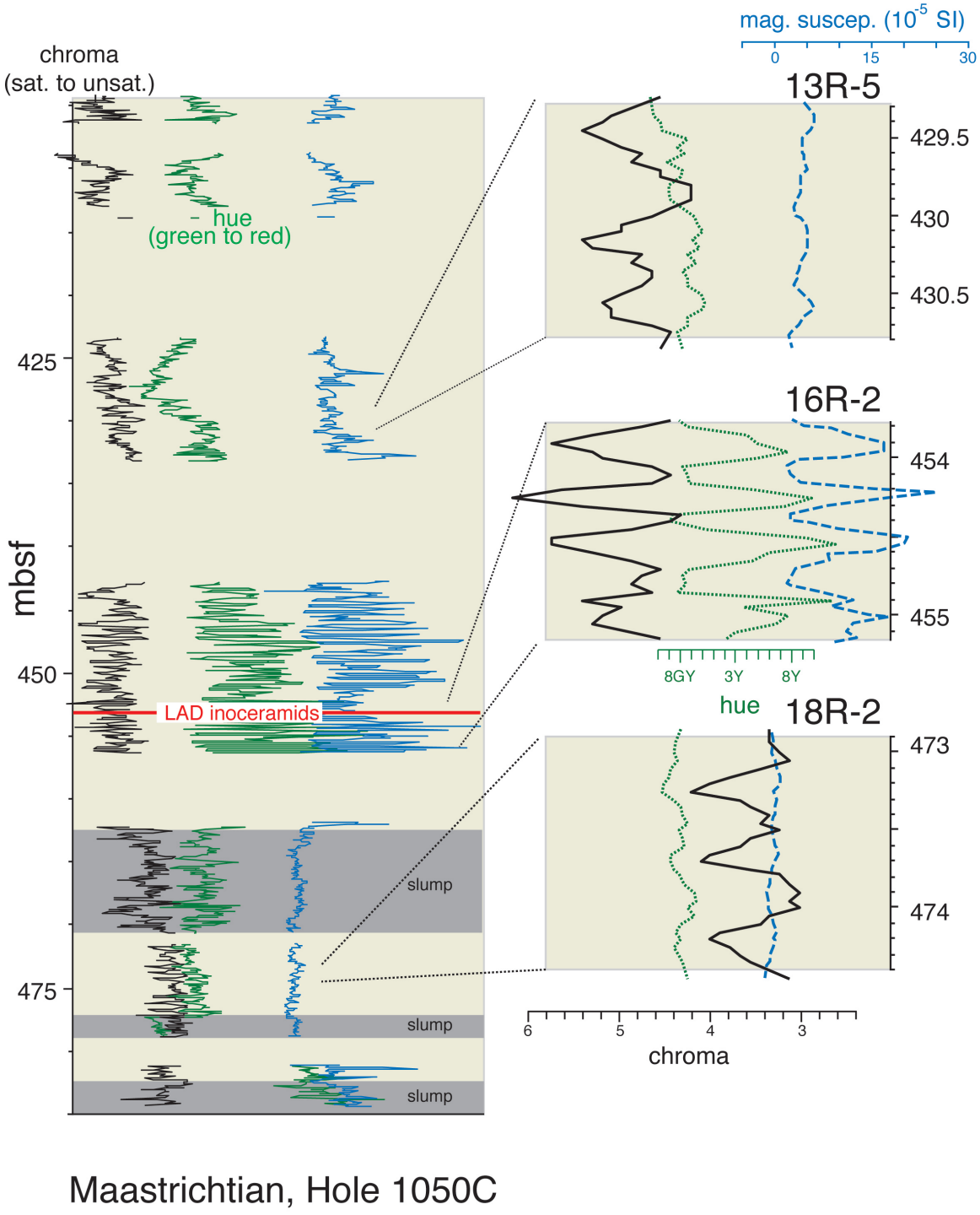

Figure 2.2. Shipboard color (Munsell chroma and hue) and magnetic susceptibility data plotted against depth for the Maastrichtian in Hole 1050C. Enlargements show nature of cyclic alternations and the study intervals from this site.

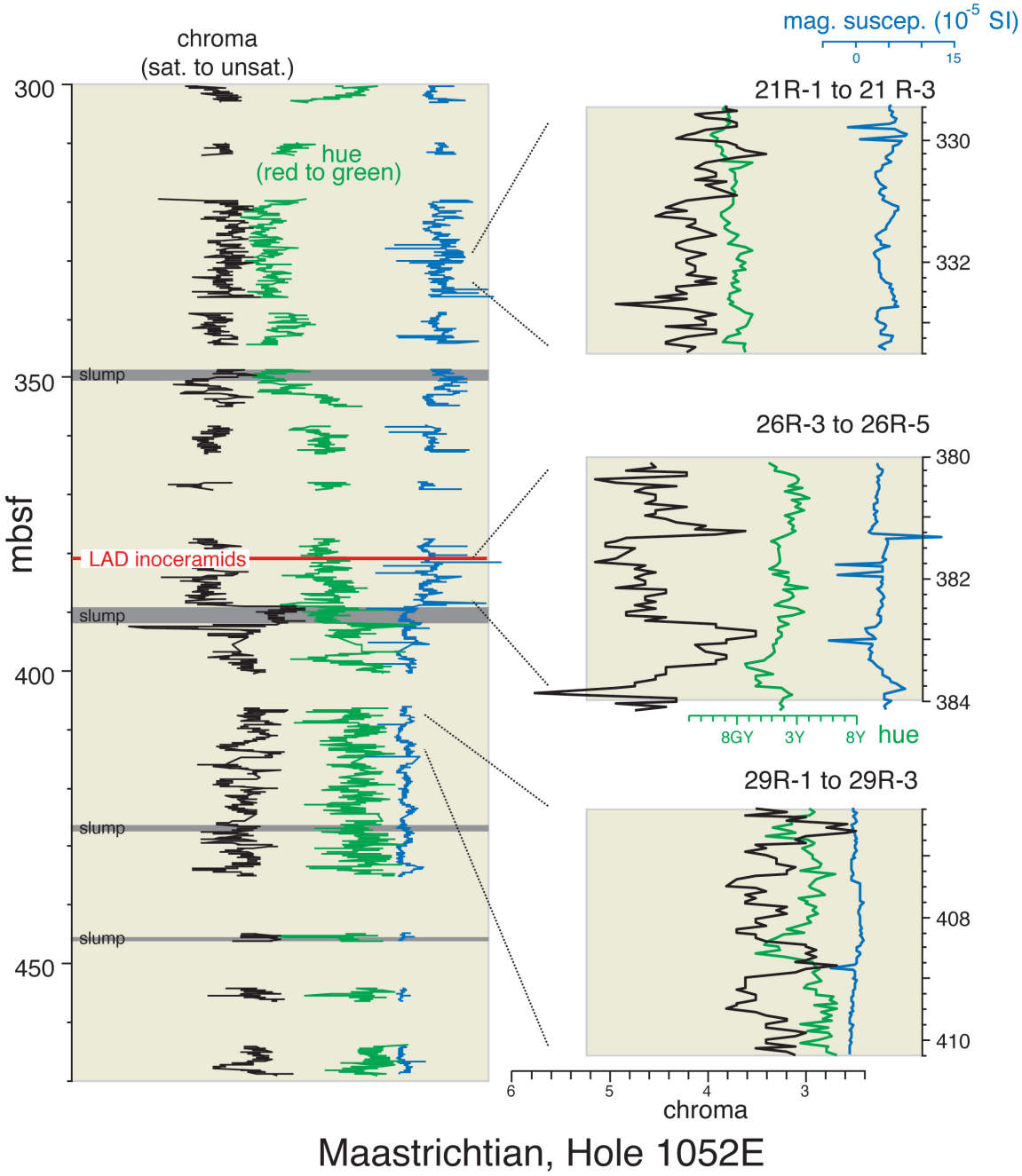

Figure 2.3. Shipboard color (Munsell chroma and hue) and magnetic susceptibility data plotted against depth for the Maastrichtian in Hole 1052E. Enlargements show nature of cyclic alternations and the study intervals from this site.

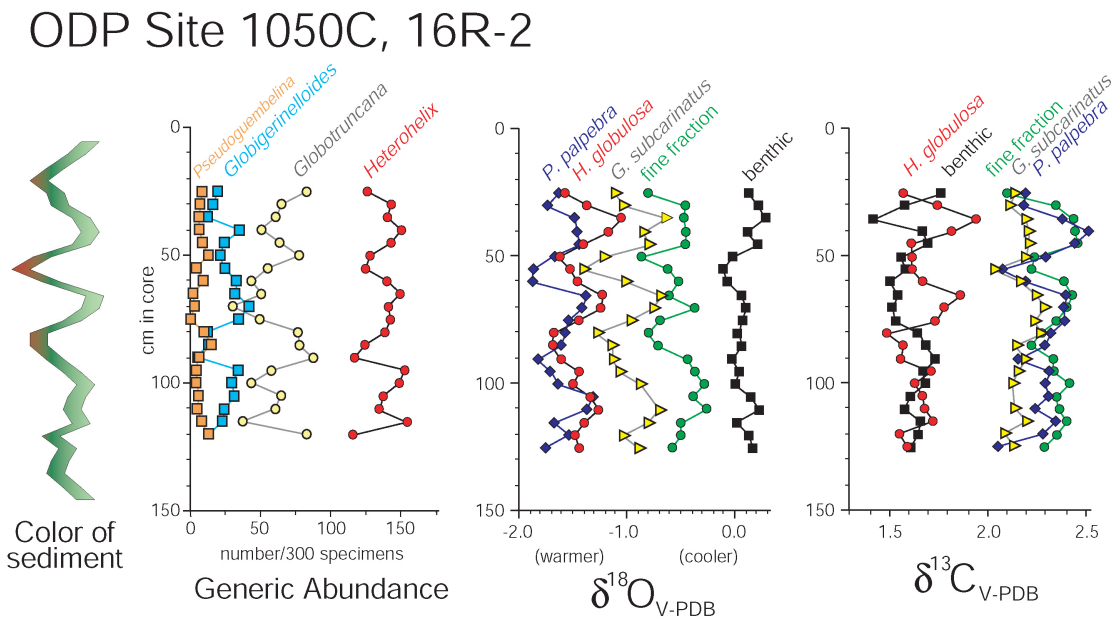

Figure 2.4. Variations of color, geochemical, and foraminifera abundances across mid Maastrichtian interval 16R-2, at site 1050C. (MacLeod et al, 2001)

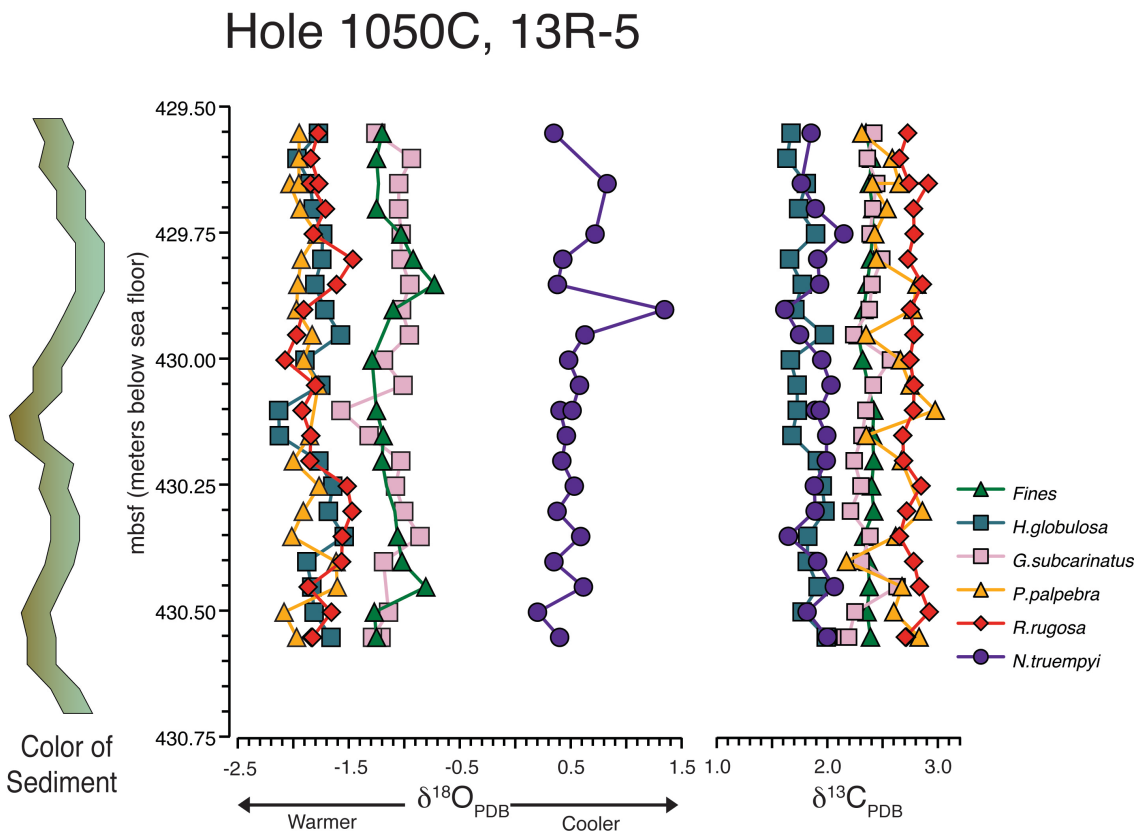

Figure 2.5. Sediment color variation and stable $\delta^{13}C$ and $\delta^{18}O$ isotopes for fine fraction, and selected planktonic and benthic foraminifera for late Maastrichtian interval at site 1050C.

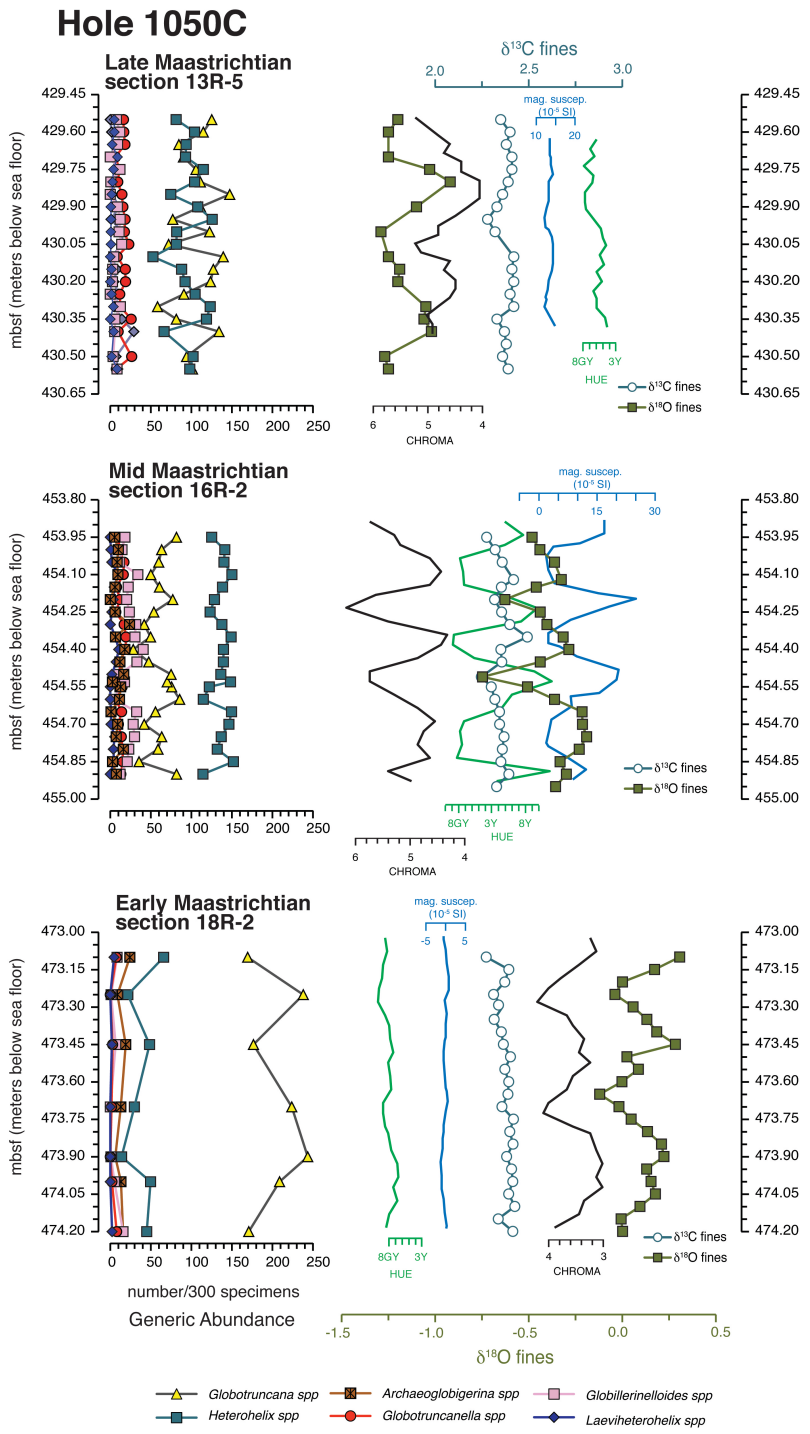

Figure 2.6. Foraminifera population assemblages, Munsell (chroma and hue) and Magnetic susceptibility, and fine fraction stable $\delta^{18}O$ and $\delta^{13}C$ isotopes, from early Maastrichtian to late Maastrichtian intervals at site 1050C.

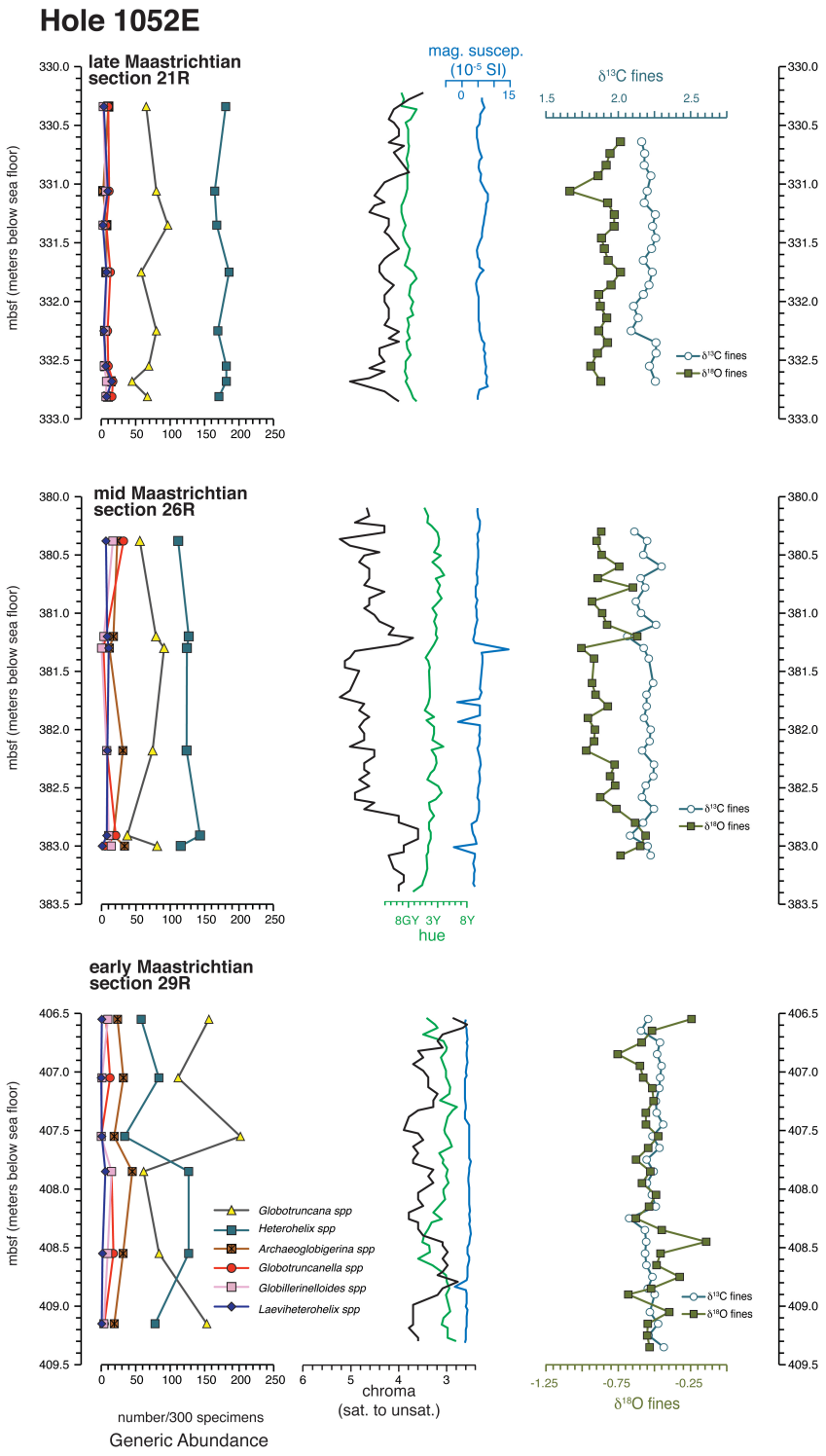

Figure 2.7. Foraminifera population assemblages, Munsell (chroma and hue) and Magnetic susceptibility, and fine fraction stable $\delta^{18}O$ and $\delta^{13}C$ isotopes, from early Maastrichtian to late Maastrichtian intervals at site 1052E.

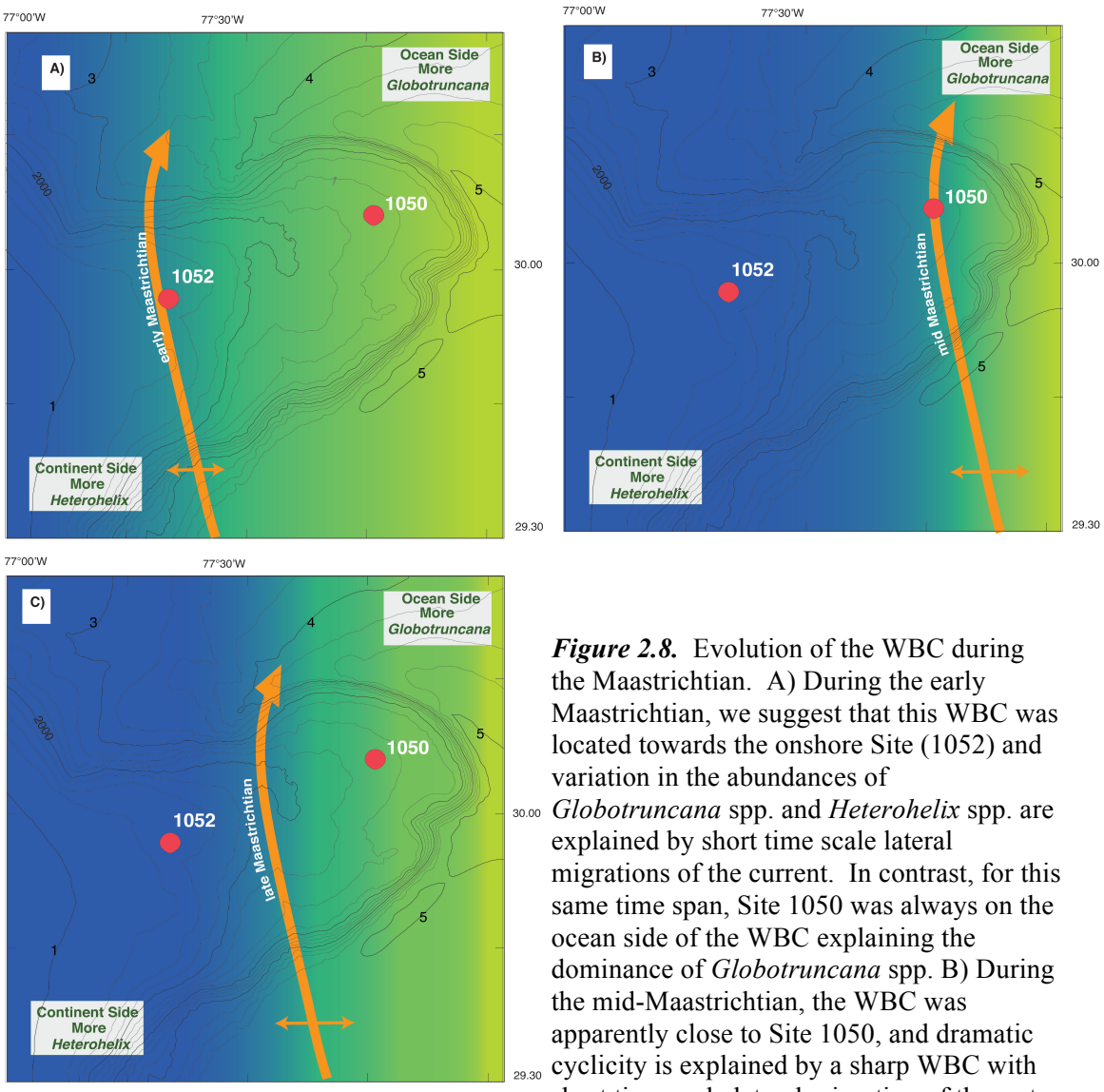

Figure 2.8. Evolution of the WBC during the Maastrichtian. A) During the early Maastrichtian, we suggest that this WBC was located towards the onshore Site (1052) and variation in the abundances of *Globotruncana* spp. and *Heterohelix* spp. are explained by short time scale lateral migrations of the current. In contrast, for this same time span, Site 1050 was always on the ocean side of the WBC explaining the dominance of *Globotruncana* spp. B) During the mid-Maastrichtian, the WBC was apparently close to Site 1050, and dramatic cyclicity is explained by a sharp WBC with short time scale lateral migration of the water mass boundary. C) Late Maastrichtian, the western boundary current would have been located between the two sites explaining not only the lower magnitude of cyclicity and the lack of difference in the abundance between *Globotruncana* spp. or *Heterohelix* spp. on the offshore Site 1050 but also the high dominance of *Heterohelix* spp. on onshore samples in Site 1052.

CHAPTER 3

DEEP TO SHALLOW MAASTRICHTIAN TIME TRANSGRESSIVE SHIFT IN THE SOURCE OF BOTTOM WATERS ON DEMERARA RISE INFERRED FROM NEODYMIUM ISOTOPES IN FISH DEBRIS

ABSTRACT

Between the early Maastrichtian and mid Danian, $\varepsilon_{Nd(t)}$ values of fish debris from three sites on Demerara Rise shift by ~6 units from -17 to -11. Extremely low values during the early Maastrichtian are similar to most other Late Cretaceous values for Demerara Rise and suggest intermediate to deep water formation in the tropical North Atlantic. The shift that begins in the Maastrichtian is gradual within the sites, is diachronous among the sites, and provides the most direct evidence yet presented for reorganization of ocean circulation patterns during the Maastrichtian. Although results are only from one region, the ε_{Nd} pattern is consistent with previous suggestions that mid Maastrichtian paleontological and paleoclimate shifts are related to initiation or intensification of deep water formation at high latitudes.

3.1. INTRODUCTION

The Late Cretaceous is well established as a greenhouse climate interval with a rich sedimentological archive that allows us to acquire a high resolution records of biotic and paleoceanographic responses to climate change during extreme climatic conditions. In general, the Late Cretaceous is characterized by high temperatures and atmospheric

CO_2 concentrations 3 to 16 times greater than the modern values(Jenkyns, 1994; Abramovich et al, 1998; Huber et al, 2002; Royer, 2006). Substantial evidence for warmth includes $\delta^{18}O$ bathyal temperatures reaching 20°C in the subtropical North Atlantic (Norris, 1998; Fassell and Bralower, 1999; Huber et al, 1999), upper ocean isotopic paleotemperatures of 22-28°C at southern high latitude sites (Huber et al, 1995), tropical sea surface temperatures of 33 to 34°C (Norris et al, 2002), and fauna intolerant of freezing conditions discovered at 71°N (Tarduno et al, 1998).

However, conditions were not uniformly hot during this 35 million year time span. Progressive warming starting in the Aptian (Huber et al, 1995) reached peak values during the Cenomanian/Turonian interval and early Turonian when globally averaged surface temperatures were up to 14°C higher than today and persisted into the early Campanian (Tarduno et al, 1998; Huber et al, 2002; Wilson et al, 2002; Forster et al, 2007). Short term cooling episodes have been documented during this interval of extreme warmth including the possibility of greenhouse glaciers (Barrera et al, 1987; Miller et al, 1999; Voigt et al, 2004; Forster et al, 2007; Bornemann et al, 2008; Ando et al, 2009). Long term cooling started during the Campanian and continued to the end of the Cretaceous (Huber et al, 2002). While the Maastrichtian was relatively cool it still was warmer than the present (Pearson, 2001). The Maastrichtian age also includes well documented paleobiological and paleoceanographic perturbations, such as the extinction of inoceramid bivalves (MacLeod and Huber, 1996; MacLeod et al, 2000) and rudist bivalves (Johnson et al, 1996; Johnson and Kauffman, 1996, 2001; Steuber et al, 2002).

The inoceramid extinction is well documented in all ocean basins during late Campanian-Maastrichtian. However, at mid-low latitude sites like the Blake Nose in the North Atlantic, the extinction occurs later than in mid to high southern latitudes (MacLeod and Huber, 1996; MacLeod et al, 2000; MacLeod et al, 2001). This diachronous behavior is difficult to explain with a single trigger but could be explained by progressive changes in intermediate and deep water sources and circulation patterns (MacLeod and Huber, 1996). Moreover, significant climate differences are observed among ocean basins during the Maastrichtian. Specifically, during the late Maastrichtian in the North Atlantic basin shows a 3 million year warming trend of approximately 6°C (MacLeod et al, 2005; Isaza-Londoño et al, 2006) at the same time other basins show cooling of the same magnitude (D'Hondt and Lindinger, 1994; Barrera and Savin, 1999; Frank and Arthur, 1999). During regional warming, some species of planktonic foraminifera in the subtropical North Atlantic show isotopic divergence and a trend to increase size, which could be indicative of changes in the water column structure in the basin (Kucera, 1998; MacLeod et al, 2005; Isaza-Londoño et al, 2006). Finally, a negative excursion in the $\delta^{13}C$ values of benthic foraminifera during the Maastrichtian has been interpreted as the record of changes in the intermediate and/or deep water sources (from low to high latitude) (Kucera and Malmgren, 1996; MacLeod and Huber, 1996; Barrera et al, 1997; Frank and Arthur, 1999).

If these conclusions are correct, the mid to late Maastrichtian could be a time where reorganization in circulation on ocean basin scales influenced by regional heat distributions could have played an important role in global cooling. Demonstrating this correlation would advance our understanding of Cretaceous paleoceanographic evolution

and provide key tests for numerical models attempting to simulate greenhouse climate (which have not predicted such changes).

The most often used approach for water mass reconstructions is based on the oxygen and carbon isotopic composition and the Cd/Ca ratio of calcite tests in foraminifera. It is generally agreed that there is a linear correlation between the $\delta^{13}C_{\Sigma CO2}$ values and nutrient contents of deep water masses because the distribution of both is controlled by biological uptake in the surface and decomposition in bottom waters. This $\delta^{13}C$ and Cd/Ca signal is recorded in benthic foraminifera and used as a nutrient proxy to track deep water circulation. As water masses circulate or "age" they accumulate remineralized nutrients from decaying plankton depleted in ^{13}C. As a result younger/ nutrient depleted waters have higher $\delta^{13}C$, while the opposite is true for older waters. Similarly, cadmium concentrations in seawater follow a nutrient-like (phosphate, nitrate) distribution. Benthic foraminifera incorporate cadmium and calcium into their shells in proportion to their relative abundance in seawater, which allows for the reconstruction of deep-water cadmium (and thus macronutrient) concentrations (Frank, 2002). However, it is difficult to make quantitative estimates of mixing between water masses on the basis of Cd/Ca or $\delta^{13}C$ data because neither of the two proxies exclusively mirrors the nutrient content of ambient deep water (Frank, 2002).

Neodymium (Nd) isotopes are a powerful alternative proxy for past water mass structure and mixing that could help constrain major circulation changes in the past. The $^{143}Nd/^{144}Nd$ ratio (expressed as ε_{Nd}) of sea water is a quasi-conservative water mass tracer (Goldstein and Hemming, 2004). The residence time of Nd in the ocean is about 600 -

1000 years (Tachikawa et al, 1999), which is shorter than the total mixing time of the oceans (~1500 years) (Broecker et al, 1960). Water mass $\varepsilon_{Nd(t)}$ signatures reflect the surrounding geology of their source region, with considerable differences among water masses. Therefore, source region and mixing of different water masses can be inferred from the $\varepsilon_{Nd(t)}$ signatures (Stille and Shields, 1997). Furthermore the $\varepsilon_{Nd(t)}$ of a water mass is recorded by fish teeth, scale, bones (herein fish debris) during early diagenesis at the seafloor (Elderfield and Pagett, 1986; Martin and Scher, 2004) and this signature is quite resistant to later alteration (Martin and Scher, 2004). Therefore, stratigraphic trends in the $\varepsilon_{Nd(t)}$ of fish debris should record changes in local bottom $\varepsilon_{Nd(t)}$ values through time.

Applications of this proxy have been used to determine the isotopic composition and mixing of modern water masses, and their evolution through time. For instance, neodymium profiles in the North Atlantic showed $\varepsilon_{Nd(t)}$ values for North Atlantic Deep Water (NADW) of -13 (Piepgras and Wasserburg, 1987) and the isotopic composition of Nd in modern deep waters of the central and northeastern Atlantic Ocean is thought to reflect mixing of North Atlantic with Antarctic Bottom Water (ABW). Furthermore, Frank et al (2003) demonstrated that the isotopic ε_{Nd} signature for the NADW has changed from -10 to -13 over the last 33 million years.

This study provides a high resolution $\varepsilon_{Nd(t)}$ record from multiple sites for the Maastrichtian in the Demerara Rise. Demerara Rise is located in the western tropical North Atlantic (figure 3.1) where MacLeod et al (2008) reported extremely low $\varepsilon_{Nd(t)}$ values (~ -16) throughout most of the Late Cretaceous and proposed to represent a

distinct bottom water mass (that they called "Demerara bottom water mass" (DBWM)) indicative of regional low latitude sinking. These low values were associated with black shale deposition but continued into chalks. Data at one Demerara site showed a shift to -11 between the Maastrichtian and Danian (Bourbon, 2008) but sampling resolution was low. If a reorganization of intermediate and/or deep water circulation was part of the mid Maastrichtian paleoceanographic evolution, any $\varepsilon_{Nd(t)}$ shift should begin at that time. The data generated in this research will test this prediction.

3.2. MATERIAL AND METHODS

Demerara Rise is a submarine plateau located off the coasts of Suriname and French Guyana at ~9°N (Figure 3.1). It was drilled during Ocean Drilling Program (ODP) leg 207. During this expedition five sites were cored on the northern margin of Demerara Rise, three of which are examined during this study: 1258 (3192.2 m), 1260 (2549 m) and 1261 (1899 m). Late Cretaceous paleodepths for these sites range from 1500m to 600m (Friedrich et al, 2008).

Maastrichtian and Danian sediments recovered from Demerara Rise are composed of nannofossil chalk with foraminifers, clay and zeolitic nannofossil claystone. Some sections display apparent cyclic color banding between light greenish gray and greenish gray on a decimeter scale, and there are more dramatic reddish intervals in some core sections (Erbacher et al, 2004). The Maastrichtian sequence varies in thickness from 75m to 25m, and the Danian from 90m to 20m among the three study sites. Age estimates are based on shipboard biostratigraphy (Erbacher et al, 2004). The Maastrichtian at all sites was subdivided by the presence of key species from biozones KS31 (*Abathomphalus*

mayaroensis), KS30a (*Racemiguembelina fructicosa*/ *Contusotruncana contusa*) and upper KS30b (*Gansserina gansseri*). Among the three sites discussed in this paper, sites 1258 and 1260 contain an apparently complete Cretaceous/Tertiary (K/T) interval with ejecta layer (MacLeod et al, 2007; Schulte et al, 2009). At site 1261, a 4 m.y. hiatus that includes the basal Danian and K/T boundary is reported; also in this location the Maastrichtian section is condensed and presents the lowest sedimentation rate among the sites is observed (Erbacher et al, 2004). Where present, the K/T boundary occurs in an interval of pelagic sediment and is placed at the contact between the *Plummerita hantkeninoides* foraminiferal zone (upper part of the *Abathomphalus mayaroensis* zone) and the lowest Paleogene P0 foraminiferal zone (MacLeod et al, 2007). The ejecta layer is characterized by normal graded green spherules with an approximate thickness of 1.7-1.9 cm (Erbacher et al, 2004).

Forty-five samples covering the Maastrichtian/Danian were selected from all three sites (two to three per core). Fish debris was present and relatively common (100s of fragments per sample) in most samples (figure 3.2). Bulk dried samples of approximately 10 cm^3 were disaggregated by soaking them first in kerosene, then in Calgon solution before washing them on a 63 μm screen. To increase picking efficiency, foraminifera and other carbonate grains were dissolved using a buffered 10% acetic acid solution. The insoluble residue was thoroughly rinsed and washed again in a 63 μm screen. Approximately 100 μg of fish debris was picked from this residue and analyzed for Nd isotopes using a Nu Plasma Multi-Collector-Inductively Coupled Plasma-Mass Spectrometer (MC-ICP-MS) at University of Florida Isotope laboratory in the Geology department. JNdi-1 standard was run every 6 samples to obtain a daily average for the

standard. This average was compared to the long-term running average of the JNdi-1 standard from the TIMS (Micromass Sector 54 Thermal Ionization Mass Spectrometer) of ~0.512103 (± 0.000012, 2σ) in order to determine a correction factor for all samples run on that day. The long term error for the Nd MC-ISP-MS is determined by comparing the corrected JNdi-1 values. The calculated 2σ error varies on a daily basis, but the long-term 2σ error is ~0.3 ε_{Nd} units.

3.3. RESULTS

At all three sites $\varepsilon_{Nd(T)}$ values of fish debris shift by ~ 4-6 units from ~-17 to ~-11 between the early Maastrichtian and mid Danian (Figure 3.3) (Appendix 2). In addition, at the two deeper sites the shift begins near the base of the Maastrichtian *Abathomphalus mayaroensis* planktonic foraminifera zone and values increase over an interval representing several million years of deposition. In the shallow site, on the other hand, $\varepsilon_{Nd(t)}$ values remain low (<-16) through the highest Cretaceous samples measured, which are from near the end of the *A. mayaroensis* Zone. In samples of mid-Danian or younger age, $\varepsilon_{Nd(t)}$ values are around -11, with no difference observed among sites. In contrast, during the Campanian and early Maastrichtian, the two deeper sites have consistently higher (~-15 to ~-16) values than the shallower site (~-16 to ~-17). Finally, superimposed on the long term shift are one or two short-term reversals at the deeper sites that bracket the K/T boundary and are associated with reddish colored sediment.

3.4. DISCUSSION

The similar shift at all three sites suggests that a change in the source region for local bottom waters occurred during the Maastrichtian at Demerara Rise. Further, time/depth trends show that low values (<-15) persisted for several million years longer at the shallower site than at the deeper sites. From the middle Danian on, samples at all three sites show consistent, similar $\varepsilon_{Nd(t)}$ values of -11 (figure 3.3) indicating that by this time all three sites were under the influence of a water mass that had consistent $\varepsilon_{Nd(t)}$ values similar to those found widely in the Cenozoic North Atlantic (Piepgras and Wasserburg, 1987; Frank et al, 2003; Thomas, 2005).

In contrast, low radiogenic values (-15 to -17) observed for upper Campanian and Early Maastrichtian samples (~80 Ma to ~68 Ma) are similar to those seen in older samples at site 1258 (MacLeod et al, 2008) and very different from other Cretaceous-Modern values (Frank et al, 2003; Pucéat et al, 2005; Thomas, 2005; Soudry et al, 2006). These low values are interpreted as the signature of an intermediate/deep water mass being formed at low latitudes during most of the Late Cretaceous. Demerara sites are close to Brazil's Guyana shield and Goldstein (1997) determined that sediment in rivers draining the shield have $\varepsilon_{Nd(t)}$ values as low as -30. Therefore, water masses formed in proximity to these rocks would be imprinted with low radiogenic $\varepsilon_{Nd(t)}$ values. Because of the latitude of formation for this water mass, it is implicit that this water mass will be warm (which is consistent with $\delta^{18}O$ values, Bornemann et al, 2008) and salty (MacLeod et al, 2008).

An intriguing detail of the early Maastrichtian samples is that the deeper sites have slightly but consistently higher values (-15 to -16) than the shallower site (-16 to -17). One possible explanation for this pattern is to invoke a model based on Mediterranean Intermediate Water. Mediterranean water reaches neutral buoyancy at a depth of ~1000m (Garrett et al, 1993) partially due to entraining some of the waters through which is moving. If a similar process occurred with the DBWM, the low radiogenic values observed on the three sites could be a reflection of the source (Guayana shield) with the depth gradient in $\varepsilon_{Nd(t)}$ being a reflection of mixing. That Site 1261 has the lowest values could indicate the site was situated at the least mixed core of this water mass.

The two deepest sites show a gradual increase in $\varepsilon_{Nd(t)}$ starting at the base of the *Abathomphalus mayaroensis* biozone, providing new evidence supporting circulation as an important variable in mid Maastrichtian change. Other studies have revealed different changes at the same time as this $\varepsilon_{Nd(t)}$ shift. For instance, geochemical studies at two Indian Ocean sites revealed changes in the rank order of $\delta^{18}O$ in benthic and deep dwelling planktic foraminifera that suggest that bottom waters became cooler and/or less salty (MacLeod and Huber, 1996). Frank and Arthur (1999) suggested a Maastrichtian reorganization on ocean circulation driven by the final breaching of the Walvis Ridge and Rio Grande Rise at the same time and Barrera and Savin (1999) invoke the correlation of a mid Maastrichtian regression (Haq et al, 1987; Hallam, 1992; Elder and Kirkland, 1994) with a negative $\delta^{13}C$ of oceanic total dissolved carbon (TDC) as an indication of changes in the source of deep waters for that time.

During this interval, the North Atlantic samples exhibit a negative $\delta^{18}O$ trend of ~1.5‰, which would correspond to an increase in temperature of approximately 6°C over the last 3 million years of the late Maastrichtian (MacLeod et al, 2005; Isaza-Londoño et al, 2006) accompanied by an increase in diversification and a $\delta^{13}C$ divergence in planktonic foraminifera. These observations suggest changes in the structure of the water column. Previous studies have suggested that the North Atlantic became an intermediate or deep-water source during the Maastrichtian (MacLeod and Huber, 1996; Barrera and Savin, 1999; Frank and Arthur, 1999; D'Hondt and Arthur, 2002). Import of heat from the South Atlantic basin into the North Atlantic would warm the mid latitude ocean and this could explain the $\delta^{18}O$ negative trend. Moreover, foraminifera observations (Isaza-Londoño et al, 2006) suggest increased stratification of the water column with a more strongly developed thermocline. This stratification could result from an intensification of the North Atlantic polar front. A stronger polar front would not only contribute to reinforce heating in the North Atlantic but also would lead to arctic cooling and North Atlantic downwelling.

Short term reversal of the $\varepsilon_{Nd(t)}$ values observed at the two deepest sites bracketing the Cretaceous/Tertiary boundary (K/T) (figure 3.3) demonstrates that the long term trend is not monotonic and local/ short term effects are recorded in the Nd signatures. Similar rapid shifts have been observed during the mid Cenomanian (Jiménez Berrocoso et al, 2009) and Cenomanian/Turonian (MacLeod et al, 2008). However, the Maastrichtian-Danian shifts differ from the older ones in that they represent reversals during long-term gradual trends. The shifts are not closely tied to the K/T event bed, but their cause cannot be uniquely determined.

Uncertainty notwithstanding, these shifts suggest short term variability. Rapid changes in the neodymium signatures could be explained by high frequency variation in continental inputs, related to increased weathering or a sudden increase in volcanism that could rapidly change the sea water $\varepsilon_{Nd(t)}$. The volcanic explanation is an intriguing possibility because of Deccan volcanism at this time. Direct basalts inputs would change seawater $\varepsilon_{Nd(t)}$ towards higher values (opposite in sign to the short-term reversal from sites 1258 and 1260) and it is unclear why only the deeper sites would be affected. Predicted indirect effect of large Deccan scale volcanic eruptions, though, is addition of carbon dioxide and sulfur oxides on the atmosphere. Resulting warming and acid rain could accelerate the rate of continental weathering (Wilf et al, 2003) leading to negative $\varepsilon_{Nd(t)}$ excursions.

Recent K/Ar, $^{40}Ar/^{39}Ar$ and Re/Os geochronology coupled with palaeomagnetic and palaeontological studies, it has been suggested, that the Deccan Traps erupted around the KT boundary 65.5 Myr ago (Courtillot et al, 1988; Allégre et al, 1999; Courtillot et al, 1999). Major eruptions were apparently quite short on a geological time scale, spanning less than 1 Myr, within the ranges of the short term $\varepsilon_{Nd(t)}$ shifts are the results of Deccan-forced weathering, we should also see evidence of increase continental input in other basins, not only in the neodymium signatures but also in other geochemical markers. An alternative possibility is the correlation of pulses of DBWM with red layers (figure 3.4), which suggests a circulation-benthic-O_2 link. Ongoing work is focused on studying more red layers. Regardless, it is important to note that these short-term shifts do not obscure the importance and significance of the long term trends.

Based on the long term signatures, we believe that the 6 unit $\varepsilon_{Nd(t)}$ shift from the base of the *A. mayaroensis* zone up to the mid Danian is evidence that a reversal in the location of sources for deep water formation occurred (from low latitude to high latitude). Perhaps as greenhouse conditions waned through the Maastrichtian the rates of evaporation decreased, leading to a reduction in the strength of the DBWM. Alternatively, cooling in high latitudes could have resulted in initiation/intensification of formation of high latitude deep water masses that displaced overlaying waters explaining. This would explain why the shift is observed first at the two deeper sites (figure 3.5). Moreover, displacement of the DBWM could result in changes in surface waters elsewhere, like the regional expressions observed in the North Atlantic region such as warming and increased stratification (MacLeod et al, 2005., Isaza-Londoño et al, 2006). Furthermore, cooling at high latitudes will increase latitudinal thermal gradients and promote the development of features characteristic of an ocean where deep water is formed at high latitudes.

3.5. IMPLICATIONS

High-resolution $\varepsilon_{Nd(t)}$ data presented in this study demonstrate that deep ocean circulation changes in the North Atlantic were happening at shorter time scales than originally assumed for greenhouse intervals and that local changes in the intermediate/deep water formation sources were having an effect on greater regional scales than originally believed for Late Cretaceous studies. The shift to higher $\varepsilon_{Nd(t)}$ values beginning in the mid Maastrichtian at sites 1258 and 1260 provides a new line of evidence supporting a role for intermediate/deep water circulation patterns in explaining

climate evolution at the end of the Cretaceous. In addition, this study confirms that low ε_{Nd} values characteristic of most of the Late Cretaceous on Demerara Rise are the signature of a locally formed intermediate water mass (DBWM) and demonstrate that main ocean intermediate to deep water masses were being formed at low latitudes.

REFERENCES

Abramovich, S., Almogi-Labin, A., and Benjamini, C., 1998. Decline of the Maastrichtian pelagic ecosystem based on planktic foraminifera assemblage change: implication for the terminal Cretaceous faunal crisis: Geology, v. 26, p. 63-66.

Adatte, T., Keller, G., and Stinnesbeck, W., 2002. Late Cretaceous to early Paleocene climate and sea-level fluctuations: the Tunisian record: Palaeogeography, Palaeoclimatology, Palaeoecology, v. 178, p. 165-196.

Allégre, C.J., Birck, J.L., Capmas, F., and Courtillot, V., 1999. Age of the Deccan traps using 187Re-187Os systematics: Earth and Planetary Science Letters, v. 170, p. 197-204.

Ando, A., Huber, B.T., MacLeod, K.G., Ohta, T., and Khim, B.K., 2009. Blake Nose stable isotopic evidence against the mid-Cenomanian glaciation hypothesis: Geology, v. 37, p. 451-454.

Barrera, E., Huber, B.T., Savin, S.M., and Webb, P.N., 1987. Antarctic marine temperatures: late Campanian through early Paleocene: Paleoceanography, v. 2, p. 21-47.

Barrera, E., Savin, S.M., Thomas, E., and Jones, C.E., 1997. Evidence for thermohaline-circulation reversals controlled by sea-level change in the latest Cretaceous: Geology, v. 25, p. 715-718.

Barrera, E., and Savin, S.M., 1999. Evolution of late Campanian-Maastrichtian marine climates and oceans: Evolution of the Cretaceous Ocean-Climate System, v. 332, p. 245-282.

Bornemann, A., Norris, R.D., Friedrich, O., Beckmann, B., Schouten, S., Damst√©, J.S.S., Vogel, J., Hofmann, P., and Wagner, T., 2008. Isotopic evidence for glaciation during the cretaceous supergreenhouse: Science, v. 319, p. 189-192.

Bourbon, É., 2008. Nd isotopes throughout the North Atlantic in the Late Cretaceous and across the Oceanic Anoxic Event 2: M.S. Thesis. Geological Sciences. Gainesville, University of Florida.

Broecker, W.S., Gerard, R., Ewing, M., and Heezen, B.C., 1960. Natural radiocarbon in the Atlantic Ocean: J. Geophys. Res., v. 65, p. 2903-2931.

Courtillot, V., Féraud, G., Maluski, H., Vandamme, D., Moreau, M.G., and Besse, J., 1988. Deccan flood basalts and the Cretaceous/Tertiary boundary: Nature, v. 333, p. 843-846.

Courtillot, V., Jaupart, C., Manighetti, I., Tapponnier, P., and Besse, J., 1999. On causal links between flood basalts and continental breakup: Earth and Planetary Science Letters, v. 166, p. 177-195.

D'Hondt, S., and Lindinger, M., 1994. A stable isotopic record of the Maastrichtian ocean-climate system: South Atlantic DSDP Site 528: Palaeogeography, Palaeoclimatology, Palaeoecology, v. 112, p. 363-378.

D'Hondt, S., and Arthur, M.A., 2002. Deep water in the late Maastrichtian ocean: Paleoceanography, v. 17, p. 8-1-8-11.

Elder, W.P., and Kirkland, J.I., 1994. Cretaceous paleogeography of the southern Western Interior region: Mesozoic Systems of the Rocky Mountain Region, p. 415-440.

Elderfield, H., and Pagett, R., 1986. Rare earth elements in ichthyoliths: Variations with redox conditions and depositional environment: Science of the Total Environment, The, v. 49, p. 175-197.

Erbacher, J., Mosher, D.C., Malone, M.J., Berti, D., Bice, K.L., Bostock, H., Brumsack, H.J., et al., 2004, Proceedings of the Ocean Drilling Program; Demerara Rise; equatorial Cretaceous and Paleogene paleoceanographic transect, western Atlantic. Leg 207 Proceedings of the Ocean Drilling Program, Part A: Initial Reports, Volume 207: United States, Texas A&M University, Ocean Drilling Program : College Station, TX, United States.

Fassell, M.L., and Bralower, T.J., 1999. Warm, equable mid-Cretaceous: Stable isotope evidence: Evolution of the Cretaceous Ocean-Climate System, v. 332, p. 121-142.

Forster, A., Schouten, S., Moriya, K., Wilson, P.A., Sinninghe, D., and Jaap, S., 2007. Tropical warming and intermittent cooling during the Cenomanian/Turonian oceanic anoxic event 2: Sea surface temperature records from the equatorial Atlantic: Paleoceanography, v. 22.

Frank, M., 2002. Radiogenic isotopes: Tracers of past ocean circulation and erosional input: Rev. Geophys., v. 40.

Frank, M., van de Flierdt, T., Halliday, A.N., Kubik, P.W., Hattendorf, B., and G√ºnther, D., 2003. Evolution of deepwater mixing and weathering inputs in the central Atlantic Ocean over the past 33 Myr: Paleoceanography, v. 18, p. 15-1.

Frank, T.D., and Arthur, M.A., 1999, Tectonic forcings of Maastrichtian ocean-climate evolution, *in* Arthur, M.A., ed., Paleoceanography, Volume 14: United States, American Geophysical Union : Washington, DC, United States, p. 103.

Friedrich, O., Erbacher, J., Moriya, K., Wilson, P.A., and Kuhnert, H., 2008. Warm saline intermediate waters in the Cretaceous tropical Atlantic Ocean: Nature Geosci, v. 1, p. 453-457.

Garrett, C., Outerbridge, R., and Thompson, K., 1993. Interannual Variability in Meterranean Heat and Buoyancy Fluxes: Journal of Climate, v. 6, p. 900-910.

Goldstein, S.L., Arndt, N.T., and Stallard, R.F., 1997. The history of a continent from U-Pb ages of zircons from Orinoco River sand and Sm-Nd isotopes in Orinoco basin river sediments: Chemical Geology, v. 139, p. 271-286.

Goldstein, S.L., and Hemming, S.R., 2004. Long-lived isotopic tracers in oceanography, paleoceanography, and ice-sheet dynamics: Treatise on Geochemistry: The Oceans and Marine Geochemistry, v. 6, p. 453-489.

Hallam, A., 1992. Phanerozoic sea-level changes: Perspectives in Paleobiology and Earth History Ser., p. 266.

Haq, B.U., Hardenbol, J., and Vail, P.R., 1987. Chronology of fluctuating sea levels since the Triassic: Science, v. 235, p. 1156-1167.

Huber, B.T., Hodell, D.A., and Hamilton, C.P., 1995. Middle-late Cretaceous climate of the southern high latitudes: stable isotopic evidence for minimal equator-to-pole thermal gradients: Geological Society of America Bulletin, v. 107, p. 1164-1191.

Huber, B.T., Leckie, R.M., Norris, R.D., Bralower, T.J., and CoBabe, E., 1999. Foraminiferal assemblage and stable isotopic change across the Cenomanian-Turonian boundary in the Subtropical North Atlantic: Journal of Foraminiferal Research, v. 29, p. 392-417.

Huber, B.T., Norris, R.D., and MacLeod, K.G., 2002. Deep-sea paleotemperature record of extreme warmth during the Cretaceous: Geology, v. 30, p. 123-126.

Isaza-Londoño, C., MacLeod, K.G., and Huber, B.T., 2006. Maastrichtian North Atlantic warming, increasing stratification, and foraminiferal paleobiology at three timescales: Paleoceanography, v. 21.

Jenkyns, H.C., Gale, A.S. and Corfield, R.M, 1994. Carbon- and oxygen-isotope stratigraphy of the English Chalk and Italian Scaglia and its palaeoclimatic significance: Geology Magazine, v. 131, p. 1-34.

Jiménez Berrocoso, A., MacLeod, K.G., Martin, E.E., Bourbon, E., Basak, C., and Isaza-Londoño, C., 2009. Water-mass changes in the western tropical North Atlantic across the Cenomanian (Late Cretaceous) inferred from bioapatite Nd isotopes (in review).

Johnson, C.C., Barron, E.J., Kauffman, E.G., Arthur, M.A., Fawcett, P.J., and Yasuda, M.K., 1996. Middle cretaceous reef collapse linked to ocean heat transport: Geology, v. 24, p. 376-380.

Johnson, C.C., and Kauffman, E.G., 1996. Maastrichtian extinction patterns of Caribbean province rudistids: Cretaceous-Tertiary Mass Extinctions: Biotic and Environmental Changes, p. 231-273.

—, 2001. Cretaceous evolution of reef ecosystems; a regional synthesis of the caribbean tropics: Topics in Geobiology, v. 17, p. 311-349.

Kucera, M., and Malmgren, B.A., 1996. Latitudinal variation in the planktic foraminifer *Contusotruncana contusa* in the terminal Cretaceous ocean: Marine Micropaleontology, v. 28, p. 31-52.

Kucera, M., 1998, Terminal Cretaceous warming event in the mid-latitude South Atlantic Ocean; evidence from poleward migration of *Contusotruncana contusa* (planktonic Foraminifera) morphotypes, *in* Malmgren, B.A., ed., Palaeogeography, Palaeoclimatology, Palaeoecology, Volume 138: Netherlands, Elsevier : Amsterdam, Netherlands, p. 1.

MacLeod, K.G., and Huber, B.T., 1996. Reorganization of deep ocean circulation accompanying a late Cretaceous extinction event: Nature, v. 380, p. 422-425.

MacLeod, K.G., Huber, B.T., and Ducharme, M.L., 2000. Paleontological and geochemical constraints on the deep ocean during the Cretaceous greenhouse interval: Warm Climates in Earth History, p. 241-274.

MacLeod, K.G., Kucera, M., Huber, B.T., Pletsch, T., and Röhl, U., 2001. Maastrichtian foraminiferal and paleoceanographic changes on Milankovitch timescales: Paleoceanography, v. 16, p. 133-154.

MacLeod, K.G., Huber, B.T., and Isaza-Londoño, C., 2005. North Atlantic warming during global cooling at the end of the Cretaceous: Geology, v. 33, p. 437-440.

MacLeod, K.G., Whitney, D.L., Huber, B.T., and Koeberl, C., 2007. Impact and extinction in remarkably complete Cretaceous-Tertiary boundary sections from Demerara Rise, tropical western North Atlantic: Bulletin of the Geological Society of America, v. 119, p. 101-115.

MacLeod, K.G., Martin, E.E., and Blair, S.W., 2008. Nd isotopic excursion across Cretaceous ocean anoxic event 2 (Cenomanian-Turonian) in the tropical North Atlantic: Geology, v. 36, p. 811-814.

Martin, E.E., and Scher, H.D., 2004. Preservation of seawater Sr and Nd isotopes in fossil fish teeth: bad news and good news: Earth and Planetary Science Letters, v. 220, p. 25-39.

Miller, K.G., Savin, S.M., Barrera, E., Olsson, R.K., and Sugarman, P.J., 1999. Does ice drive early Maastrichtian eustasy?: Geology, v. 27, p. 783-786.

Norris, R.D., 1998. Planktonic foraminifer biostratigraphy: Eastern equatorial Atlantic: Proceedings of the Ocean Drilling Program: Scientific Results, v. 159, p. 445-479.

Norris, R.D., Bice, K.L., Magno, E.A., and Wilson, P.A., 2002. Jiggling the tropical thermostat in the Cretaceous hothouse: Geology, v. 30, p. 299-302.

Pearson, P.N., 2001, Warm tropical sea surface temperatures in the Late Cretaceous and Eocene epochs, *in* Ditchfield, P.W., Singano, J., Harcourt-Brown, K.G., Nicholas, C.J., Olsson, R.K., Shackleton, N.J., and Hall, M.A., eds., Nature London, Volume 413: United Kingdom, Macmillan Journals : London, United Kingdom, p. 481.

Piepgras, D.J., and Wasserburg, G.J., 1987. Rare earth element transport in the western North Atlantic inferred from Nd isotopic observations: Geochimica et Cosmochimica Acta, v. 51, p. 1257-1271.

Pucéat, E., Lecuyer, C., and Reisberg, L., 2005. Neodymium isotope evolution of NW Tethyan upper ocean waters throughout the Cretaceous: Earth and Planetary Science Letters, v. 236, p. 705-720.

Royer, D.L., 2006. CO2-forced climate thresholds during the Phanerozoic: Geochimica et Cosmochimica Acta, v. 70, p. 5665-5675.

Schulte, P., Deutsch, A., Salge, T., Berndt, J., Kontny, A., MacLeod, K.G., Neuser, R.D., and Krumm, S., 2009. A dual-layer Chicxulub ejecta sequence with shocked carbonates from the Cretaceous-Paleogene (K-Pg) boundary, Demerara Rise, western Atlantic: Geochimica et Cosmochimica Acta, v. 73, p. 1180-1204.

Soudry, D., Glenn, C.R., Nathan, Y., Segal, I., and VonderHaar, D., 2006. Evolution of Tethyan phosphogenesis along the northern edges of the Arabian-African shield

during the Cretaceous-Eocene as deduced from temporal variations of Ca and Nd isotopes and rates of P accumulation: Earth-Science Reviews, v. 78, p. 27-57.

Steuber, T., Mitchell, S.F., Buhl, D., Gunter, G., and Kasper, H.U., 2002. Catastrophic extinction of Caribbean rudist bivalves at the Cretaceous-Tertiary boundary: Geology, v. 30, p. 999-1002.

Stille, P., and Shields, G.A., 1997. Radiogenic isotope geochemistry of sedimentary and aquatic systems: Lecture Notes in Earth Science, v. 68.

Tachikawa, K., Jeandel, C., and Roy-Barman, M., 1999. A new approach to the Nd residence time in the ocean: The role of atmospheric inputs: Earth and Planetary Science Letters, v. 170, p. 433-446.

Tarduno, J.A., Brinkman, D.B., Renne, P.R., Cottrell, R.D., Scher, H., and Castillo, P., 1998. Evidence for extreme climatic warmth from late cretaceous arctic vertebrates: Science, v. 282, p. 2241-2244.

Thomas, D.J., 2005, Reconstructing ancient deep-sea circulation patterns using the Nd isotopic composition of fossil fish debris, Special Paper - Geological Society of America, Volume 395: United States, Geological Society of America (GSA) : Boulder, CO, United States, p. 1.

Voigt, S., Gale, A.S., and Flügel, S., 2004. Midlatitude shelf seas in the Cenomanian-Turonian greenhouse world: Temperature evolution and North Atlantic circulation: Paleoceanography, v. 19, p. 1-17.

Wilf, P., Johnson, K.R., and Huber, B.T., 2003. Correlated terrestrial and marine evidence for global climate changes before mass extinction at the Cretaceous-Paleogene boundary: Proceedings of the National Academy of Sciences of the United States of America, v. 100, p. 599-604.

Wilson, P.A., Norris, R.D., and Cooper, M.J., 2002. Testing the Cretaceous greenhouse hypothesis using glassy foraminiferal calcite from the core of the Turonian tropics on Demerara Rise: Geology, v. 30, p. 607-610.

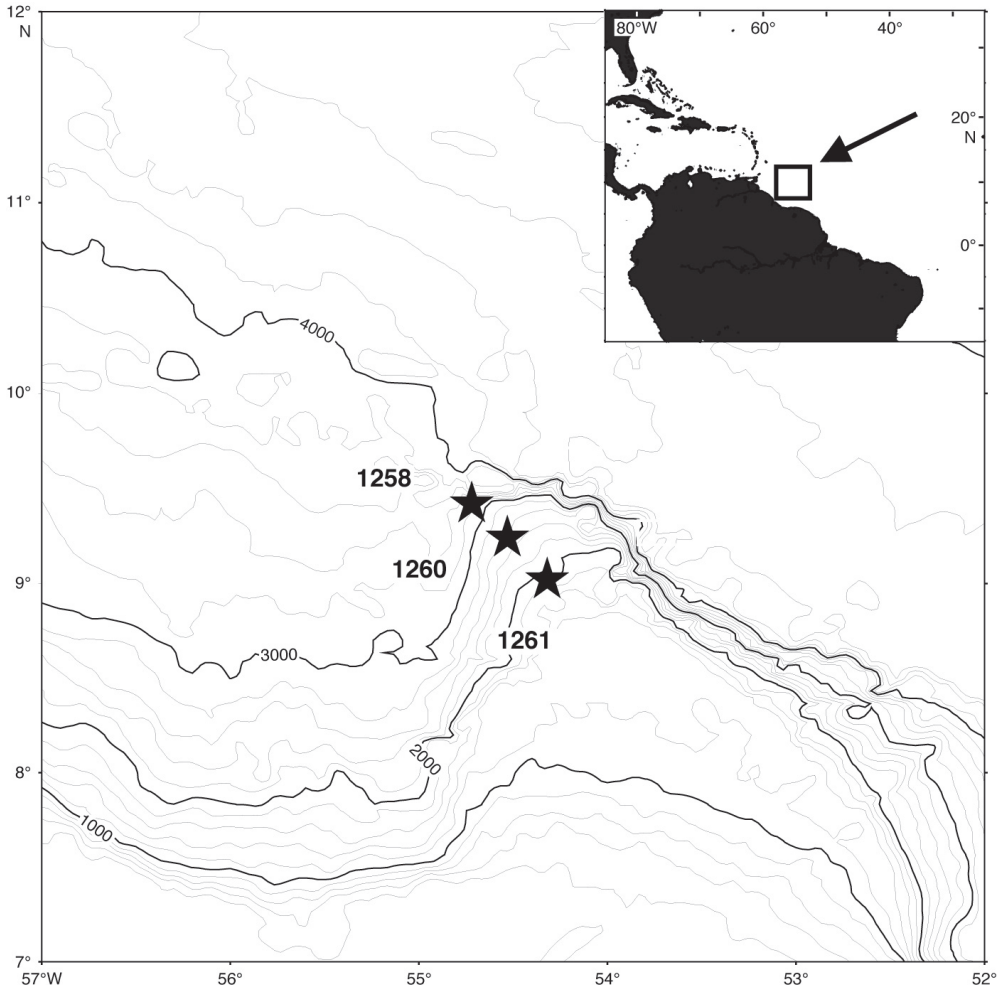

Figure 3.1. Location and modern bathymetry of study sites 1258, 1260 and 1261. Inset show the regional location map, where the boxed area represents the approximate location of sites drilled during ODP Leg 207 (modified after Erbacher et al, 2004).

Figure 3.2. Typical fish teeth and fish debris fragments found in samples from the study sites.

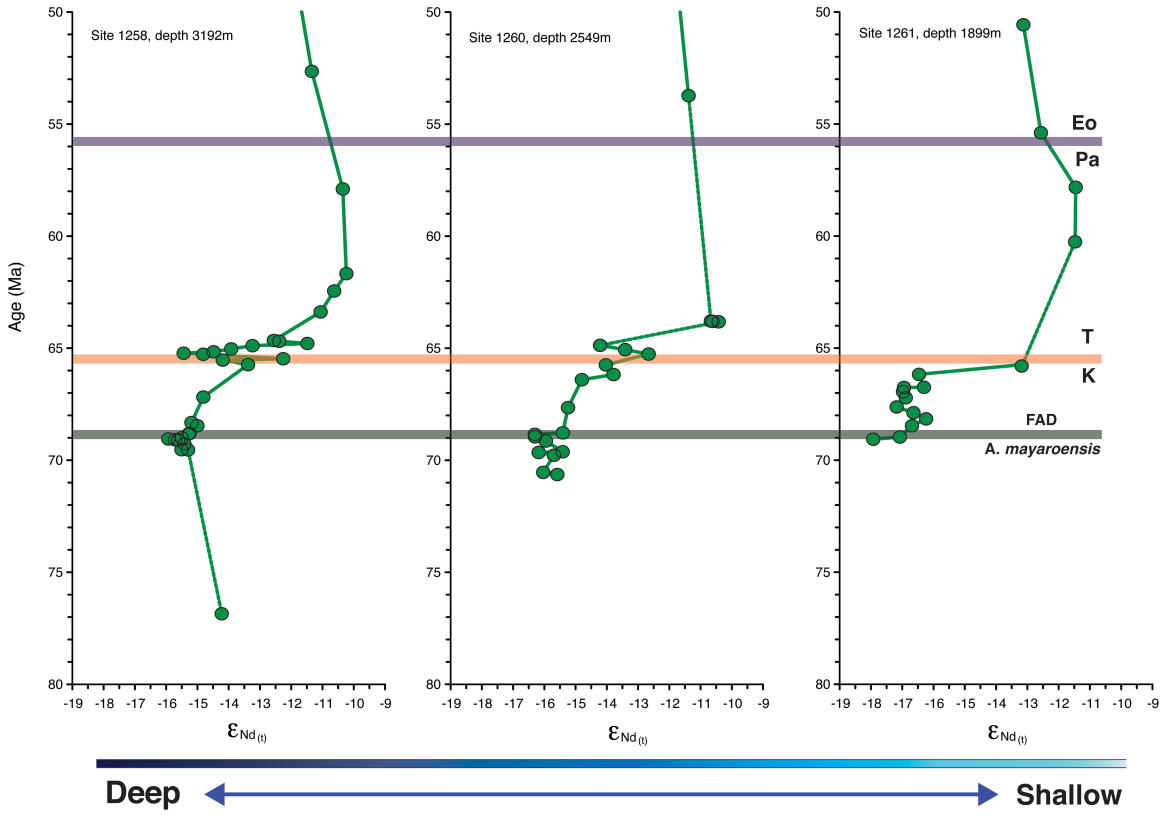

Figure 3.3. Campanian-early Eocene neodymium isotopic values for three sites at the Demerara Rise (Campanian data are from Bourbon, 2008). All sites show a large positive shift across the interval studied, but the shift starts earlier and seems more gradual at the deeper two sites than at the shallower site. Calculations for age model were made based on biostratigraphy analysis and identification of Late Cretaceous nannofossil and foraminifera index taxa in Erbacher et al (2004). Variable sedimentation rates are observed between the points, but in general there is a decrease in sedimentation rate from deep to shallow and through time. Some datums for index fossils and boundaries, were modified following the chronostratigraphy/biostratigraphy on Time Scale creator professional (2008). Abbreviations are: T (Tertiary), K (Cretaceous), Pa (Paleocene), Eo (Eocene).

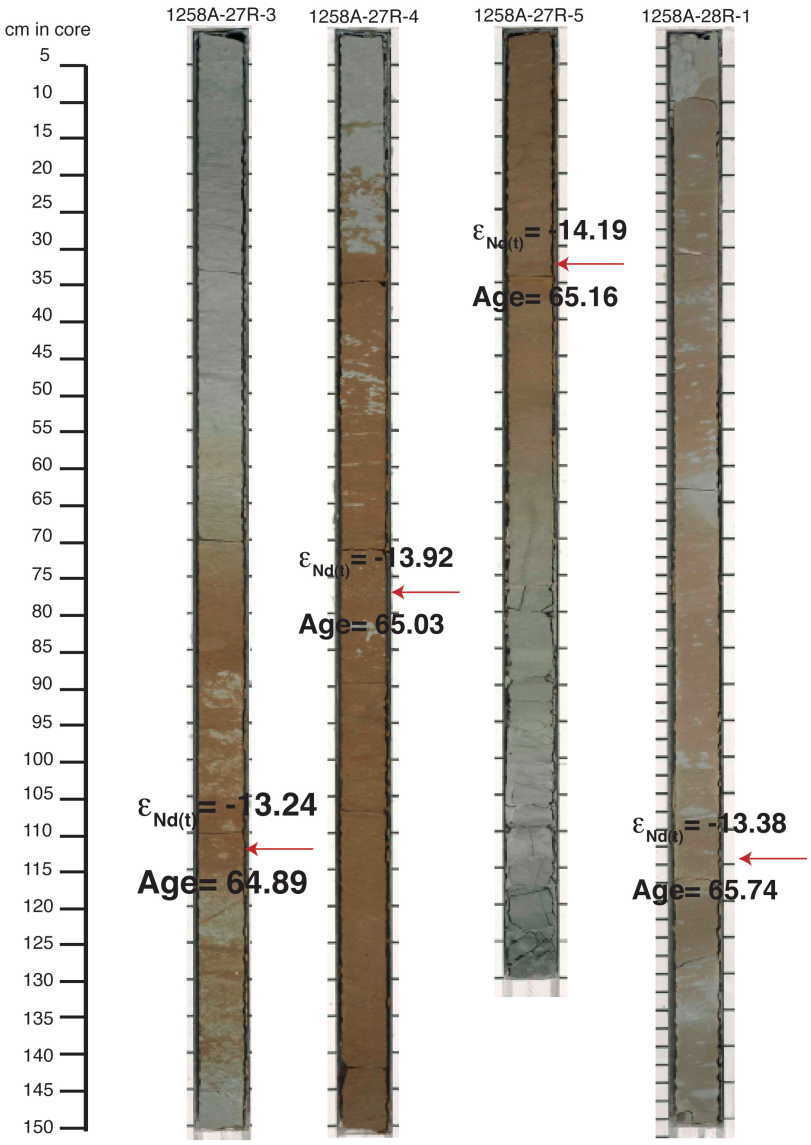

Figure 3.4. Shipboard core photographs, showing some of the core intervals in Site 1258, where the red layers are present, accompanied by the estimated age and $\varepsilon_{Nd(t)}$ value for specific red layer samples.

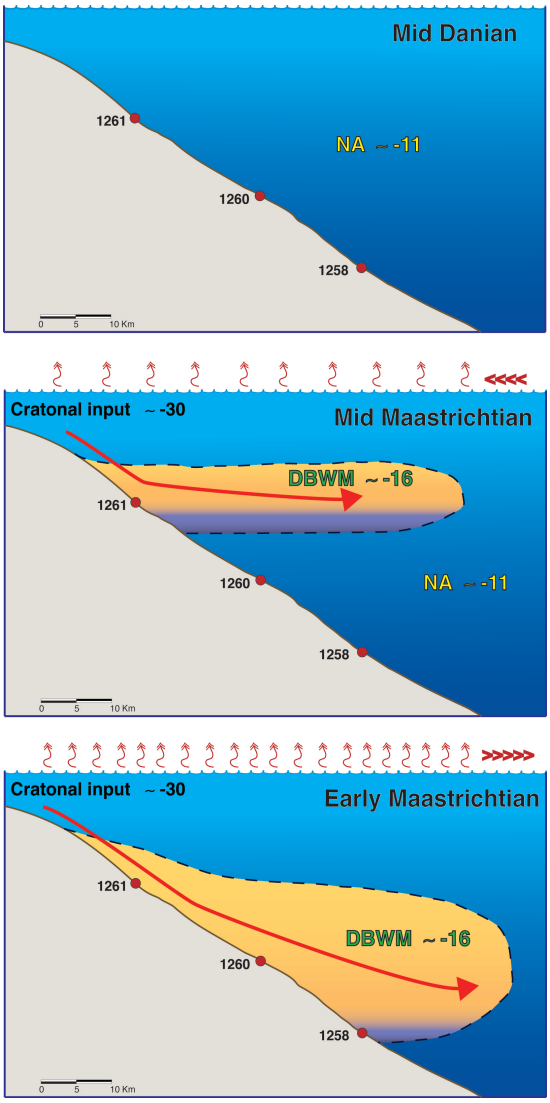

Figure 3.5. Simplified model of ocean circulation evolution during the Maastrichtian at Demerara rise. During the early Maastrichtian all sites were under the influence of the DBWM (Demerara bottom water mass). Greenhouse conditions were high therefore it is possible that strength of this water mass was intensified during this time interval and boundary conditions between DBWM and surrounding waters were more well defined. By the mid Maastrichtian, several lines of evidence including neodymium isotopes (this study) demonstrate that a dramatic reorganization in ocean circulation was initiated. It is probable that an increase in deep water formation at high latitude took place, with newly formed water masses exhibiting isotopic characteristics similar to modern NADW (North Atlantic Deep Water). As greenhouse conditions started to wane the DBWM shrank (less evaporation, therefore less weathering of craton with low radiogenic values) boundary conditions between the DBWM and newly formed North Atlantic (NA) type water was less defined. Furthermore, this NA mass could have a displacing effect on DBWM, this process continues up to late Maastrichtian until mid Danian, where any evidence of DBWM has disappeared and Demerara Basin looks homogenous with isotopes values typical of the NA.

CHAPTER 4

MAASTRICHTIAN NORTH ATLANTIC EVOLUTION FROM ABBYSAL TO BATHYAL DEPTHS

ABSTRACT

Sources and circulation patterns of intermediate and deep water masses are a much discussed but poorly constrained aspect of Late Cretaceous paleoceanography. To address this problem we measured Nd isotopes, a quasi-conservative water mass tracer, in Maastrichtian through Danian samples from four regions throughout the North Atlantic that represent different latitudes and different depths. Results demonstrate that during the Cenomanian-Campanian interval, deep water was dominated by a water mass with $\varepsilon_{Nd(t)}$ values of around -9, and that a likely source for this water was the Tethyan region. During the early/mid Maastrichtian abyssal waters in the tropical transect shift to very non-radiogenic values that can be linked to a deep/intermediate water mass (Demerara Bottom Water Mass) that reached true deep water depths. Finally, between the mid Maastrichtian and Danian all sites show a shift towards radiogenic values between -9 to -11, indicating that sometime during this interval a dramatic reorganization of deepwater formation took place, resulting in patterns similar to the modern ocean circulation.

4.1. INTRODUCTION

Deep-water circulation is a key control on the distribution of nutrients and heat in the Earth's ocean, and changes in its patterns can affect climatic conditions. The

International Panel on Climate Change (IPCC, 2008) recognized that global warming could have a dramatic effect on the intermediate and deep water thermohaline circulation. As we move towards a new greenhouse world it is important to understand how ocean circulation might respond to warming. Warm intervals in the geologic past provide the only empirical record of ocean circulation during greenhouse conditions.

The Late Cretaceous has been widely recognized as a time of extreme high temperatures and high CO_2 levels (Jenkyns et al, 1994; Huber et al, 2002; MacLeod et al, 2004; Royer, 2006). Late Cretaceous thermal gradients (horizontal and vertical) were different from what we see in modern times (Barron and Peterson, 1989; Bice et al, 1997; Poulsen et al, 1998; Barrera and Savin, 1999), but whether ocean circulation patterns changed to a world with a low latitude source of deep waters as a result has been debated for over 100 years (Chamberlin, 1906; Brass et al, 1982; Barrera and Savin, 1987; Barrera and Keller, 1990; Stott and Kennett, 1990; Corfield and Norris, 1996; MacLeod and Huber, 1996; Brady et al, 1998; Frank and Arthur, 1999; Bice and Marotzke, 2001; Bice and Norris, 2002; Friedrich et al, 2008; MacLeod et al, 2008). To date, ocean circulation studies during this interval have relied on indirect inferences of paleoceanographic proxies based on theory or analysis of calcareous microorganisms. Beyond uncertainties in the proxies (chapter 3), interpretations are limited because true deep water data are absent as these sites were deposited below the carbon compensation depth (CCD) and, thus, lack calcareous microfossils.

A solution lies in exploiting a geochemical water-mass tracer such as the neodymium (Nd) isotopic composition of seawater. This proxy provides a relatively

direct way to track water masses and paleocirculation patterns (Frank et al, 2003; Goldstein and Hemming, 2003). Neodymium is supplied to the oceans mainly via continental weathering and runoff of dissolved and particulate fluxes (Bertram and Elderfield, 1993; Frank, 2002; Goldstein and Hemming, 2003). The residence time of Nd in the modern oceans is ~1000 years (Elderfield and Greaves, 1982; Piepgras and Wasserburg, 1985; Jeandel et al, 1995; Tachikawa et al, 1999; Tachikawa et al, 2003), which is shorter than the total mixing time of the ocean ~1500 years (Broecker and Peng, 1982). Nd isotopes are quasi-conservative tracers of water mass that reflect the Nd signature of the source region and are only slightly modified by weathering inputs along the flow path. Among the archives for Nd in the geologic record, fish remains have proven to be effective for paleoceanographic studies (Elderfield and Pagett, 1986; Martin, 2000; Thomas, 2003; Martin and Scher, 2004; Thomas, 2005). Nd is incorporated into fossil fish remains during early diagenesis when they are still often in contact with deep ocean water (Elderfield and Pagett, 1986; Martin and Haley, 2000). Moreover, fossil teeth are found in all ocean basins so they can record detailed variations in the deep water signal through time and they can be dated based on the surrounding sediment using biostratigraphic, magnetostratigraphic and chemostratigraphic data.

The $^{143}Nd/^{144}Nd$ is measured in samples and commonly reported as ε_{Nd}. This expression allows small, but significant, variation in the isotopic ratio to be reported in whole numbers relative to a bulk Earth value (DePaolo and Wasserburg, 1976) and is obtained by the following equation:

$$\varepsilon_{Nd} = \left[\frac{\left({}^{143}Nd/_{144}Nd \right)_{Sample}}{\left({}^{143}Nd/_{144}Nd \right)_{CHUR}} - 1 \right] \times 10^4$$

CHUR (Chondritic uniform reservoir): equivalent to the bulk Earth $^{143}Nd/^{144}Nd$ ratio (~0.512638) (DePaolo and Wasserburg, 1976)

The use of this proxy during the Late Cretaceous is still in its early stages and most of the existing Nd data from this interval are limited to shallow water masses and single localities (Frank et al, 2005; Pucéat et al, 2005; Soudry et al, 2006; Pucéat et al, 2007; MacLeod et al, 2008). In chapter 3 we used Nd isotopes to examine bottom water sources along a depth transect in Demerara Rise in the western tropical North Atlantic and found evidence for deep to intermediate water formation at low latitudes during the Campanian- early Maastrichtian. Furthermore, we found evidence for a dramatic reorganization in ocean circulation that took place between the mid Maastrichtian and the Danian. The changes are consistent with a switch from downwelling at low latitudes to a more Tertiary pattern with high latitude water formation by mid-Danian. While exciting, those observations only represent conditions in a small region from a relatively narrow depth range.

The objective of this study is to expand the coverage of the data geographically and bathymetrically. A multisite approach (figure 4.1) is designed to try to track intermediate and deep water circulation in the North Atlantic from bathyal to abyssal depths during the Maastrichtian. First, by extending the Demerara transect to abyssal depths in the Cape Verde Site (367) we can possibly test the downstream fate of the Demerara Bottom Water Mass (DBWM) (MacLeod et al, 2008) and, thus, the possibility of low latitude deep-water formation during the Maastrichtian. Second, by studying a similar depth transect in the Subtropical North Atlantic in the Blake Nose Site 1050C

(bathyal) and Bermuda Rise Sites 386-387 (abyssal), we can provide new insights into deep water circulation patterns during a greenhouse interval and test our hypothesis for a dramatic reorganization of deep water circulation during the Maastrichtian.

4.2. AREA OF STUDY

4.2.1. NORTHERN (SUBTROPICAL) TRANSECT

The shallow end of our northern transect is Site 1050. It was drilled during ODP leg 171B at the intermediate Site in the Blake Nose transect. Blake Nose is in the western North Atlantic (figure 4.1). During Maastrichtian time, Blake Nose was located at bathyal paleodepths in the northwestern boundary of the Tethys Seaway at a paleolatitude of ~30ºN. The Maastrichtian at this site is comprised of an 85 m section with a sedimentation rate of ~18 m/m.y. for most of the interval (Huber et al, 2008). The section consists mostly of gray nannofossil ooze or chalk containing abundant well preserved foraminifera (Norris et al, 1998). Fish debris is present in low abundances in most samples. There are subtle meter-scale alternations between lighter and darker intervals in the section that have been attributed to a ~20 Kyr Milankovitch precessional cycle (MacLeod et al, 2001) (chapter 2). Hiatuses and slumping disturb the Maastrichtian sequence in places. Nonetheless, the Maastrichtian sequence is relatively complete and age estimates above and below these features are continuous (Huber et al, 2008). There are two working hypotheses regarding the slumping. The first one attributes the slumps to a large-magnitude earthquake produced by the Chicxulub impact (Klaus et al, 2000; Norris et al, 2000). The second one invokes pelagic deposition punctuated by gravity flows supported by an increase in $^{87}Sr/^{86}Sr$ throughout the Maastrichtian and the presence

of burrows in the surface of the slumps (MacLeod et al, 2003).

The Maastrichtian is subdivided biostratigraphically by recognition of the key species that define the *Abathomphalus mayaroensis* Partial-range Zone, *Racemiguembelina fructicosa* Partial-range Zone, *Gansserina gansseri* Partial-range Zone, and *Pseudoguembelina palpebra* Partial-range Zone (Huber et al, 2008). An incomplete Cretaceous/Tertiary boundary (K/T) was recovered in Hole 1050C core 10R-2, 36 cm (405.93 Mbsf); the top most Maastrichtian *Micula prinsii* nannofossil zone is present, as is the early Paleocene Pα foraminifera zone. The ejecta layer was not recovered probably due to some combination of bioturbation, coring gaps, and slumping (Norris et al, 1998). In addition, Huber et al (2008) developed a high resolution age model of the Blake Nose which is used for the relative age characterization of the Blake Nose samples in this project.

Deep Sea Drilling Project (DSDP) Sites 386 and 387 are the deep end of the northern transect and extend the transect to abyssal depths. Both sites were drilled during DSDP leg 41. They are located on the central Bermuda Rise and are 700 km and 1200 km offshore of the continental escarpment respectively (Norris and Firth, 2002) (figure 4.1). The Maastrichtian in Sites 386 and 387 is represented by ~100 m and ~35 m thick sections, respectively, with similar sedimentation rates of 16 m/m.y, and similar lithological features (Tucholke and Vogt, 1979).

The lower to middle Maastrichtian interval is characterized by multicolored red claystone that has been interpreted as being deposited below the carbonate compensation depth (CCD) (Tucholke and Vogt, 1979). The upper Maastrichtian interval is

characterized by an homogeneous olive to light olive-gray marly chalk with minor greenish gray calcareous claystone, that generally has been interpreted as a pelagic sediment that accumulated during a brief episode of increased depth of the CCD (Tucholke and Vogt, 1979). An alternative view, based on sedimentary structures, fossil contents, and geochemistry interpreted the chalk interval as a mass-wasting deposit derived from the North Atlantic margin (Norris and Firth, 2002). At both sites, the upper boundary of the chalk with the overlying lithology has been tied to the K/T boundary, but only at Site 386 is an ejecta layer present. It is a green spherule-rich layer that shows a Pt/Ir signature, which strongly supports an impact origin and a K/T age for the sequence (Norris and Firth, 2002).

Calcareous microfossils are rare to absent, but fish debris is quite abundant. Nonetheless, the presence of some key nannofossil and agglutinated benthic foraminifera allowed for a low-resolution biozonation of some of the Late Cretaceous horizons (Okada and Thierstein, 1979; Kuhnt, 1992; Norris and Firth, 2002). At Site 386, an upper Cenomanian/ early Turonian age was assigned between ~738 mbsf (meters below sea floor) and ~724 mbsf based on the recognition of Oceanic Anoxic Event 2 (OAE2) (Jiménez Berrocoso et al, 2009) and the first occurrence (FO) of agglutinated foraminifera *Uvigerinammina jankoi* above the Cenomanian/Turonian boundary (Kuhnt and Moullade, 1991). Based on the last occurrence (LO) of *U. jankoi* (Kuhnt et al, 1992) a Turonian/mid Campanian age is assigned between ~724 mbsf and ~642 mbsf. Mid/upper Maastrichtian is present between ~639 mbsf ~636 mbsf based on shipboard identification of calcareous nannofossils *Micula mura* and *Lithraphidites quadratus*

(Okada and Thierstein, 1979) and lithologic interpretation of the K/T boundary (Norris and Firth, 2002). Above this level, samples are assumed to be Paleocene in age. At Site 387, between ~474 mbsf and ~471 mbsf, the FO of *Tetralithus trifidus* (Okada and Thierstein, 1979) suggests an age of upper Campanian/ early Maastrichtian. From ~471 mbsf to ~445 mbsf, we assigned an early Maastrichtian/ late Maastrichtian age based on the identification of FO of *M. micura* (Okada and Thierstein, 1979) and the lithological characterization of the K/T boundary (Norris and Firth, 2002). Superjacent the K/T boundary, samples are assumed to be Paleocene in age.

4.2.2. SOUTHERN (TROPICAL) TRANSECT

The Demerara Rise described in chapter 3 represents the shallow end of the southern transect. Site 367 represents the abyssal end of our tropical transect. It was drilled during Deep Sea Drilling Program (DSDP) leg 41 and is located at the base of the continental rise, in the Cape Verde Basin (figure 4.1). The Upper Cretaceous was spot cored; therefore, specific details about thickness, gaps, and sedimentation rates are difficult to estimate. The Maastrichtian is assumed to be contained within a unit dominated by multicolored silty clay with sharp boundaries that was deposited below the CCD (Lancelot and Seibold, 1977). A relatively low resolution age model was constructed based on biostratigraphic observations of calcareous nannofossils, agglutinated benthic foraminifera, and identifications of critical intervals such as Oceanic Anoxic Event 2 (OAE2). (Cepek, 1978; Holbourn et al, 1999; Forster et al, 2007; Jiménez Berrocoso et al, 2009). A Turonian/Campanian age is assigned between ~636 mbsf and ~548 mbsf based on the recognition of OAE2 (Jiménez Berrocoso et al, 2009)

and the presence of *U. jankoi* (Houlborn et al, 1999). Early Campanian/ mid Campanian is identified between ~548 mbsf and ~479 mbs based on the LO of *U. jankoi* (Houlborn et al, 1999). Between ~479 mbsf and ~474 mbsf the presence of *Caudammina* (*Hormosina) gigantea* (Houlborn et al, 1999) allows us to assign a mid Campanian-Maastrichtian age to this interval. Cepek (1978) identified the base of nannofossil biozone NP12 at ~378 mbsf; therefore higher samples are assigned a Paleocene age. The K/T boundary occurs in an approximately 85 m thick coring gap between cores 14 and 15.

4.3. MATERIALS AND METHODS

New samples for this study concentrated on Maastrichtian and Danian intervals with the goal of getting the same degree of resolution that was acquired for Demerara Rise (where available) and extending the record to abyssal depths.

A total of thirty-nine samples (25 from Blake Nose, 5 from Bermuda Rise, and 9 from Cape Verde) were selected for the development of this study. Additionally, values from Bourbon (2008), MacLeod et al (2008), and (Jiménez Berrocoso et al, 2009) Jiménez Berrocoso et al (2009) were added to the pool data in order to get a more complete representation of North Atlantic intermediate and deep water evolution. Samples were obtained from the Integrated Ocean Drilling Program (IODP) core repository and were approximately 10 cm^3 each. The bulk sediment was dried overnight in an oven at 50°C, then disaggregated by soaking overnight in a beaker containing kerosene, followed by decanting and adding Calgon solution. The resulting slurry was washed on a 63 μm screen. To increase picking efficiency, where present, foraminifera

and other carbonates grains were dissolved using a buffered 10% acetic acid. The insoluble residue was thoroughly rinsed and washed again in a 63 μm screen. Fish debris was relatively common in all sample residues and approximately 0.5 mg of fish debris was used for analysis.

Nd isotopes were analyzed using a Nu Plasma Multi-Collector-Inductively Coupled Plasma-Mass Spectrometer (MC-ICP-MS) at the University of Florida Isotope laboratory in the Geology department. The samples were dissolved in 0.3 ml of 2% optima HNO_3 then 10μl was pipetted out and placed in a sampling beaker and diluted with 0.99 ml of 2% optima HNO_3. Samples were then scanned on the MC-ICP-MS. JNdi-1 standard was run every 6 samples to obtain a daily average for the standard (Bourbon, 2008). This average was compared to the long-term running average of the JNdi-1 standard from the TIMS (Micromass Sector 54 Thermal Ionization Mass Spectrometer) of ~0.512103 (± 0.000012, 2σ) in order to determine a correction factor for all samples run on that day. The long term error for the Nd MC-ISP-MS is determined by comparing the corrected JNdi-1 values. The calculated 2σ error varies on a daily basis, but the long-term 2σ error is ~0.3 ε units (Bourbon, 2008).

As mentioned previously, age models for the Maastrichtian at Blake Nose are well resolved. However, in the abyssal sites, ages are difficult to constrain because coring gaps introduced considerable uncertainty in the precise depth of the few available datums. As a result, neodymium data are presented against depth (meters below sea floor), but the plots are annotated with the low resolution age estimates in order to compare our results to previous isotopic data from other ocean basins.

Most importantly, conclusions regarding $\varepsilon_{Nd(t)}$ isotopic trends through the sections on all sites are not dependent on the age model. That is, association of data and depth to relative ages are more than enough to test observations regarding North Atlantic evolution during the Maastrichtian.

4.4. RESULTS

Samples from the upper bathyal Site 1050C in the Blake Nose exhibit a gradual increase to more radiogenic values with $\varepsilon_{Nd(t)}$ ranging from ~-6.5 (Cenomanian), ~-8.6 (Mid Campanian) to ~-7.5 (close to the K/T boundary). After the Cretaceous/Tertiary interval $\varepsilon_{Nd(t)}$ values decrease to mid Danian where we observe low radiogenic signatures of -9.7. A tendency toward more radiogenic signatures is again observed in the highest samples analyzed (figure 4.2) (Appendix 3).

Sites 386 and 387 extend the Blake Nose to abyssal depths. Despite poor age control, both sites show that in the abyssal depths in the subtropical North Atlantic, $\varepsilon_{Nd(t)}$ values maintain a range between -8 to -7 units through most of the Late Cretaceous, but somewhere between the Upper Maastrichtian and Danian there is a sharp shift to less radiogenic values of -11 (figure 4.3) (appendix 3) similar to the post K/T shift in the Blake Nose (figure 4.2).

Demerara Rise values (chapter 3) (figure 4.4) showed that between the early Maastrichtian and mid Danian, $\varepsilon_{Nd(t)}$ values of fish debris from three sites shift by ~6 units from -17 to -11, where the extremely low values during the early Maastrichtian are similar to most other Late Cretaceous values for Demerara Rise and suggest

intermediate to deep water formation, the post mid Maastrichtian values suggest a switch in the source of the deep/intermediate water.

The Cape Verde Site 367 is the abyssal end member of our tropical transect in the tropical Atlantic and extends the Demerara Rise values to true deep depth. Age resolution is poor due to extensive coring gaps and minimum biostratigraphic control, but as noted combined data from Bourbon (2008), Jiménez Berrocoso et al (2009), and this study show that between the Cenomanian and Campanian/Maastrichtian the basin exhibits $\varepsilon_{Nd(t)}$ values between -8 to -10. Then, during the Campanian-Maastrichtian the basin shows a shift towards very low radiogenic values (-13 to -15) that return to more radiogenic (-9.5 to -11) by the Paleocene (figure 4.5) (appendix 3).

4.5. DISCUSSION

Neodymium records derived from the four study sites representing different regions and different depths of the North Atlantic demonstrate large differences among the sites and within the sites through time. Some trends are observed to be parallel between bathyal and abyssal sites, whereas at other times trends are distinct. These differences suggest multiple water masses were present during the Late Cretaceous and their distribution changed through time. Although considerable uncertainty remains, these records greatly increase controls on the source and circulation patterns of intermediate and deep water masses in the Late Cretaceous North Atlantic.

During the Cenomanian, in the subtropical transect, the deep Bermuda Rise site has $\varepsilon_{Nd(t)}$ values between -8 and -9 while the shallow Blake Nose site exhibits a more

radiogenic signature of -6, suggesting at least two water masses separated at depth. Following the Cenomanian, similar values (-9) are observed at both sites, suggesting homogenization with respect to its source from the Cenomanian on. Values of $\varepsilon_{Nd(t)}$ of -7 to -9 have been reported for fish debris and other phosphates from shelf deposits of the Northwestern Tethys (Pucéat et al, 2005)and central Tethys (Soudry et al, 2006). Similar values of -8.5 to -9 have been reported from the South Atlantic (Robinson and Vance, 2009) whereas, contemporary central Pacific $\varepsilon_{Nd(t)}$ values range from -2.5 to -5.5 (Frank et al, 2005). These low Pacific values mixed with Tethyan or South Atlantic waters could explain low values at Site 1050C during the Cenomanian. The lower values at the Bermuda Rise though, suggest the deep subtropical North Atlantic basin may have been dominated by a water mass that originated in the Tethyan or South Atlantic region. Because paleogeographic reconstructions show that connections between the North Atlantic and South Atlantic were very restricted during the Cenomanian and the Bermuda Rise was closer to the Tethys than to the South Atlantic, we think that Bermuda Rise deep waters were more likely sourced largely within the North Atlantic-Tethyan region (figure 4.6). By the Campanian this deep water mass seems to have expanded into bathyal depths with one possible cause being the restriction of the gateway between North and South America, which coincides with the time where "cool" greenhouse conditions started (Huber et al, 2002).

In the tropical sites, values between bathyal (Demerara) and abyssal (Cape Verde) are different for most of the Cenomanian-Campanian interval, and only converge during the Campanian-Maastrichtian. The only exception to this pattern is that both sites exhibit a positive excursion to $\varepsilon_{Nd(t)}$ values of ~-8 at the level of OAE2 event (MacLeod et al,

2008; Jiménez Berrocoso et al, 2009). During the Cenomanian-Campanian interval, the Cape Verde site $\varepsilon_{Nd(t)}$ values are about -9, similar to those at Bermuda Rise and raising the possibility of a Tethyan source for deep waters at this site. At the same time Demerara Rise sites show an unusually non-radiogenic signature (-16 to -17) that has been interpreted as evidence of a locally formed intermediate water mass "Demerara Bottom Water Maas" (DBWM), that persisted in the region until at least mid Maastrichtian time (MacLeod et al, 2008, Chapter 3).

Addition of the Cape Verde abyssal data to the North Atlantic data set show that very low radiogenic values were also present at >3 km depth during the Campanian-Maastrichtian (figure 4.5). Cape Verde is the extension of the Demerara transect to abyssal depth, therefore the shift could demonstrate that the DBWM reached true deep-water depths during this time period. A second possibility would be a different water mass with similar isotopic characteristics to those in DBWM filled the Cape Verde Basin.

Many features and sedimentary sequences show strong parallels on the African and South American side of the North Atlantic. In particular Cape Verde Site 367 presents similar succession of Mesozoic facies to those described in the western North Atlantic (Hollister et al, 1972; Lancelot and Seibold, 1978), and river particles from the western margin of Africa exhibit $\varepsilon_{Nd(t)}$ values that varied from -27 to -19 similar to those sourced on the Guayana shield (Jeandel et al, 2007). That is, if there was a water mass formed due to excess evaporation in African seaways, it might be characterized by very non radiogenic values similar to the ones suggested for the DBWM. Either way, the fact that these very low radiogenic signatures are observed from bathyal to abyssal depths in

the tropical North Atlantic suggests rather directly that deep water formation at low latitudes was active during the Late Cretaceous (Chamberlin, 1906; Brass et al, 1982; MacLeod and Huber, 1996) contrary to the conclusions of modeling studies (D'Hondt and Arthur, 1996; Bice and Marotzke, 2001; D'Hondt and Arthur, 2002).

The most interesting aspect of this research is observed during the Maastrichtian/ Danian interval, where all sites at both transects shift towards ε_{Nd} values between -9 to -11. These results fall near the ε_{Nd} North Atlantic Deep Water (NADW) values (-10 to -13) established by Frank et al (2003) for the last 33 million years. Therefore, we believe that this multisite shift provides the first direct line of evidence for the timing of the reorganization of deep water circulation from a Cretaceous type to a Cenozoic type (figure 4.6)

4.6. IMPLICATIONS

Neodymium data from two depths transects in the subtropical and tropical North Atlantic from bathyal to abyssal depths demonstrate that during most of the Late Cretaceous the main source of intermediate/deep water was likely the Tethyan region and the Demerara Region. The data also support the much debated hypothesis first proposed by Chamberlin (1906) that greenhouse ocean circulation could have been driven in part by low latitude intermediate/deep water formation. These results also suggest dynamic and active patterns of intermediate and deep water circulation contrary to the idea for a sluggish Late Cretaceous ocean.

REFERENCES

Barrera, E., and Savin, S.M., 1987. Effect of sample preparation on the delta p18sO-value of fine- grained calcite: Chemical Geology (Isotope Geoscience Section), v. 66, p. 301-305.

Barrera, E., and Keller, G., 1990. Stable isotope evidence for gradual environmental changes and species survivorship across the Cretaceous/Tertiary boundary: Paleoceanography, v. 5, p. 867-890.

Barrera, E., and Savin, S.M., 1999. Evolution of late Campanian-Maastrichtian marine climates and oceans: Evolution of the Cretaceous Ocean-Climate System, v. 332, p. 245-282.

Barron, E.J., and Peterson, W.H., 1989. Model simulation of the cretaceous ocean circulation: Science, v. 244, p. 684-686.

Bertram, C.J., and Elderfield, H., 1993. The geochemical balance of the rare earth elements and neodymium isotopes in the oceans: Geochimica et Cosmochimica Acta, v. 57, p. 1957-1986.

Bice, K.L., Barron, E.J., and Peterson, W.H., 1997. Continental runoff and early Cenozoic bottom-water sources: Geology, v. 25, p. 951-954.

Bice, K.L., and Marotzke, J., 2001. Numerical evidence against reversed thermohaline circulation in the warm Paleocene/Eocene ocean: Journal of Geophysical Research C: Oceans, v. 106, p. 11529-11542.

Bice, K.L., and Norris, R.D., 2002. Possible atmospheric CO_2 extremes of the Middle Cretaceous (late Albian-Turonian): Paleoceanography, v. 17, p. 22-1 - 22-17.

Bourbon, É., 2008. Nd isotopes throughout the North Atlantic in the Late Cretaceous and across the Oceanic Anoxic Event 2: M.S. Thesis. Geological Sciences. Gainesville, University of Florida.

Brady, E.C., DeConto, R.M., and Thompson, S.L., 1998. Deep water formation and Poleward Ocean heat transport in the warm climate extreme of the Cretaceous (80 Ma): Geophysical Research Letters, v. 25, p. 4205-4208.

Brass, G.W., Southam, J.R., and Peterson, W.H., 1982. Warm saline bottom water in the ancient ocean: Nature, v. 296, p. 620-623.

Broecker, W.S., and Peng, T.H., 1982. Tracers in the sea: Lamont-Doherty Geological Observatory, p. 690.

Cepek, P., 1978. Mesozoic calcareous nannoplankton of the eastern North Atlantic, Leg. 41: Initial Reports of the Deep Sea Drilling Project 41, p. 667-688.

Chamberlin, T.C., 1906. On a possible reversal of deep-sea circulation and its influence on geologic climates: J. Geol., v. 14, p. 363-373.

Corfield, R.M., and Norris, R.D., 1996, Deep water circulation in the Paleocene Ocean, Geological Society Special Publication, p. 443-456.

D'Hondt, S., and Arthur, M.A., 1996. Late cretaceous oceans and the cool tropic paradox: Science, v. 271, p. 1838-1841.

—, 2002. Deep water in the late Maastrichtian ocean: Paleoceanography, v. 17, p. 8-1-8-11.

DePaolo, D.J., and Wasserburg, G.J., 1976. Inferences about magma source and mantle structure from variation of 143Nd/144 Nd: Geophys Res Lett, v. 3, p. 743746.

Elderfield, H., and Greaves, M.J., 1982. The rare earth elements in seawater: Nature, v. 296, p. 214-219.

Elderfield, H., and Pagett, R., 1986. Rare earth elements in ichthyoliths: Variations with redox conditions and depositional environment: Science of the Total Environment, The, v. 49, p. 175-197.

Forster, A., Schouten, S., Moriya, K., Wilson, P.A., Sinninghe, D., and Jaap, S., 2007. Tropical warming and intermittent cooling during the Cenomanian/Turonian oceanic anoxic event 2: Sea surface temperature records from the equatorial Atlantic: Paleoceanography, v. 22.

Frank, M., 2002. Radiogenic isotopes: Tracers of past ocean circulation and erosional input: Rev. Geophys., v. 40.

Frank, M., van de Flierdt, T., Halliday, A.N., Kubik, P.W., Hattendorf, B., and G√ºnther, D., 2003. Evolution of deepwater mixing and weathering inputs in the central Atlantic Ocean over the past 33 Myr: Paleoceanography, v. 18, p. 15-1.

Frank, T.D., and Arthur, M.A., 1999, Tectonic forcings of Maastrichtian ocean-climate evolution, *in* Arthur, M.A., ed., Paleoceanography, Volume 14: United States, American Geophysical Union : Washington, DC, United States, p. 103.

Frank, T.D., Brown, P.R., Jones, K., Lees, J.A., Thomas, D.J., Leckie, R.M., and Arthur, M.A., 2005. The Maastrichtian record from Shatsky Rise (northwest Pacific): A tropical perspective on global ecological and oceanographic changes: Paleoceanography, v. 20, p. 1-14.

Friedrich, O., Erbacher, J., Moriya, K., Wilson, P.A., and Kuhnert, H., 2008. Warm saline intermediate waters in the Cretaceous tropical Atlantic Ocean: Nature Geosci, v. 1, p. 453-457.

Goldstein, S.L., and Hemming, S.R., 2003. Long-lived isotopic tracers in oceanography, paleoceanography, and ice-sheet dynamics: Treatise on Geochemistry, v. 6, p. 453-489.

Holbourn, A., Kuhnt, W., El Albani, A., Ly, A., Gomez, R., and Herbin, J.P., 1999. Palaeoenvironments and palaeobiogeography of the Late Cretaceous Casamance transect (Senegal, NW Africa): Distribution patterns of benthic foraminifera, organic carbon and terrigenous flux: Neues Jahrbuch fur Geologie und Palaontologie - Abhandlungen, v. 212, p. 335-377.

Hollister, C.D., Ewing, J.I., Habib, D., Hathaway, J.C., Lancelot, Y., Luterbacher, H., Paulus, F.J., et al., 1972. Init. Rep. Deep Sea Drilling Project (DSDP).

Huber, B.T., Norris, R.D., and MacLeod, K.G., 2002. Deep-sea paleotemperature record of extreme warmth during the Cretaceous: Geology, v. 30, p. 123-126.

Huber, B.T., MacLeod, K.G., and Tur, N.A., 2008. Chronostratigraphic Framework For Upper Campanian-Maastrichtian Sediments On The Blake Nose (Subtropical North Atlantic): Journal of Foraminiferal Research, v. 38, p. 162-182.

IPCC, 2008. Climate Change 2007: The Physical Science Basis: Contribution of Working Group I to the Fourth Assessment Report of the Intergovernmental Panel on Climate Change [Solomon, S., D. Qin, M. Manning, Z. Chen, M. Marquis, K.B. Averyt, M. Tignor and H.L. Miller (eds.)]. Cambridge University Press, Cambridge, United Kingdom and New York, NY, USA, 996 pp.

Jeandel, C., Bishop, J.K., and Zindler, A., 1995. Exchange of neodymium and its isotopes between seawater and small and large particles in the Sargasso Sea: Geochimica et Cosmochimica Acta, v. 59, p. 535-547.

Jeandel, C., Arsouze, T., Lacan, F., Téchiné, P., and Dutay, J.C., 2007. Isotopic Nd compositions and concentrations of the lithogenic inputs into the ocean: A compilation, with an emphasis on the margins: Chemical Geology, v. 239, p. 156-164.

Jenkyns, H.C., Gale, A.S., and Corfield, R.M., 1994. Carbon- and oxygen-isotope stratigraphy of the English Chalk and Italian Scaglia and its palaeoclimatic significance: Geology Magazine, v. 131, p. 1-34.

Jiménez Berrocoso, A., MacLeod, K.G., Martin, E.E., Bourbon, E., Basak, C., and Isaza-Londoño, C., 2009. Water-mass changes in the western tropical North Atlantic across the Cenomanian (Late Cretaceous) inferred from bioapatite Nd isotopes (in review).

Klaus, A., Norris, R.D., Kroon, D., and Smit, J., 2000. Impact-induced mass wasting at the K-T boundary: Blake Nose, western North Atlantic: Geology, v. 28, p. 319-322.

Kuhnt, W., and Moullade, M., 1991. Quantitative analysis of Upper Cretaceous abyssal agglutinated foraminiferal distribution in the North Atlantic - paleoceanographic implications: Revue de Micropaleontologie, v. 34, p. 313-349.

Kuhnt, W., 1992. Abyssal recolonization by benthic foraminifera after the Cenomanian/Turonian boundary anoxic event in the North Atlantic: Marine Micropaleontology, v. 19, p. 257-274.

Lancelot, Y., and Seibold, E., 1977. Site 367: Cape Verde Basin: Init. Rep. DSDP, v. 41, p. 163-232.

—, 1978. The evolution of the central northeastern Atlantic - Summary of results of DSDP Leg 41: Initial Reports of the Deep Sea Drilling Project, v. 41, p. 1215-1245.

MacLeod, K.G., and Huber, B.T., 1996. Reorganization of deep ocean circulation accompanying a late Cretaceous extinction event: Nature, v. 380, p. 422-425.

MacLeod, K.G., Kucera, M., Huber, B.T., Pletsch, T., and Röhl, U., 2001. Maastrichtian foraminiferal and paleoceanographic changes on Milankovitch timescales: Paleoceanography, v. 16, p. 133-154.

MacLeod, K.G., Fullagar, P.D., and Huber, B.T., 2003. $^{87}Sr/^{86}Sr$ test of the degree of impact-induced slope failure in the Maastrichtian of the western North Atlantic: Geology, v. 31, p. 311-314.

MacLeod, K.G., Huber, B.T., and Ducharme, M.L., 2004. Paleontological and geochemical constraints on changes in the deep ocean during the Cretaceous greenhouse interval: Warm Climates in Earth History.

MacLeod, K.G., Martin, E.E., and Blair, S.W., 2008. Nd isotopic excursion across Cretaceous ocean anoxic event 2 (Cenomanian-Turonian) in the tropical North Atlantic: Geology, v. 36, p. 811-814.

Martin, E.E., 2000, Fossil fish teeth as proxies for seawater Sr and Nd isotopes, *in* Haley, B.A., ed., Geochimica et Cosmochimica Acta, Volume 64: International, Pergamon : Oxford, International, p. 835.

Martin, E.E., and Haley, B.A., 2000. Fossil fish teeth as proxies for seawater Sr and Nd isotopes: Geochimica et Cosmochimica Acta, v. 64, p. 835-847.

Martin, E.E., and Scher, H.D., 2004. Preservation of seawater Sr and Nd isotopes in fossil fish teeth: bad news and good news: Earth and Planetary Science Letters, v. 220, p. 25-39.

Norris, R.D., Kroon, D., Klaus, A., and et al., 1998. Proceedings of the Ocean drilling program, initial reports, 171B, Ocean Drilling program, College Station, TX.

Norris, R.D., Firth, J., Blusztajn, J.S., and Ravizza, G., 2000. Mass failure of the North Atlantic margin triggered by the Cretaceous-Paleogene bolide impact: Geology, v. 28, p. 1119-1122.

Norris, R.D., and Firth, J.V., 2002. Mass wasting of Atlantic continental margins following the Chicxulub impact event: Catastrophic Events and Mass Extinctions: Impacts and Beyond, v. 356, p. 79-95.

Okada, H., and Thierstein, H.R., 1979. Calcareous nannoplankton-Leg 43, Deep Sea Drilling Project: Initial Reports of the Deep Sea Drilling Project, v. 43, p. 507-573.

Piepgras, D.J., and Wasserburg, G.J., 1980. Neodymium isotopic variations in seawater: Earth and Planetary Science Letters, v. 50, p. 128-138.

—, 1985. Strontium and neodymium isotopes in hot springs on the East Pacific Rise and Guaymas Basin: Earth and Planetary Science Letters, v. 72, p. 341-356.

Poulsen, C.J., Seidov, D., Barron, E.J., and Peterson, W.H., 1998. The impact of paleogeographic evolution on the surface oceanic circulation and the marine environment within the mid-Cretaceous Tethys: Paleoceanography, v. 13, p. 546-559.

Pucéat, E., Lecuyer, C., and Reisberg, L., 2005. Neodymium isotope evolution of NW Tethyan upper ocean waters throughout the Cretaceous: Earth and Planetary Science Letters, v. 236, p. 705-720.

Pucéat, E., Lécuyer, C., Donnadieu, Y., Naveau, P., Cappetta, H., Ramstein, G., Huber, B.T., and Kriwet, J., 2007. Fish tooth $\delta^{18}O$ revising Late Cretaceous meridional upper ocean water temperature gradients: Geology, v. 35, p. 107-110.

Robinson, S.A., and Vance, D., 2009. The Nd-isotopic composition of late Cretaceous bathyal–abyssal seawater from fossil fish skeletal debris: Geophysical Research Abstracts, v. Vol. 11, EGU2009-5320, 2009.

Royer, D.L., 2006. CO_2-forced climate thresholds during the Phanerozoic: Geochimica et Cosmochimica Acta, v. 70, p. 5665-5675.

Soudry, D., Glenn, C.R., Nathan, Y., Segal, I., and VonderHaar, D., 2006. Evolution of Tethyan phosphogenesis along the northern edges of the Arabian-African shield

during the Cretaceous-Eocene as deduced from temporal variations of Ca and Nd isotopes and rates of P accumulation: Earth-Science Reviews, v. 78, p. 27-57.

Stott, L.D., and Kennett, J.P., 1990. The paleoceanographic and paleoclimatic signature of the Cretaceous/Paleogene boundary in the Antarctic: stable isotopic results from ODP Leg 113: Proc., scientific results, ODP, Leg 113, Weddell Sea, Antarctica, p. 829-848.

Tachikawa, K., Jeandel, C., and Roy-Barman, M., 1999. A new approach to the Nd residence time in the ocean: The role of atmospheric inputs: Earth and Planetary Science Letters, v. 170, p. 433-446.

Tachikawa, K., Athias, V., and Jeandel, C., 2003. Neodymium budget in the modern ocean and paleo-oceanographic implications: Journal of Geophysical Research C: Oceans, v. 108, p. 10-1.

Thomas, D.J., 2003, Neodymium isotopic reconstruction of late Paleocene-early Eocene thermohaline circulation, *in* Bralower, T.J., and Jones, C.E., eds., Earth and Planetary Science Letters, Volume 209: Netherlands, Elsevier : Amsterdam, Netherlands, p. 309.

—, 2005, Reconstructing ancient deep-sea circulation patterns using the Nd isotopic composition of fossil fish debris, Special Paper - Geological Society of America, Volume 395: United States, Geological Society of America (GSA) : Boulder, CO, United States, p. 1.

Tucholke, B.E., and Vogt, P.R., 1979. Introduction and explanatory notes, Leg 43 Deep Sea Drilling Project, (western North Atlantic): Initial reports of the Deep Sea Drilling Project, Leg 43, Istanbul, Turkey to Norfolk, Virginia, 1975, (Scripps Institution of Oceanography; UK distributors IPOD Committee, NERC, Swindon), p. 5-28.

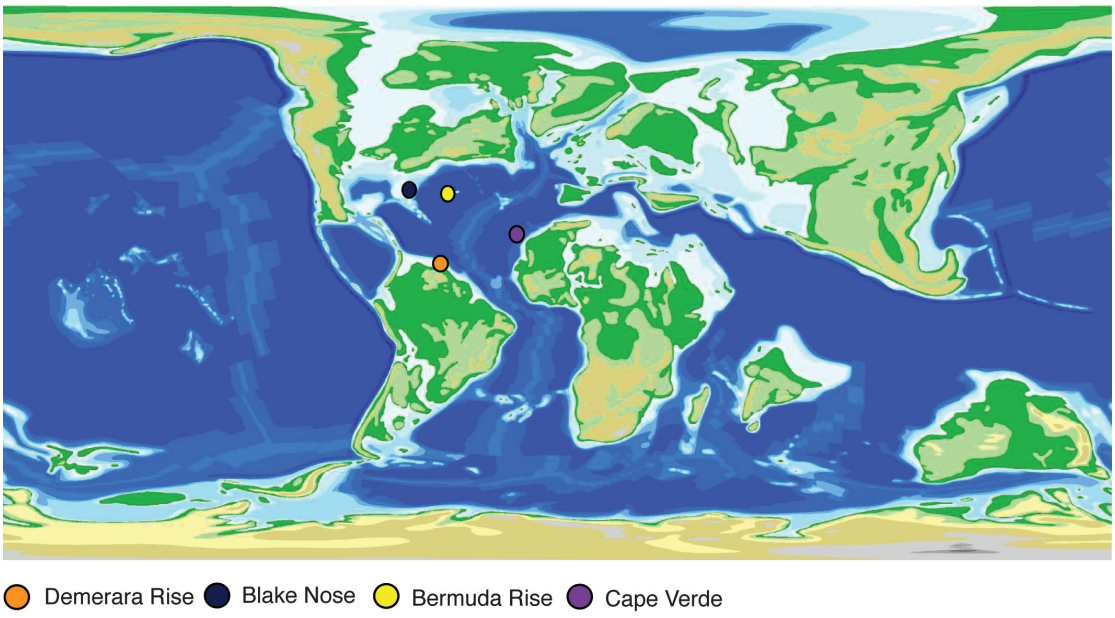

Figure 4.1. Approximate location of the study sites. Tropical transect Site 1050C (Blake Nose) and Sites 386-387 (Bermuda Rise. Subtropical transect Sites 1258-1260-1261 (Demerara Rise), and Site 367 (Cape Verde).

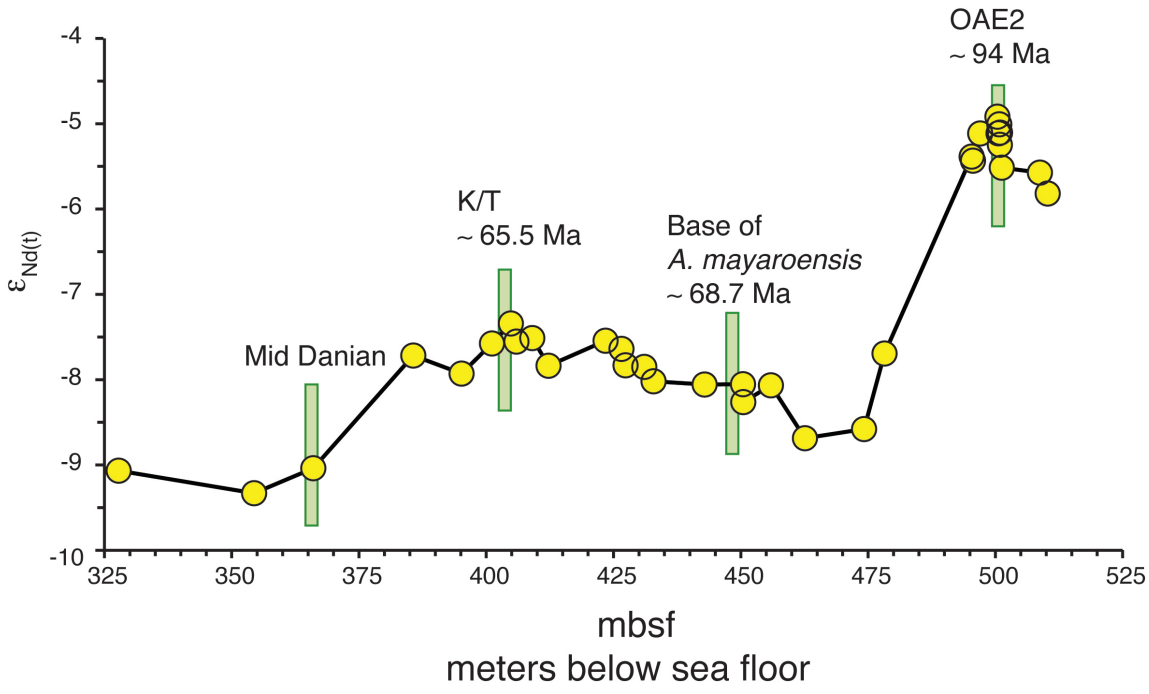

Figure 4.2. Evolution of the $\varepsilon_{Nd(t)}$ signature in the Subtropical bathyal site 1050C, in the Blake Nose. $\varepsilon_{Nd(t)}$ ranging from ~-6.5 (Cenomanian) to ~-8.6 (Mid Campanian) to ~-7.5 (close to the K/T boundary). After the Cretaceous/Tertiary interval $\varepsilon_{Nd(t)}$ values decrease to mid Danian where we observe low radiogenic signatures of -9.3. (see discussion for interpretations)

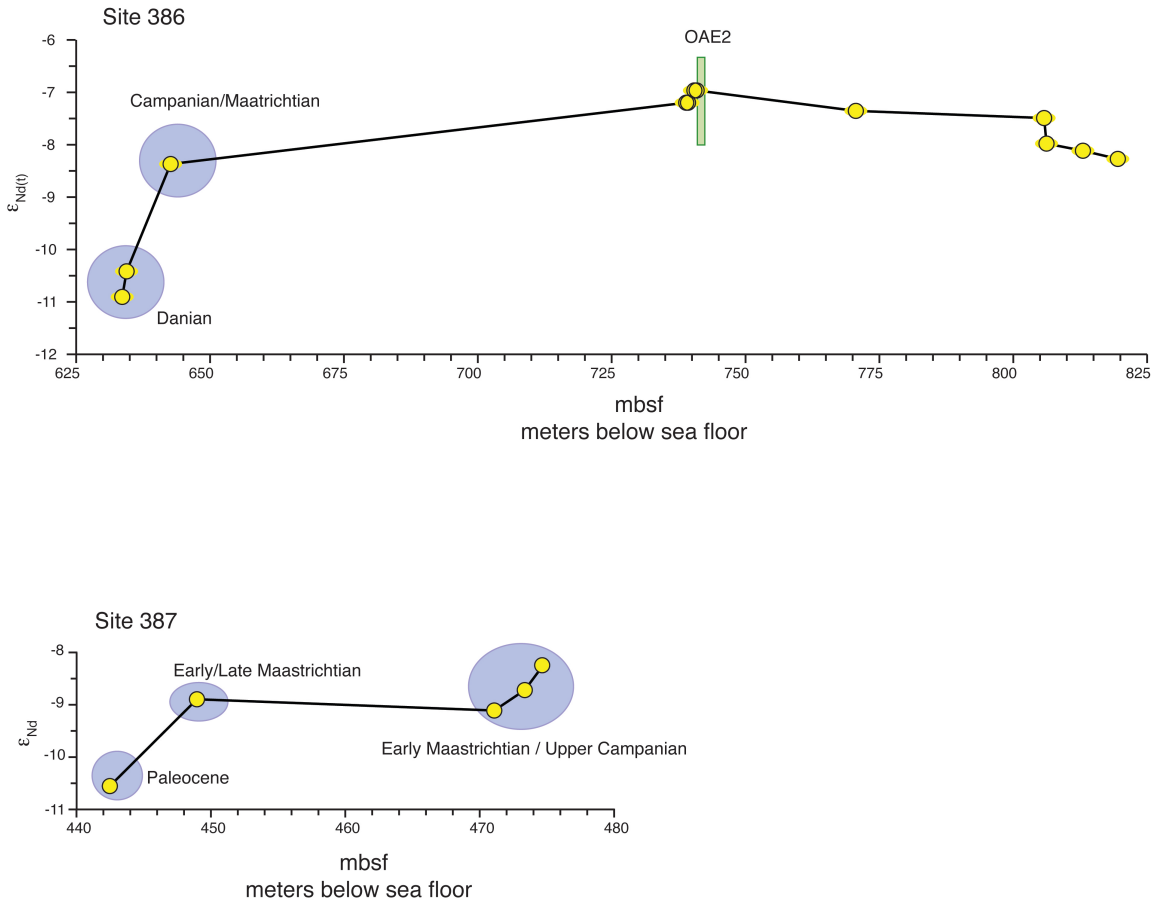

Figure 4.3. Evolution of the $\varepsilon_{Nd(t)}$ signature in the Subtropical abyssal sites 386-387 in the Bermuda Rise. $\varepsilon_{Nd(t)}$ values maintain a range between -8 to -7 units through most of the Late Cretaceous, but somewhere between the Upper Maastrichtian and Danian there is a sharp shift to less radiogenic values of -11 similar to the post K/T shift in the Blake Nose. (see discussion for interpretations)

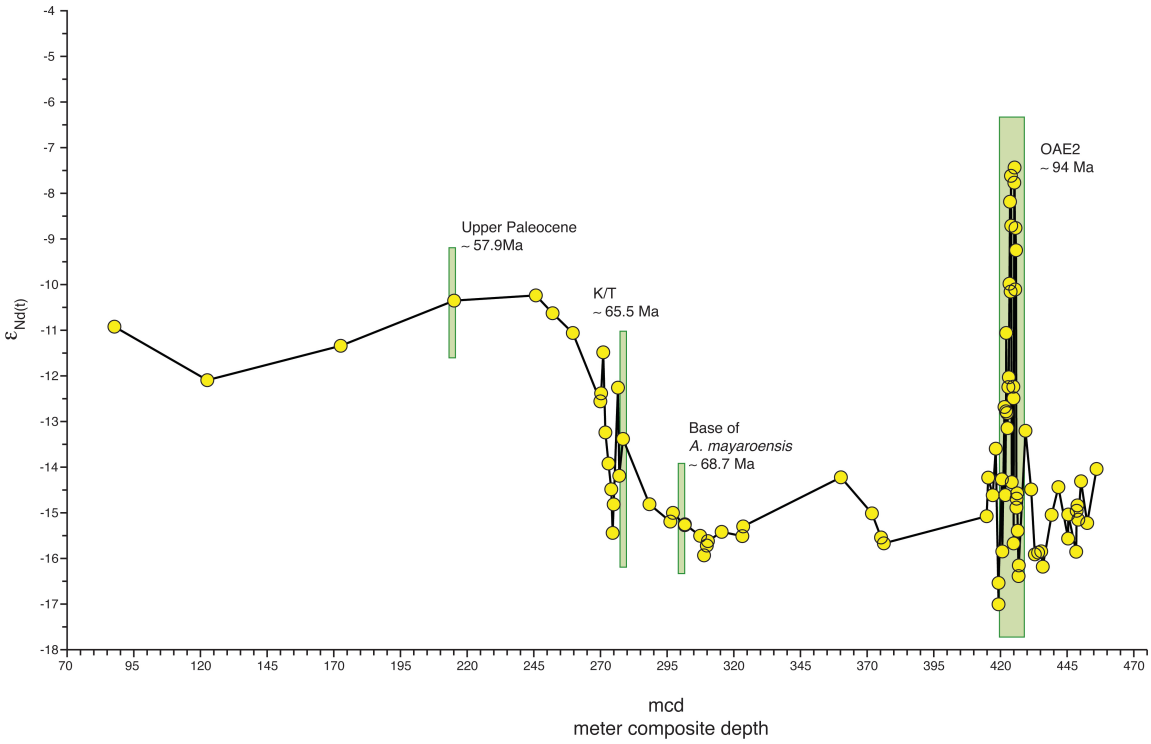

Figure 4.4. Evolution of the $\varepsilon_{Nd(t)}$ signature in the Tropical bathyal site 1258, in the Demerara Rise. $\varepsilon_{Nd(t)}$ values showed that between the early Maastrichtian and mid Danian, $\varepsilon_{Nd(T)}$ values of fish debris from three sites shift by ~6 units from -17 to -11 (chapter 3). Where the extremely low values during the early Maastrichtian are similar to most other Late Cretaceous values for Demerara Rise and suggest intermediate to deep water formation. The post mid Maastrichtian values suggest a switch in the source of the deep/intermediate water. Even though there are interesting differences among the sites in the Demerara Rise (Chapter 3) the general trend is expressed in similar ways at the three sites. Therefore, for purpose of generalization only site 1258 is showed.

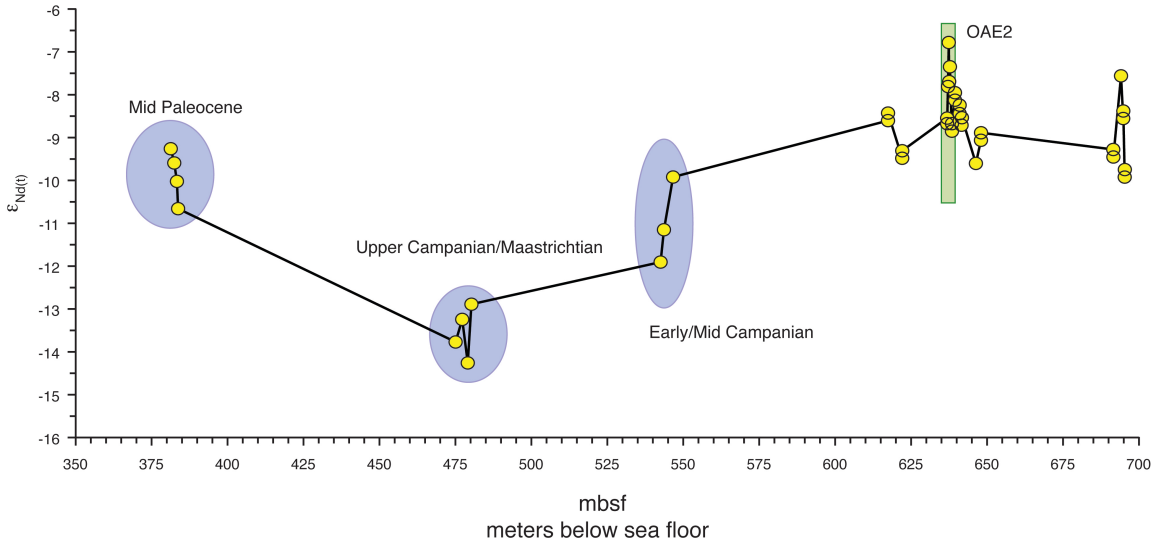

Figure 4.5. Evolution of the $\varepsilon_{Nd(t)}$ signature in the Tropical abyssal site 376, in Cape Verde. Between the Cenomanian and Campanian-Maastrichtian the basin exhibits $\varepsilon_{Nd(t)}$ values between -9 to -10. Then, during the Campanian-Maastrichtian the basin shows a shift towards very low radiogenic values (-13 to -15), then returns to more radiogenic (-9.5 to -11) by the Paleocene (see discussion for interpretations)

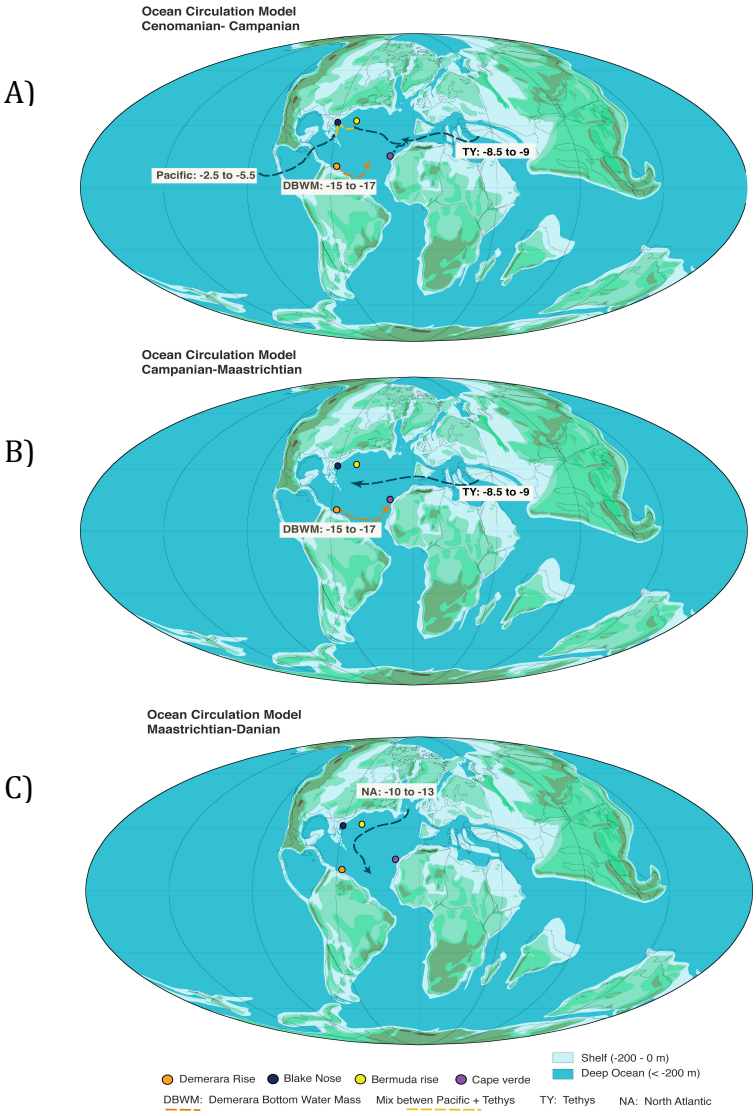

Figure 4.6. Circulation Model for the North Atlantic Basin during the Late Cretaceous based on $\varepsilon_{Nd(t)}$ isotopes. A) During the Cenomanian-Campanian main sources for deep/intermediate water formation were the Tethys Ocean and the tropical North Atlantic (Demerara). Both abyssal sites are dominated by a Tethys component. Bathyal Blake Nose is dominated by a mixture of Pacific and Tethys waters, and Demerara sites are dominated by DBWM. B) During the Campanian-Maastrichtian, water at the abyssal and bathyal sites in the Subtropical transect becomes homogenized with respect to its source (Tethyan Ocean). In the tropical transect, $\varepsilon_{Nd(t)}$ values in the abyssal site become less radiogenic, indicating the possibility of DBWM reaching deep depths. C) Sometime between the Maastrichtian-Danian all sites at all depth switch to radiogenic values typical of North Atlantic water, suggesting a switch in the sources of deep/intermediate water from a Cretaceous type (low latitude formation) to a Tertiary type (high latitude formation).

CHAPTER 5

IMPLICATIONS

Knowledge of past climates can provide important lessons about current and future climate evolution. Knowledge of climate evolution is a particularly pressing issue in light of the current debate about climatic change in our immediate future. Furthermore, global climate changes may be rapid or slow, and different components of the climate system could dampen or amplify the signals on either regional or global scales. Because of these uncertainties, it is important to recognize and to separate both global and regional components (oceanic and atmospheric) in order to understand the sensitivity of the climate system. The Intergovernmental Panel on Climate Change (IPCC, 2008) recognized that global warming could have a dramatic effect on thermohaline circulation, and, as we move towards a new greenhouse word, it is important to understand how ocean circulation might respond to this warming. Questions regarding how stable present climate is, and what might be the effects of rapid climate change in the biosphere can be answered by looking at the natural experiment that is the history of past climates in the geologic record. For the immediate future, studying warm intervals in the geologic past is especially important as these times provide the only empirical record of ocean circulation during greenhouse conditions.

As noted in previous chapters, the Late Cretaceous is widely recognized as a time of extreme high temperatures and high CO_2 levels (Jenkyns, 1994; Huber et al, 2002;

MacLeod et al, 2004; Royer, 2006). As climate is the result of redistribution of heat (from incoming solar radiation) by the flow of the air and ocean system on the rotating earth, it is influenced by geographic setting determined by the arrangement of land and sea, depth of the oceans and ocean gateways. Cretaceous paleogeography had many differences from the present, and this, combined with high pCO_2 levels is expected to result in ocean circulation and thermal gradients (horizontal and vertical) during this interval that were different from what we see in modern times (Barron and Peterson, 1989; Bice et al, 1997; Poulsen et al, 1998; Barrera and Savin, 1999).

Divergent temperature trends among ocean basins are observed during the Maastrichtian, the last 7 million years of the Cretaceous. Notably, the North Atlantic basin shows a 3 million year long warming trend of approximately 6°C whereas the other basins show cooling (MacLeod et al, 2005; Isaza-Londoño et al, 2006). To explain this difference as well as a number of other Maastrichtian events, changes in the intermediate and/or deep water sources have been invoked (Barrera et al, 1997; Frank and Arthur, 1999; MacLeod et al, 2005). Details vary among study sites with primary differences residing in source regions for intermediate and deep waters as well as cause and effects relationships at local scales (MacLeod et al, 2005; Isaza-Londoño et al, 2006).

The research presented in the previous 3 chapters provides the first of its kind empirical data regarding evolution of Maastrichtian surface to deep ocean circulation in the North Atlantic, and provides compelling evidence that helps solve regional and global uncertainties such as the regional warming trend in the North Atlantic and the source of deep water formation in the Maastrichtian ocean. Specifically, we demonstrate the

presence of deep water forming at low latitudes during the Late Cretaceous and the presence of an apparently sharp water mass boundary in the subtropical western North Atlantic throughout the Maastrichtian.

For surface waters, through parallel examination of foraminiferal populations and stable isotopes we argued that a well established Water Mass Boundary (WMB) was present in the subtropical western North Atlantic throughout the Maastrichtian (Chapter 2). Furthermore, we were able both to narrow the position of the WMB to 40 km (distance between the study sites) and also to demonstrate that this WMB migrated both on short and long time scales. In regards to regional observations, though, it seems that surface water circulation patterns were not a not a big influence in North Atlantic warming at this time. The presence of a strong, relatively stable WMB throughout the Maastrichtian (and present), at the same time that significant regional change through Maastrichtian is observed, demonstrates that WMB change is not needed for regional change. In fact, a strong WMB seems to be a persistent feature of the North Atlantic occurring both across the Maastrichtian and in the present. So, while changes in the strength and/or position of do not correlate with regional warming of the North Atlantic during the Maastrichtian, models attempting to capture significant features of Maastrichtian surface ocean circulation should create a sharp WMB in the western North Atlantic.

Regarding deep ocean circulation, the neodymium records derived from four study sites representing different regions and different depths of the North Atlantic demonstrate large differences among the sites and within the sites through the Late

Cretaceous. Specifically, we argued, based on the data in chapters 3 and 4, that low Pacific values mixed with Tethyan or South Atlantic waters could explain relatively high values at bathyal Site 1050 in the subtropical North Atlantic during the Cenomanian-Campanian (figure 5.1). The lower values at the deeper Bermuda Rise sites, though, suggest the deep subtropical North Atlantic basin may have been dominated by a water mass that originated in the Tethyan or South Atlantic region. Because paleogeographic reconstructions show that connection between the North Atlantic and South Atlantic were very restricted during the Cenomanian and because Bermuda Rise was closer to the Tethys than to the South Atlantic, we think that Bermuda Rise deep waters were more likely sourced within the North Atlantic-Tethyan region than the South Atlantic (figure 5.1). In the tropical North Atlantic, $\varepsilon_{Nd(t)}$ values in the abyssal Cape Verde site are similar to those in the Bermuda Rise, so we think that the Tethys was also the source of deep water in this deep site. On the other hand, the very low values in Demerara sites at this time are interpreted as reflecting a separate, low-latitude-sourced, intermediate water mass (MacLeod et al, 2008). These results demonstrate that during the Cenomanian-Campanian interval at least three different water masses were active in the North Atlantic, one sourced in the Tethyan region dominated the subtropical and tropical North Atlantic at abyssal depths, while its mixture with Pacific waters resulted in a different water mass at subtropical bathyal depths. The third water mass (Demerara Bottom Water Mass [DBWM]) mass dominated the intermediate/surface waters in the tropical North Atlantic.

During the Campanian-Maastrichtian, deep water masses from Bermuda Rise seem to have expanded to bathyal depths at Blake Nose (figure 5.1). During this interval

there was a restriction of the gateway between North and South America that could have blocked waters coming from the Pacific (Mann et al, 2007) allowing the homogenization of the subtropical North Atlantic with respect to the Tethyan source. In the tropical North Atlantic, $\varepsilon_{Nd(t)}$ values in the abyssal site Cape Verde show that very low values were present at depths greater that 3 km indicating the possibility of DBWM reaching deep depths during this time interval (figure 5.1). A second possibility would be a different water mass with similar isotopic characteristics that those in DBWM filled the Cape Verde Basin. Either way, the fact that these very low values are observed from bathyal to abyssal depths in the tropical North Atlantic suggest rather directly that deep water formation at low latitudes was active during the Late Cretaceous (Chamberlin, 1906; Brass et al, 1982; MacLeod and Huber, 1996) contrary to the conclusions of modeling studies (D'Hondt and Arthur, 1996; Bice and Marotzke, 2001; D'Hondt and Arthur, 2002).

An interesting aspect of this research is observed during the Maastrichtian - Danian interval, where all sites at both transects shift towards $\varepsilon_{Nd(t)}$ values between -9 to -11(figure 5.1). These results fall near the $\varepsilon_{Nd(t)}$ of North Atlantic values of -10 to -13 for the last 33 million year (Frank et al, 2003). Furthermore, the high resolution time/depth trends observed in the Demerara Rise sites (chapter 3) demonstrate that the positive $\varepsilon_{Nd(t)}$ shift (6 units) was initiated during the mid Maastrichtian at the level of the base of the *Abathomphalus mayaroensis* foraminifera biozone.

If this shift is the result of initiation and/or intensification of formation of high latitude deep water masses (similar isotopically to Cenozoic North Atlantic water

masses), it could result in export of relatively cool waters from the North Atlantic to the South Atlantic at depth. To compensate, warm tropical waters could flow northward from the South Atlantic into the North Atlantic generating a heat piracy affect and leading to the regional warming previously mentioned (MacLeod et al, 2005; Isaza-Londoño et al, 2006). Deep water formation at low latitudes imply rates of evaporations in the subtropics were high enough to create saline warm waters dense enough to sink to abyssal depths. High evaporation in the subtropics, in turn, implies large changes in the hydrological cycles potentially including higher poleward latent heat transport and more precipitation at high latitudes. Warmth at depth would also result in changes in the distribution of oxygen in the ocean and therefore could affect marine productivity and faunal distribution.

All combined (surface and deep water results), indicates that the Maastrichtian was a transitional time where a dramatic reorganization on ocean circulation took place. Our data demonstrate that surface and especially intermediate and deep water circulation patterns are an important (and measurable) variable that help determine greenhouse temperature distributions on regional and global scales. This finding is important for current environmental discussions because, as a consequence of global warming, IPCC pCO_2 estimates for 2100 are similar to those observed in the Maastrichtian, raising the possibility for reversal in ocean circulation from high latitude to low latitude sources of deep water directly affecting climate, ocean/land ecosystems, and human activities in general. At the simplest level, this possibility suggests the a future greenhouse North Atlantic could see deep water forming at low latitudes in the next 100 years. Some of the effects would be increase of temperatures in the poles, a decrease of latitudinal thermal

gradients, and changes in ocean circulation and productivity all of which would have a direct effect on human life. A more measured statement of the implication of this study is that coupled Ocean-Atmospheric Global Circulation Models that can reproduce the patterns of circulation inferred through the Maastrichtian given changing forcing (i.e., pCO_2) arguably have the best chance of accurately predicting future climate evolution.

REFERENCES

Barrera, E., Savin, S.M., Thomas, E., and Jones, C.E., 1997. Evidence for thermohaline-circulation reversals controlled by sea-level change in the latest Cretaceous: Geology, v. 25, p. 715-718.

Barron, E.J., and Peterson, W.H., 1989. Model simulation of the cretaceous ocean circulation: Science, v. 244, p. 684-686.

Bice, K.L., Barron, E.J., and Peterson, W.H., 1997. Continental runoff and early Cenozoic bottom-water sources: Geology, v. 25, p. 951-954.

Bice, K.L., and Marotzke, J., 2001. Numerical evidence against reversed thermohaline circulation in the warm Paleocene/Eocene ocean: Journal of Geophysical Research C: Oceans, v. 106, p. 11529-11542.

Brass, G.W., Southam, J.R., and Peterson, W.H., 1982. Warm saline bottom water in the ancient ocean: Nature, v. 296, p. 620-623.

Chamberlin, T.C., 1906. On a possible reversal of deep-sea circulation and its influence on geologic climates: J. Geol., v. 14, p. 363-373.

D'Hondt, S., and Arthur, M.A., 1996. Late cretaceous oceans and the cool tropic paradox: Science, v. 271, p. 1838-1841.

—, 2002. Deep water in the late Maastrichtian ocean: Paleoceanography, v. 17, p. 8-1-8-11.

Frank, M., van de Flierdt, T., Halliday, A.N., Kubik, P.W., Hattendorf, B., and Günther, D., 2003. Evolution of deepwater mixing and weathering inputs in the central Atlantic Ocean over the past 33 Myr: Paleoceanography, v. 18, p. 15-1.

Frank, T.D., and Arthur, M.A., 1999, Tectonic forcings of Maastrichtian ocean-climate evolution, *in* Arthur, M.A., ed., Paleoceanography, Volume 14: United States, American Geophysical Union : Washington, DC, United States, p. 103.

Huber, B.T., Norris, R.D., and MacLeod, K.G., 2002. Deep-sea paleotemperature record of extreme warmth during the Cretaceous: Geology, v. 30, p. 123-126.

IPCC, 2008. Climate Change 2007: The Physical Science Basis: Contribution of Working Group I to the Fourth Assessment Report of the Intergovernmental Panel on Climate Change [Solomon, S., D. Qin, M. Manning, Z. Chen, M. Marquis, K.B. Averyt, M. Tignor and H.L. Miller (eds.)]. Cambridge University Press, Cambridge, United Kingdom and New York, NY, USA, 996 pp.

Isaza-Londoño, C., MacLeod, K.G., and Huber, B.T., 2006. Maastrichtian North Atlantic warming, increasing stratification, and foraminiferal paleobiology at three timescales: Paleoceanography, v. 21.Jenkyns, H.C., Gale, A.S. and Corfield, R.M, 1994. Carbon- and oxygen-isotope stratigraphy of the English Chalk and Italian Scaglia and its palaeoclimatic significance: Geology Magazine, v. 131, p. 1-34.

MacLeod, K.G., and Huber, B.T., 1996. Reorganization of deep ocean circulation accompanying a late Cretaceous extinction event: Nature, v. 380, p. 422-425.

MacLeod, K.G., Huber, B.T., and Ducharme, M.L., 2004. Paleontological and geochemical constraints on changes in the deep ocean during the Cretaceous greenhouse interval: Warm Climates in Earth History.

MacLeod, K.G., Huber, B.T., and Isaza-Londoño, C., 2005. North Atlantic warming during global cooling at the end of the Cretaceous: Geology, v. 33, p. 437-440.

MacLeod, K.G., Martin, E.E., and Blair, S.W., 2008. Nd isotopic excursion across Cretaceous ocean anoxic event 2 (Cenomanian-Turonian) in the tropical North Atlantic: Geology, v. 36, p. 811-814.

Mann, P., Rogers, R., and Gahagan, L., 2007. Overview of plate tectonic history and its unsolved tectonic problem: Central America: Geology, Resources, and Natural Hazards, p. 205-241.

Poulsen, C.J., Seidov, D., Barron, E.J., and Peterson, W.H., 1998. The impact of paleogeographic evolution on the surface oceanic circulation and the marine environment within the mid-Cretaceous Tethys: Paleoceanography, v. 13, p. 546-559.

Royer, D.L., 2006. CO2-forced climate thresholds during the Phanerozoic: Geochimica et Cosmochimica Acta, v. 70, p. 5665-5675.

O'Nions, R.K., Frank, M., Von Blanckenburg, F., and Ling, H.F., 1998. Secular variation of Nd and Pb isotopes in ferromanganese crusts from the Atlantic, Indian and Pacific Oceans: Earth and Planetary Science Letters, v. 155, p. 15-28.

Pucéat, E., Lecuyer, C., and Reisberg, L., 2005. Neodymium isotope evolution of NW Tethyan upper ocean waters throughout the Cretaceous: Earth and Planetary Science Letters, v. 236, p. 705-720.

Soudry, D., Glenn, C.R., Nathan, Y., Segal, I., and VonderHaar, D., 2006. Evolution of Tethyan phosphogenesis along the northern edges of the Arabian-African shield during the Cretaceous-Eocene as deduced from temporal variations of Ca and Nd isotopes and rates of P accumulation: Earth-Science Reviews, v. 78, p. 27-57.

Thomas, D.J., 2004. Evidence for deep-water production in the North Pacific Ocean during the early Cenozoic warm interval, v. 430, p. 65-68

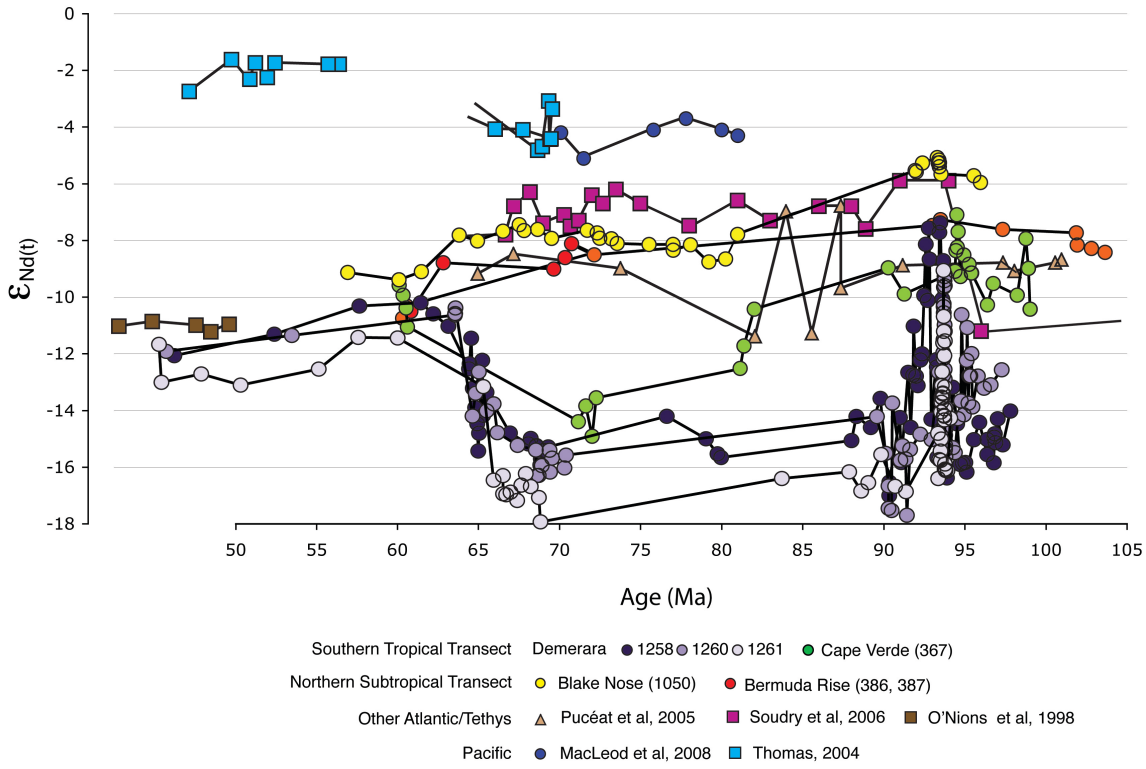

Figure 5.1. Evolution of Neodymium ($\varepsilon_{Nd(t)}$) values through the Late Cretaceous, in several ocean basins. The data demonstrate the presence of different waters masses and sources through time (see text for description of trends).

APPENDIX 1

FORAMINIFERA COUNTS, AND STABLE ISOTOPES HOLES 1050C AND 1052E

Species counts Hole 1050C Section 13R-5

meter below sea floor (mbsf)	cm in core	Benthics	*Archaeoglobigerina sp.*	*Contusotruncana contusa*	*Contusotruncana walfischensis*	*Gansserina wiedenmayeri*	*Globigerinelloides prairiehillensis*	*Globigerinelloides subcarinatus*	*Globigerinelloides sp.*	*Globigerinelloides ultimicrus*	*Globotruncana aegyptiaca*	*Globotruncana arca*	*Globotruncana bulloides*	*Globotruncana dupueblei*	*Globotruncana esnehensis*	*Globotruncana falsostuarti*	*Globotruncana mariey*	*Globotruncana orientalis*	*Globotruncana rosetta*
429.55	25	1					3	5			12	56			18	1	31	5	8
429.60	30	5	6	2	1	2		3		4	30	82					66		4
429.65	35	2	6			4	3	5			3	41		1	2		23	4	1
429.70	40	3	4	1							2	54		1	8			5	1
429.75	45	2		1			13	5			8	89		4	9	1	24	10	2
429.80	50	3	7					1			36	42		7	19		36	15	2
429.85	55	5	10								25	172			10			40	
429.90	60	3		3			6	13	2		18	103	1		11			15	10
429.95	65	4	16	2				12			3	49		1	3		20		
430.00	70	5						9											
430.05	75	2	30	2				16			6	42		2	10		20		2
430.15	85	4	12					7			38	55		1	3	1	52	4	1
430.20	90						11	16	13		14	46			6			8	1
430.25	95		7			5					10	60		9	6		22	9	9
430.30	100	1				3	2	11			4	39			4		5	4	5
430.35	105	5	10	1		2		4			16	19		3	3		13		3
430.40	110	2		3			8	4	1		11	71	3	1	4			13	6
430.50	120	4	17	1		3	1	3			21	45			2		31	8	
430.55	125	6		1			25	16	20		3	58		2	5			8	4

meter below sea floor (mbsf)	cm in core	*Globotruncana sp.*	*Globotruncanella minuta*	*Globotruncanella petaloidea*	*Globotruncanita pettersi*	*Globotruncanita stuarti*	*Globotruncanita stuartiformis*	*Globotruncanita conica*	*Gublerina acuta*	*Hedbergella sp.*	*Heterohelix globulosa*	*Heterohelix navarroensis*	*Heterohelix moremanni*	*Heterohelix planata*	*Heterohelix punctulata*	*Heterohelix sphenoides*	*Heterohelix sp.*	*Laeviheterohelix dentata*	*Laeviheterohelix glabrans*	*Planoglobulina acervulinoides*	*Planoglobulina multicamerata*
429.55	25			17			1				74	9		2					5		3
429.60	30		3	47		1	1		2		172	34		4	1	1			2		1
429.65	35			16			3				40	27		16					2		4
429.70	40			5		2	3				56	8		7	2				7		3
429.75	45			27		2						14		6					1		2
429.80	50			13							95	18		33	1				4		3
429.85	55		4	20		2	1				116			7	2				3		
429.90	60			18	2	3	3				114	1		15	4	20	2		4		3
429.95	65			18		2	1				89	19		16					1		2
430.00	70			24															5		1
430.05	75			26		3	3				85			8					1		1
430.15	85			10		2	3				54	8		6	1	2			1		2
430.20	90			37			5			13	125		6	6	6	73	1		33		1
430.25	95			16		1	2			13	131	7		6					2	1	2
430.30	100			13		1	4				73	20		35	1				4		4
430.35	105			18			1				61	8		12	2						1
430.40	110			28	1		3			2	106		1	5	2	10		1	15		1
430.50	120			30		1					70	12		30	4				2	1	
430.55	125	2		11		4	2	1		5	132	1	1	18		77			32		4

meter below sea floor (mbsf)	cm in core	*Pseudoguembelina costulata*	*Pseudoguembelina excolata*	*Pseudoguembelina hariaensis*	*Pseudoguembelina carinata*	*Pseudoguembelina palpebra*	*Pseudotextularia elegans*	*Pseudotextularia intermedia*	*Pseudotextularia nuttali*	*Racemiguembelina fructicosa*	*Rugoglobigerina hexacamerata*	*Rugoglobigerina millamensis*	*Rugoglobigerina rugosa*	*Rugoglobigerina sp.*	*Trinitella scotti*	Total planktics
429.55	25	13				1	2	13	14	21						314
429.60	30	30				6	49	16	34	20	5		2	1		631
429.65	35				0	4	23	6	20	19	3					276
429.70	40	8	4				7	10	11	29	2					240
429.75	45	18		2		12	12	24	8	24						318
429.80	50	16				3	29	9		34	8					431
429.85	55	18				3	25	17	12	22	3		1			513
429.90	60	7		3			19	5	23	32	10	1	2	5		478
429.95	65	4				6	7	16	13	11			1			312
430.00	70					4	23	18	4	13			2			103
430.05	75	14				4	17	21	15	27	17					372
430.15	85	9				6	27	23	8	69	12		3			420
430.20	90			1		2	2	2	17	13	29	1		4	1	493
430.25	95	10			0	1	25	25	10	22	13		1			425
430.30	100	4	3			3	27	10		33	5					317
430.35	105	4				2	13	4	3	9	10					222
430.40	110			3			8	4	22	31	25			10		403
430.50	120	9				2	22	5	6	27	7		1			361
430.55	125	3		4		3	8	10	12	24	20	2				519

Species counts Hole 1050C Section 16R-2
(MacLeod et al 2001)

meter below sea floor (mbsf)	cm in core	Benthics	*Archaeoglobigerina* sp.	*Contusotruncana contusa*	*Contusotruncana walfischensis*	*Gansserina wiedenmayeri*	*Globigerinelloides prairiehillensis*	*Globigerinelloides subcarinatus*	*Globigerinelloides ultimicrus*	*Globotruncana aegyptiaca*	*Globotruncana arca*	*Globotruncana dupueblei*	*Globotruncana esnehensis*	*Globotruncana falsostuarti*	*Globotruncana linneiana*	*Globotruncanella havanensis*	*Globotruncanella minuta*	*Globotruncanella petaloidea*	*Globotruncanita pettersi*
453.95	25	5	5	1	2	2	1	12	4	2	51		18	1	5			10	
454.00	30	9	13	1	1	1		12	7	1	59		20	1	2			14	
454.05	35	4	9	1				9	3		35		27		2		5	13	2
454.10	40	4	10				10	20	6		42		11					17	1
454.15	45	13	6				2	16	5		38	1	24					8	
454.20	50	2		1			1	15	6		34		50					13	
454.25	55	7	6				3	14	7		21		30	1	3			7	
454.30	60	9	25					17	16		37		6		1			18	
454.35	65	4	7	1			2	23	8	1	27		25		1	1		20	
454.40	70	7	19	1				30	13		11		15	4				20	
454.45	75	11	13			1	7	18	11	1	22		22	5	2			13	
454.50	80	8	17				1	4	6	2	35		28	6	6			12	
454.53	83	8	3		1		2	7	11	2	50	4	22	1	1	3		10	
454.55	85	9	14		1		1	9	3	9	36		28		10	1		15	
454.60	90	9	12	3	2			4	1	2	46	2	37		4			7	
454.65	95	10	1				2	17	16	5	25		24	3	3			15	
454.70	100	9	10		4		4	17	10	3	19		15		9			11	
454.75	105	5	8		3	1	9	23	1	1	45	1	19		4		3	12	
454.80	110	9	17	1	1		4	15	5		44		16		2	1		15	
454.85	115	9	3	1	2		3	14	6		17		22			2		15	
454.90	120	7	8	3	1		2	7	4	7	34		34	7	6	3		11	
455.95	125	5	20	4	2		3	10	12	1	64		38		6	1		39	

meter below sea floor (mbsf)	cm in core	*Globotruncanita stuartiformis*	*Gublerina acuta*	*Hedbergella monmouthensis*	*Heterohelix globulosa*	*Heterohelix navarroensis*	*Heterohelix planata*	*Heterohelix semicostata*	*Laeviheterohelix glabrans*	*Planoglobulina acervulinoides*	*Planoglobulina multicamerata*	*Pseudoguembelina costulata*	*Pseudoguembelina excolata*	*Pseudoguembelina kempensis*	*Pseudoguembelina palpebra*	*Pseudotextularia elegans*	*Pseudotextularia intermedia*	*Pseudotextularia nuttali*	*Racemiguembelina fructicosa*
453.95	25	6		5	108	8	2			1	3	4	2		1	6	3	4	3
454.00	30	15		7	168	16	1		1	2	2	2		3	3	8	2	3	3
454.05	35	7		10	136	10	4		2		2				6	3		10	3
454.10	40	3		6	139	12	8		10	1		3			3		1	5	1
454.15	45	7		5	135	1	8		5		1	4			4	3	3	13	4
454.20	50	4	1	5	130	7	3		4		6	3	1	2	7	1		6	
454.25	55	4		3	117	8	1		2		1		1	2		1	3	4	6
454.30	60	3		2	127	17	1				1	5			3	3	3	6	3
454.35	65	7		4	140	14	6	2	7	6	1				1	3		8	1
454.40	70	3		3	112	24	11	1	11	1				1	1	2		9	2
454.45	75	6		1	116	19	14	4	8	1	1					3	3	6	3
454.50	80	6		2	109	16	12	3	2		3		3		6	1	2	7	
454.53	83	6	1	4	154	14	1		5		2		2	3	2	7	2	7	1
454.55	85	4	4	2	113	18	3				1		8	1	6	1	1	15	5
454.60	90	4		3	113	5	4			2	1				6	3	5	22	8
454.65	95	3	1	1	124	14	23		1	1	1	1	1		2	1		5	2
454.70	100	11		9	133	10	18		1		2			2	2	1		7	1
454.75	105	1		8	135	11	5		6	1	1	1		1	3	1	1	4	3
454.80	110	5		4	122	15	2		4	1			1		3	5		4	1
454.85	115	8		5	131	18	18		5			1	4		3	2	2	18	2
454.90	120	10	1		96	18	9				4	5	3	1	4	5	1	16	2
455.95	125	8		9	180	18	3		3					3	3	11	10	10	3

meter below sea floor (mbsf)	cm in core	*Rugoglobigerina hexacamerata*	*Rugoglobigerina rugosa*	*Trinitella scotti*	*Schackoina multispinata*	Total planktics
453.95	25	5	3			278
454.00	30	9	7			384
454.05	35	9	9			317
454.10	40	1	4			314
454.15	45	2	4			299
454.20	50	17	7	1		325
454.25	55	21	31	3		300
454.30	60	8	5			307
454.35	65	2	4			322
454.40	70	6	11			311
454.45	75	4	13	1		318
454.50	80	10	1			300
454.53	83	5	1			334
454.55	85	6	5			320
454.60	90	7	7			310
454.65	95	6	13	2		313
454.70	100	13	9			321
454.75	105	9	5			326
454.80	110	13	6			307
454.85	115	6	11	2		321
454.90	120	5	6	3		316
455.95	125	8	6		1	476

Counts at generic level (normalized)
Hole 1050C, section 13R-5

meter below sea floor (mbsf)	cm in core	*Archaeoglobigerina* spp.	*Contusotruncana* spp.	*Globigerinelloides* spp.	*Globotruncana* spp.	*Globotruncanella* spp.	*Globotruncanita* spp.	*Hedbergella* spp.	*Heterohelix* spp.	*Laeviheterohelix* spp.	*Planoglobulina* spp.	*Pseudoguembelina* spp.	*Pseudotextularia* spp.	*Racemiguembelina* spp.	*Rugoglobigerina* spp.	benthic	Total
429.55	25	0	0	8	125	16	1	0	81	5	3	13	28	20	0	0	300
429.60	30	5	0	11	113	16	0	0	102	5	2	3	20	20	2	2	300
429.65	35	7	0	9	83	18	3	0	92	2	4	4	54	21	3	0	300
429.70	40	5	1	0	89	6	6	0	91	9	4	15	35	36	3	0	300
429.75	45	0	1	12	106	11	2	0	115	4	1	6	16	18	8	1	300
429.80	50	5	0	1	109	9	0	0	102	3	2	13	26	24	6	0	300
429.85	55	6	0	0	144	14	2	0	73	2	0	12	32	13	2	0	300
429.90	60	0	0	9	111	16	1	0	108	1	1	13	13	17	11	0	300
429.95	65	15	2	12	73	17	3	0	119	1	2	10	35	11	1	0	300
430.00	70	0	0	11	122	17	0	0	82	1	0	4	33	13	14	1	300
430.05	75	24	2	13	66	21	5	0	75	1	1	15	43	22	14	0	300
430.10	80	0	3	4	139	9	6	0	53	0	1	3	43	38	1	0	300
430.15	85	9	0	3	123	18	3	0	85	1	3	6	22	17	8	2	300
430.20	90	0	0	3	124	19	2	4	92	0	3	4	23	21	4	0	300
430.25	95	5	0	0	89	11	2	9	103	1	2	8	43	16	10	0	300
430.30	100	0	0	12	58	12	5	0	123	4	4	10	35	32	5	0	300
430.35	105	14	1	5	78	25	1	0	113	0	1	8	27	12	14	0	300
430.40	110	0	0	6	134	10	0	0	66	4	3	6	29	14	29	0	300
430.50	120	14	1	3	90	25	1	0	97	2	1	9	28	23	7	0	300
430.55	125	0	0	8	101	7	1	0	98	8	4	16	23	21	9	2	300

Counts at generic level (normalized)
Hole 1050C, section 16R-2

meter below sea floor (mbsf)	cm in core	*Archaeoglobigerina* spp.	*Contusotruncana* spp.	*Gansserina* spp.	*Globigerinelloides* spp.	*Globotruncana* spp.	*Globotruncanella* spp.	*Globotruncanita* spp.	*Hedbergella* spp.	*Heterohelix* spp.	*Laeviheterohelix* spp.	*Planoglobulina* spp.	*Pseudoguembelina* spp.	*Pseudotextularia* spp.	*Racemiguembelina* spp.	*Rugoglobigerina* spp.	other	Benthics	Total
453.95	25	5	3	2	18	82	11	6	5	125	0	4	7	14	3	8	0	5	300
454.00	30	10	2	1	15	63	11	11	5	141	1	3	6	10	2	12	0	7	300
454.05	35	8	1	0	11	60	17	8	9	140	2	2	6	12	3	17	0	4	300
454.10	40	9	0	0	34	50	16	4	6	150	9	1	6	6	1	5	0	4	300
454.15	45	6	0	0	22	61	8	7	5	138	5	1	8	18	4	6	0	13	300
454.20	50	0	1	0	20	77	12	4	5	128	4	6	12	6	0	22	2	2	300
454.25	55	6	0	0	23	54	7	4	3	123	2	1	3	8	6	51	3	7	300
454.30	60	24	0	0	31	42	17	3	2	138	0	1	8	11	3	12	0	9	300
454.35	65	6	1	0	30	50	19	6	4	149	6	6	1	10	1	6	0	4	300
454.40	70	18	1	0	41	28	19	3	3	140	10	1	2	10	2	16	0	7	300
454.45	75	12	0	1	33	47	12	5	1	140	7	2	0	11	3	16	1	10	300
454.50	80	17	0	0	11	75	12	6	2	136	2	3	9	10	0	11	0	8	300
454.53	83	3	1	0	18	70	11	5	4	148	4	2	6	14	1	5	1	7	300
454.55	85	13	1	0	12	76	15	4	2	122	0	1	14	16	5	10	4	8	300
454.60	90	11	5	0	5	86	7	4	3	115	0	3	6	28	8	13	0	8	300
454.65	95	1	0	0	33	56	14	3	1	150	1	2	4	6	2	18	3	9	300
454.70	100	9	4	0	28	42	10	10	8	146	1	2	4	7	1	20	0	8	300
454.75	105	7	3	1	30	63	14	1	7	137	5	2	5	5	3	13	0	5	300
454.80	110	16	2	0	23	59	15	5	4	132	4	1	4	9	1	18	0	9	300
454.85	115	3	3	0	21	35	15	7	5	152	5	0	7	20	2	15	2	8	300
454.90	120	7	4	0	12	82	13	9	0	114	0	4	12	20	2	10	4	7	300
455.95	125	12	4	0	16	68	25	5	6	125	2	0	4	19	2	9	1	3	300

Counts at generic level (normalized)
Hole 1050C, section 18R-2

meter below sea floor (mbsf)	cm in core	*Archaeoglobigerina* spp.	*Contusotruncana* spp.	*Gansserina* spp.	*Globigerinelloides* spp.	*Globotruncana* spp.	*Globotruncanella* spp.	*Globotruncanita* spp.	*Hedbergella* spp.	*Heterohelix* spp.	*Laeviheterohelix* spp.	*Planoglobulina* spp.	*Pseudoguembelina* spp.	*Pseudotextularia* spp.	*Racemiguembelina* spp.	*Rugoglobigerina* spp.	benthic	Total
473.10	20	24	4	6	8	169	7	5	0	66	5	0	1	0	0	3	2	300
473.25	35	9	5	12	1	238	0	8	0	22	0	2	2	0	0	0	2	300
473.45	55	19	2	24	7	177	3	12	1	48	2	2	1	0	0	1	2	300
473.70	80	13	2	15	0	224	2	5	0	30	0	6	2	1	0	0	2	300
473.90	100	6	2	19	1	244	0	8	0	14	0	3	1	0	0	0	3	300
474.00	110	13	2	9	5	209	2	4	0	50	0	3	1	0	0	0	2	300
474.20	130	16	2	11	16	171	8	13	0	45	2	4	7	2	0	1	1	300

Species counts Hole 1052C Section 26R and 29R

Core	meter below sea floor (mbsf)	cm in core	Benthics	*Archeoglobigerina cretacea*	*Archaeglobigerina mayaroensis*	*Archeoglobigerina blowi*	*Contusotruncana contusa*	*Contusotruncana patelliformis*	*Gansserina widenmayeri*	*Globigerinolloides prairihillensis*	*Globigerinolloides subcarinatus*	*Globigerinolloides ultramicrus*	*Globotruncana aegyptiaca*	*Globotruncana arca*	*Globotruncana dupueblei*	*Globotruncana esnehensis*	*Globotruncana falsostuarti*	*Globotruncana linelliana*
26R-3	380.38	28	5	25			0		0	0	14	4	7	28	0	1	0	0
26R-3	381.20	110	7	25			2		11		3	2	15	76		1		
26R-3	381.30	120	0	12			1	1	13				8	58				
26R-4	382.18	50	3	61		1	1		2		11	4	23	96	1			
26R-4	382.91	130	2	31		1			6	2	15	2	2	37				
26R-4	383.00	140	1	28	5				7		11	3	18	29	1		1	
29R-1	406.55	65	9	27	0	0	1	0	15	2	4	5	2	114	7		5	3
29R-1	407.05	115	5	30			7		17		1		3	68	1		1	
29R-2	407.55	15	1	21					16				10	169	3			1
29R-2	407.85	45	5	60					13	5	7	8		57				
29R-3	408.55	115	7	34			1		7	3	2	5	4	64			1	
29R-3	409.15	25	5	25			8		16	2		3	4	149	2		1	

Core	meter below sea floor (mbsf)	cm in core	*Globotruncana lobata*	*Globotruncana mariey*	*Globotruncana orientalis*	*Globotruncana ventricosa*	*Globotruncanella minuta*	*Globotruncanella petaloidea*	*Globotruncanella Pschadea*	*Globotruncanita conica*	*Globotruncanita stuarti*	*Globotruncanita stuartiformis*	*Hedbergella monmouthensis*	*Heterolix globulosa*	*Heterolix navarroensis*	*Heterolix planata*	*Heterolix punctulata*	*Heterohelix moremani*
26R-3	380.38	28		21	2		7	27	1		1		1	82	18	19	1	
26R-3	381.20	110		16	4		3	4	2		2	5	4	123	23	30	5	
26R-3	381.30	120		21	7			3		1	1	5	1	94	7	25	3	
26R-4	382.18	50		17	7	1		16				1	8	169	34	40	1	
26R-4	382.91	130		14	2			34	4				2	164	25	24	5	
26R-4	383.00	140	4	21	4			5			1	1	5	60	21	30	1	
29R-1	406.55	65		38	9			8	0	6	2	1		58	3	4	1	
29R-1	407.05	115		30	1			12			1			59	8	10	1	
29R-2	407.55	15		38	5					7	1	3	3	35	1	2		
29R-2	407.85	45		25				20		4			1	119	28	20		2
29R-3	408.55	115		17	4		5	14		4		1		110	13	9	3	1
29R-3	409.15	25		40	6			6		6		1	1	93	5	3	1	1

Core	meter below sea floor (mbsf)	cm in core	*Laeviheterolix glabrans*	*Laeviheterolix dentata*	*Laeviheterohelix pulchra*	*Planoglobulina multicamerata*	*Pseudoguembelina costulata*	*Pseudoguembelina excolata*	*Pseudoguembelina palpebra*	*Pseudoguembelina polypleura*	*Pseudotextularia elegans*	*Pseudotextularia intermedia*	*Pseudotextularia nutallai*	*Racemiguembelina fructicosa*	*Rugoglobigerina hexacamerata*	*Rugoglobigerina rugosa*	*Rectoguembelina cretacea*	**Total planktics**
26R-3	380.38	28	5	2			5		3		5	3	1		32	8		323
26R-3	381.20	110	2	6	4	1	14		1	1	10	4		1	27			427
26R-3	381.30	120	1	10		2	12		2		13	2		1	12			315
26R-4	382.18	50	8	7	2		13		1		19	4		3	37	9		597
26R-4	382.91	130	3	8	3		2				22	5			14	26	7	460
26R-4	383.00	140	1			3	5		1		14	2	1	1	6	5		295
29R-1	406.55	65	1			1	9				1	1		2	3			333
29R-1	407.05	115				1	5		3						16			275
29R-2	407.55	15	1			1	6		3		1	1			6	1		335
29R-2	407.85	45	8				3		3						12			395
29R-3	408.55	115	2			1	5				2	2			1			315
29R-3	409.15	25	1			4	3				1		3		4	2		391

Counts at generic level (normalized)
Hole 1052E, sections 21R, 26R, and 29R

Core	meter below sea floor (mbsf)	cm in core	Benthics	Archeoglobigerina spp	Contusotruncana spp	Gansserina spp	Globigerinolloides spp	Globotruncana spp	Globotruncanella spp	Globotruncanita spp	Hedbergella spp
21R-2	330.34	24	3	10	1	0	3	65	10	1	0
21R-2	331.06	65	2	3	1	0	7	80	11	1	0
21R-2	331.35	95	3	7	0	0	2	97	7	2	0
21R-2	331.75	135	2	7	0	0	8	58	13	2	0
21R-3	332.25	35	3	6	1	0	6	80	9	3	0
21R-3	332.55	65	7	6	0	1	4	69	10	1	0
21R-3	332.68	78	4	14	0	1	8	45	17	0	0
21R-3	332.81	91	2	10	0	1	7	67	16	0	0
26R-3	380.38	28	5	23	0	0	16	54	32	1	1
26R-3	381.20	110	5	17	1	8	3	77	6	5	3
26R-3	381.30	120	0	11	2	12	0	89	3	7	1
26R-4	382.18	50	2	31	1	1	8	73	8	1	4
26R-4	382.91	130	1	21	0	4	12	36	25	0	1
26R-4	383.00	140	1	33	0	7	14	79	5	2	5
29R-1	406.55	65	8	24	1	13	10	156	7	8	0
29R-1	407.05	115	5	32	8	18	1	111	13	1	0
29R-2	407.55	15	1	19	0	14	0	202	0	10	3
29R-2	407.85	45	4	45	0	10	15	62	15	3	1
29R-2	408.55	115	7	32	1	7	9	84	18	5	0
29R-3	409.15	25	4	19	6	12	4	153	5	5	1

Core	meter below sea floor (mbsf)	cm in core	Heterohelix spp	Laeviheterolix spp	Planoglobulina spp	Pseudoguembelina spp	Pseudotextularia spp	Racemiguembelina spp	Rugoglobigerina spp	Rectoguembelina spp	Total
21R-2	330.34	24	181	4	5	4	7	6	2	0	300
21R-2	331.06	65	165	10	3	5	1	8	5	0	300
21R-2	331.35	95	168	2	2	2	3	2	1	0	300
21R-2	331.75	135	186	7	1	3	2	6	3	0	300
21R-3	332.25	35	169	4	0	0	8	10	2	0	300
21R-3	332.55	65	182	7	1	4	4	4	1	0	300
21R-3	332.68	78	182	15	2	2	3	5	4	0	300
21R-3	332.81	91	171	8	3	5	7	2	3	0	300
26R-3	380.38	28	110	6	0	7	8	0	37	0	300
26R-3	381.20	110	125	8	1	11	10	1	19	0	300
26R-3	381.30	120	122	10	2	13	14	1	11	0	300
26R-4	382.18	50	122	9	0	7	12	2	23	0	300
26R-4	382.91	130	142	9	0	1	18	0	26	5	300
26R-4	383.00	140	114	1	3	6	17	1	11	0	300
29R-1	406.55	65	58	1	1	8	2	2	3	0	300
29R-1	407.05	115	84	0	1	9	0	0	17	0	300
29R-2	407.55	15	34	1	1	8	2	0	6	0	300
29R-2	407.85	45	127	6	0	5	0	0	9	0	300
29R-2	408.55	115	127	2	1	5	4	0	1	0	300
29R-3	409.15	25	78	1	3	2	3	0	5	0	300

Species isotopes Hole 1050C, section 13R-5

meters below sea floor (mbsf)	cm in core	*Ht. globulosa*		*Gg. subcarinatus*	
		$\delta^{13}C$	$\delta^{18}O$	$\delta^{13}C$	$\delta^{18}O$
429.55	25	1.67	-1.77	2.42	-1.26
429.60	30	1.63	-1.97	2.36	-0.94
429.65	35	1.81	-1.85	2.45	-1.05
429.70	40	1.74	-1.82	2.41	-1.05
429.75	45	1.89	-1.73	2.39	-1.03
429.80	50	1.66	-1.74	2.49	-1.03
429.85	55	1.77	-1.81	2.40	-0.95
429.90	60	1.71	-1.72	2.38	-1.02
429.95	65	1.97	-1.57	2.24	-0.95
430.00	70	1.67	-1.90	2.57	-1.19
430.05	75	1.73	-1.75	2.42	-1.01
430.10	80	1.73	-2.13	2.35	-1.57
430.15	85	1.68	-2.13	2.31	-1.32
430.20	90	1.91	-1.77	2.24	-1.03
430.25	95	1.95	-1.64	2.30	-1.08
430.30	100	1.98	-1.68	2.21	-1.00
430.35	105	1.82	-1.54	2.39	-0.86
430.40	110	1.82	-1.88	2.31	-1.19
430.45	115	1.92	-1.83	2.63	
430.50	120	1.77	-1.81	2.25	-1.14
430.55	125	1.99	-1.66	2.17	-1.25

meters below sea floor (mbsf)	cm in core	*Pb. palpebra*		*R. rugosa*		*N. Truempyi* (benthic)	
		$\delta^{13}C$	$\delta^{18}O$	$\delta^{13}C$	$\delta^{18}O$	$\delta^{13}C$	$\delta^{18}O$
429.55	25	2.31	-1.95	2.73	-1.78	1.85	0.35
429.60	30	2.59	-1.95	2.65	-1.84		
429.65	35	2.53	-1.99	2.83	-1.81	1.76	0.83
429.70	40	2.54	-1.94	2.78	-1.71	1.89	
429.75	45	2.43	-1.79	2.78	-1.82	2.15	0.72
429.80	50	2.44	-1.93	2.73	-1.46	1.91	0.43
429.85	55	2.81	-1.96	2.86	-1.61	1.93	0.38
429.90	60	2.77	-1.97	2.75	-1.91	1.62	
429.95	65	2.35	-1.83	2.78	-1.97	1.75	0.63
430.00	70	2.66	-1.91	2.75	-2.07	1.95	0.48
430.05	75	2.75	-1.78	2.78	-1.80	2.03	0.58
430.10	80	2.98		2.78	-1.92	1.91	0.46
430.15	85	2.35	-1.85	2.68	-1.84	1.99	0.46
430.20	90	2.67	-2.00	2.69	-1.85	1.99	0.42
430.25	95		-1.77	2.85	-1.51	1.88	0.53
430.30	100	2.86	-1.91	2.72	-1.47	1.89	0.38
430.35	105	2.62	-2.01	2.65	-1.56	1.65	0.59
430.40	110	2.17	-1.61	2.78	-1.56	1.91	0.35
430.45	115	2.68	-1.60	2.83	-1.87	2.06	0.61
430.50	120	2.60	-2.08	2.92	-1.66	1.82	0.20
430.55	125	2.83	-1.97	2.71	-1.83	2.00	0.40

Species isotopes Hole 1050C, section 16R-2
(MacLeod et al, 2001)

meters below sea floor (mbsf)	cm in core	*Pb. palpebra*		*Gg. subcarinatus*	
		$\delta^{13}C$	$\delta^{18}O$	$\delta^{13}C$	$\delta^{18}O$
453.95	25	2.21	-1.61	2.16	-1.08
454.00	30	2.19	-1.72	2.13	-0.99
454.05	35	2.41	-1.46	2.21	-0.61
454.10	40	2.54	-1.43	2.22	-0.84
454.15	45	2.46	-1.41	2.23	-0.77
454.20	50	2.29	-1.67	2.21	-1.20
454.25	55	2.08	-1.85	2.15	-1.22
454.30	60	2.21	-1.85	2.18	-0.98
454.35	65	2.42	-1.34	2.27	-0.65
454.40	70	2.41	-1.40	2.31	-0.74
454.45	75	2.40	-1.52	2.25	-0.95
454.50	80	2.34	-1.54	2.29	-1.25
454.53	83	2.18	-1.97	2.08	-1.10
454.55	85	2.31	-1.58	2.15	-1.11
454.60	90	2.16	-1.80	2.22	-1.11
454.65	95	2.33	-1.68	2.16	-1.03
454.70	100	2.31	-1.61	2.14	-0.86
454.75	105	2.32	-1.30		
454.80	110	2.25	-1.36	2.15	-0.69
454.85	115	2.36	-1.66	2.21	-0.79
454.90	120	2.29	-1.52	2.09	-1.01
455.95	125	2.05	-1.73	2.14	-0.87

meters below sea floor (mbsf)	cm in core	*Ht. globulosa*		benthic		benthic taxon
		$\delta^{13}C$	$\delta^{18}O$	$\delta^{13}C$	$\delta^{18}O$	
453.95	25	1.58	-1.55	0.16	1.78	*N. truempyi*
454.00	30	1.77	-1.33	0.25	1.58	*N. truempyi*
454.05	35	1.96	-1.03	0.31	1.43	*G. beccariiformis*
454.10	40	1.84	-1.15	0.14	1.68	*N. truempyi*
454.15	45	1.63	-1.39	0.25	1.71	*N. truempyi*
454.20	50	1.63	-1.61	0.00	1.57	*G. beccariiformis*
454.25	55	1.62	-1.50	-0.08	1.59	*G. beccariiformis*
454.30	60	1.69	-1.44	-0.05	1.52	*G. beccariiformis*
454.35	65	1.88	-1.19	0.09	1.55	*G. beccariiformis*
454.40	70	1.80	-1.22	0.13	1.53	*G. beccariiformis*
454.45	75	1.75	-1.43	0.08	1.54	*G. beccariiformis*
454.50	80	1.50	-1.65	0.06	1.67	*G. beccariiformis*
454.53	83	1.45	-1.73	0.05	1.63	*G. beccariiformis*
454.55	85	1.59	-1.68	0.09	1.70	*G. beccariiformis*
454.60	90	1.58	-1.60	0.00	1.75	*G. beccariiformis*
454.65	95	1.72	-1.42	0.08	1.69	*G. beccariiformis*
454.70	100	1.65	-1.48	0.03	1.70	*G. beccariiformis*
454.75	105	1.68	-1.30	0.18	1.62	*G. beccariiformis*
454.80	110	1.69	-1.22	0.26	1.59	*G. beccariiformis*
454.85	115	1.74	-1.36	0.05	1.67	*G. beccariiformis*
454.90	120	1.56	-1.45	0.16	1.66	*G. beccariiformis*
455.95	125	1.60	-1.41	0.20	1.62	*G. beccariiformis*

Fine fraction Isotopes Hole 1050C

Section	meter below sea floor (mbsf)	cm in core	Fine Fraction	
			$\delta^{13}C$	$\delta^{18}O$
13R-5	430.55	25	2.39	-1.25
13R-5	430.50	30	2.36	-1.27
13R-5	430.45	35	2.38	
13R-5	430.40	40	2.37	-1.02
13R-5	430.35	45	2.33	-1.06
13R-5	430.30	50	2.42	-1.05
13R-5	430.25	55	2.40	
13R-5	430.20	60	2.42	-1.20
13R-5	430.15	65	2.41	-1.19
13R-5	430.10	70	2.42	-1.25
13R-5	430.05	75		
13R-5	430.00	80	2.32	-1.29
13R-5	429.95	85	2.28	
13R-5	429.90	90	2.33	-1.10
13R-5	429.85	95	2.36	
13R-5	429.80	100	2.39	-0.92
13R-5	429.75	105	2.41	-1.03
13R-5	429.70	110	2.41	-1.25
13R-5	429.65	115	2.38	
13R-5	429.60	120	2.40	-1.25
13R-5	429.55	125	2.35	-1.20

Section	meter below sea floor (mbsf)	cm in core	Fine Fraction	
			$\delta^{13}C$	$\delta^{18}O$
16R-2	453.95	25	2.27	-0.48
16R-2	454.00	30	2.32	-0.44
16R-2	454.05	35	2.36	-0.36
16R-2	454.12	42	2.42	-0.33
16R-2	454.15	45	2.35	-0.46
16R-2	454.20	50	2.32	-0.63
16R-2	454.25	55	2.35	-0.44
16R-2	454.30	60	2.40	-0.40
16R-2	454.35	65	2.49	-0.32
16R-2	454.40	70	2.35	-0.29
16R-2	454.45	75	2.36	-0.44
16R-2	454.51	81	2.25	-0.75
16R-2	454.55	85	2.30	-0.51
16R-2	454.60	90	2.32	-0.36
16R-2	454.65	95	2.34	-0.21
16R-2	454.70	100	2.34	-0.21
16R-2	454.75	105	2.37	-0.19
16R-2	454.80	110	2.36	-0.23
16R-2	454.85	115	2.35	-0.33
16R-2	454.90	120	2.39	-0.30
16R-2	454.95	125	2.33	-0.36

Section	meter below sea floor (mbsf)	cm in core	Fine Fraction	
			$\delta^{13}C$	$\delta^{18}O$
18R-2	473.10	20	2.27	0.31
18R-2	473.15	25	2.39	0.17
18R-2	473.20	30	2.37	0.00
18R-2	473.25	35	2.31	-0.04
18R-2	473.30	40	2.36	0.06
18R-2	473.35	45	2.32	0.13
18R-2	473.40	50	2.35	0.18
18R-2	473.45	55	2.36	0.28
18R-2	473.50	60	2.40	0.02
18R-2	473.55	65	2.37	0.09
18R-2	473.60	70	2.39	0.00
18R-2	473.65	75	2.39	-0.12
18R-2	473.70	80	2.36	-0.02
18R-2	473.75	85	2.42	0.05
18R-2	473.80	90	2.40	0.13
18R-2	473.85	95	2.42	0.21
18R-2	473.90	100	2.38	0.22
18R-2	473.95	105	2.41	0.13
18R-2	474.00	110	2.41	0.15
18R-2	474.05	115	2.39	0.18
18R-2	474.10	120	2.43	0.09
18R-2	474.15	125	2.34	-0.01
18R-2	474.20	130	2.41	0.00

Fine fraction Isotopes Hole 1052E

Section	meter below sea floor (mbsf)	cm in core	Fine Fraction	
			$\delta^{13}C$	$\delta^{18}O$
21R-2	330.64	24	2.16	-0.74
21R-2	330.74	34	2.18	-0.81
21R-2	330.84	44	2.18	-0.83
21R-2	330.93	53	2.23	-0.89
21R-2	331.06	66	2.20	-1.09
21R-2	331.16	76	2.18	-0.82
21R-2	331.26	86	2.26	-0.78
21R-2	331.36	96	2.24	-0.78
21R-2	331.46	106	2.26	-0.87
21R-2	331.55	115	2.23	-0.85
21R-2	331.65	125	2.17	-0.82
21R-2	331.75	135	2.24	-0.73
21R-2	331.86	146	2.21	-0.80
21R-3	331.94	4	2.17	-0.89
21R-3	332.04	14	2.11	-0.87
21R-3	332.14	24	2.14	-0.83
21R-3	332.25	35	2.09	-0.88
21R-3	332.35	45	2.26	-0.82
21R-3	332.44	54	2.26	-0.89
21R-3	332.55	65	2.22	-0.94
21R-3	332.68	78	2.26	-0.87
21R-3	332.81	91	2.11	-1.11

Section	meter below sea floor (mbsf)	cm in core	Fine Fraction	
			$\delta^{13}C$	$\delta^{18}O$
26R-3	380.30	20	2.11	-0.87
26R-3	380.38	30	2.20	-0.90
26R-3	380.50	40	2.17	-0.87
26R-3	380.60	50	2.30	-0.74
26R-3	380.70	60	2.15	-0.89
26R-3	380.78	68	2.19	-0.65
26R-3	380.90	80	2.12	-0.93
26R-3	381.00	90	2.16	-0.86
26R-3	381.10	100	2.26	-0.83
26R-3	381.20	110	2.06	-0.62
26R-3	381.30	120	2.18	-1.00
26R-3	381.39	130	2.21	-0.92
26R-4	381.60	0	2.24	-0.93
26R-4	381.70	10	2.20	-0.91
26R-4	381.80	20	2.20	-0.82
26R-4	381.90	30	2.18	-0.96
26R-4	382.00	40	2.22	-0.91
26R-4	382.10	50	2.22	-0.92
26R-4	382.18	58	2.17	-0.97
26R-4	382.30	70	2.25	-0.77
26R-4	382.40	80	2.24	-0.81
26R-4	382.48	88	2.19	-0.77
26R-4	382.58	98	2.16	-0.87
26R-4	382.68	108	2.25	-0.76
26R-4	382.80	120	2.17	-0.63
26R-4	382.91	131	2.08	-0.56
26R-4	383.00	140	2.20	-0.60
26R-4	383.08	148	2.22	-0.73

Section	meter below sea floor (mbsf)	cm in core	Fine Fraction	
			$\delta^{13}C$	$\delta^{18}O$
29R-1	406.55	65	2.21	-0.24
29R-1	406.65	75	2.16	-0.52
29R-1	406.75	85	2.29	-0.59
29R-1	406.85	95	2.27	-0.75
29R-1	406.95	105	2.30	-0.60
29R-1	407.05	115	2.29	-0.58
29R-1	407.14	124	2.28	-0.52
29R-1	407.25	135	2.26	-0.51
29R-1	407.35	145	2.27	-0.56
29R-2	407.45	5	2.31	-0.56
29R-2	407.55	15	2.24	-0.47
29R-2	407.65	25	2.28	-0.54
29R-2	407.75	35	2.20	-0.63
29R-2	407.85	45	2.24	-0.53
29R-2	407.95	55	2.20	-0.59
29R-2	408.05	65	2.23	-0.49
29R-2	408.15	75	2.26	-0.54
29R-2	408.25	85	2.08	-0.63
29R-2	408.35	95	2.18	-0.45
29R-2	408.45	105	2.19	-0.14
29R-2	408.55	115	2.19	-0.46
29R-2	408.65	125	2.19	-0.49
29R-2	408.75	135	2.24	-0.32
29R-2	408.85	145	2.20	-0.52
29R-3	408.90	0	2.25	-0.68
29R-3	409.05	15	2.22	-0.40
29R-3	409.15	25	2.28	-0.55
29R-3	409.25	35	2.21	-0.55
29R-3	409.35	45	2.31	-0.53

References

MacLeod, K.G., Kucera, M., Huber, B.T., Pletsch, T., and Röhl, U., 2001. Maastrichtian foraminiferal and paleoceanographic changes on Milankovitch timescales: Paleoceanography, v. 16, p. 133-154

APPENDIX 2

DEMERARA RISE NEODYMIUM ISOTOPE DATA, AND AGE CALCULATIONS FOR SITES 1258, 1260, AND 1261

SITE 1258

source	Sample	depth (mcd)	Age	$^{143}Nd/^{144}Nd$	$\varepsilon_{Nd(0)}$	$\varepsilon_{Nd(t)}$
3	1258A 1-1W 70-73	0.7	31.46	0.511836	-15.64	-15.35
3	1258 A 1-2W 100-102	2.51	31.68	0.511985	-12.73	-12.44
3	1258 A 1-3W 100-102	4.01	31.86	0.511849	-15.38	-15.09
3	1258 A 3-1W 98-100.5	15.19	33.24	0.512010	-12.24	-11.94
3	1258A 8R-3W 20-26	67.28	39.67	0.512035	-11.76	-11.40
3	1258 A 10-4W 100-105	87.73	42.19	0.512058	-11.31	-10.92
3	1258 A 14-2W 5-7	122.56	46.48	0.511996	-12.52	-12.09
3	1258A 17R-2W 20-26	172.59	52.65	0.512032	-11.82	-11.34
3	1258A 19R-5, 114-115	198.13	55.80	P/E boundary [1]		
1	1258 A 21-3W 100-103.5	215.13	57.90	0.512080	-10.88	-10.35
1	1258 A 24-5W 4.5-6.5	245.77	61.67	0.512084	-10.80	-10.24
1	1258A 25R-3W 60-66	252.05	62.45	0.512064	-11.20	-10.63
1	1258 A 26-2W 8-10	259.63	63.38	0.512041	-11.64	-11.06
1	1258A 27R-2W, 71-75	269.96	64.66	0.511964	-13.15	-12.56
1	1258A 27R-2W 100-106	270.25	64.69	0.511973	-12.97	-12.38
1	1258A 27R-3W, 29-34	271.04	64.79	0.512019	-12.07	-11.48
1	1258A 27R-3W, 110-115	271.85	64.89	0.511929	-13.83	-13.24
1	1258A 27R-4W, 76-80	273.01	65.03	0.511894	-14.51	-13.92
1	1258A 27R-5W, 30-35	274.05	65.16	0.511865	-15.08	-14.49
1	1258A 27R-5W, 82-87	274.57	65.23	0.511816	-16.03	-15.44
1	1258A 27R-5W, 120-125	274.95	65.27	0.511848	-15.41	-14.82
1	1258B 27R-1W, 24-29	276.57	65.47	0.511979	-12.86	-12.26
1	1258B 27R-1, 49.51	276.83	65.50	K/T boundary [1]		
1	1258B 27R-1W, 72-77	277.05	65.53	0.511880	-14.79	-14.19
1	1258 A 28-1W 110-118	278.45	65.74	0.511921	-13.98	-13.38
1	1258 A 29-1W 133-140	288.38	67.18	0.511847	-15.42	-14.81
1	1258 A 29-7W 33-39	296.2	68.32	0.511827	-15.81	-15.19
1	1258A-30R-1,61-69	297.18	68.46	0.511837	-15.63	-15.00
1	1258A 29RCC 13-18	298.97	68.72	Base. *A. Mayaroensis* [1, 3]		
1	1258A,30R-4,53-59	301.60	68.81	0.511823	-15.90	-15.27
1	1258A,30R-4,59-61	301.66	68.81	0.511824	-15.88	-15.25
1	1258A-31R-1,74-80	307.38	69.00	0.511811	-16.13	-15.50
1	1258A 31R-2W 10-19	308.34	69.03	0.511948	-13.46	
1	1258A,31R-2W,70-71	308.84	69.05	0.511789	-16.56	-15.93
1	1258A 31R-3W 20-26	309.89	69.08	0.511800	-16.35	-15.72
1	1258A 31R-3W 66-72	310.30	69.10	0.511805	-16.25	-15.62
1	1258A 31R-5 81-87	315.45	69.27	0.511815	-16.05	-15.42
1	1258 A 32-5W 50-53	323.21	69.53	0.511810	-16.14	-15.51
1	1258 A 32-5W 81-87	323.52	69.54	0.511821	-15.93	-15.30
1	1258A 32R CC, 0-7	325.30	69.60	Base of KS30A *(fructicosa/contusa)* [1]		

source	Sample	depth (mcd)	Age	$^{143}Nd/^{144}Nd$	$\varepsilon_{Nd(0)}$	$\varepsilon_{Nd(t)}$
1	1258A, 36-4W 80-86	360.17	76.85	0.511873	-14.92	-14.22
1	1258 A 36-6W 51-53.5	362.88	77.41	0.511774	-16.85	
1	1258 A 37-6W 22.5-25	371.8	79.27	0.511831	-15.73	-15.01
1	1258A 38R-1, 105	375.22	79.98	0.511804	-16.27	-15.54
1	1258 A 38-2W 60-66	376.27	80.20	0.511797	-16.40	-15.67
1	1258 A 41R-3W 80-86	407.88	86.77			
2	1258A 42R-1 0-1	414.75		Campanian/Turonian boundary [1]		
2	1258A 42R-1, 8-10	414.83	88.24	0.511824	-15.88	-15.07
2	1258A 42R-1, 65-66.5	415.40	88.54	0.511867	-15.04	-14.23
2	1258A 42R-2W 85-86.5	417.10	89.43	0.511847	-15.43	-14.62
2	1258A 42R-3, 60-62	418.24	90.03	0.511899	-14.42	-13.59
2	1258B 45R-1, 95	419.28	90.57	0.511724	-17.83	-17.00
2	1258B 45R-1, 96-97	419.29	90.57	0.511748	-15.39	-16.54
2	1258A, 42R, 5R, 12-15	420.29	91.10		-15.50	
2	1258B 45R-3, 36	420.54	91.23	0.511864	-15.10	-14.27
2	1258B 45R-3, 51	420.69	91.31	0.511783	-16.68	-15.85
2	1258A 42-6, 2-4	421.51	91.74	0.511945	-13.52	-12.68
2	1258A 42-6, 32-34	421.81	91.89	0.511846	-15.45	-14.61
2	1258A 42-6, 60-62	422.09	92.04	0.511940	-13.62	-12.78
2	1258A 42R-6, 66	422.15	92.07	0.512028	-11.90	-11.06
2	1258A 42R-6, 96	422.44	92.22	0.511938	-13.65	-12.81
2	1258A 42R-6, 116	422.64	92.33	0.511921	-13.99	-13.14
2	1258A 42R-7, 7-9	422.96	92.49	0.511967	-13.09	-12.25
2	1258A 42R-7, 26	423.14	92.59	0.511978	-12.87	-12.03
2	1258A 42R-7W 50-51.5	423.39	92.72	0.512083	-10.83	-9.98
2	1258A 42R-7, 71	423.59	92.82	0.512175	-9.03	-8.18
2	1258A 42R-7, 92-94	423.81	92.94	0.512074	-11.00	-10.15
2	1258A 42R-7W 105-106.5	423.94	93.01	0.512204	-8.47	-7.62
2	1258A 42R-7W 115-116.5	424.04	93.06	0.512148	-9.56	-8.71
2	1258A 42R-7W 135-136.5	424.24	93.16	0.511860	-15.18	-14.33
2	1258C 17X-1 5-6.5	424.84	93.48	0.511967	-13.09	-12.24
2	1258C 17X-1 10-11.5	424.89	93.50	0.511954	-13.34	-12.49
2	1258A 43R-1W 66	424.94	93.53	0.511791	-16.52	-15.67
2	1258C 17X-1 40-41.5	425.19	93.66	0.512196	-8.62	-7.77
2	1258C 17X-1 50-51.5	425.29	93.71	0.512213	-8.29	-7.43
2	1258C 17X-1 75-76.5	425.54	93.84	0.512076	-10.96	-10.11
2	1258C17X1-85-86.5	425.64	93.90	0.512145	-9.62	-8.76
2	1258C17X1-105-106.5	425.84	94.00	OAE 2 [2]		

source	Sample	depth (mcd)	Age	$^{143}Nd/^{144}Nd$	$\varepsilon_{Nd(0)}$	$\varepsilon_{Nd(t)}$
2	1258C17X1-105-106.5	425.84	94.00	0.512120	-10.10	-9.25
2	1258A 43R-2W 42-44	425.98	94.02	0.511831	-15.74	-14.89
2	1258C17X1-125-126.5	426.04	94.03	0.511841	-15.55	-14.69
2	1258C17X2-10-11.5	426.28	94.06	0.511847	-15.43	-14.57
2	1258C17X2-30-31.5	426.48	94.09	0.511805	-16.25	-15.39
2	1258A 43R-2W 124	426.80	94.13	0.511754	-17.24	-16.39
2	1258C17X2-70-71.5	426.88	94.14	0.511766	-17.01	-16.15
2	1258B 47R-1, 23	429.39	94.47	0.511917	-14.06	-13.20
2	1258B 47R-2W 116-117.5	431.51	94.76	0.511851	-15.35	-14.49
2	1258B 47R-3W 124-126	432.90	94.94	0.511778	-16.78	-15.91
2	1258B 47R-4W 102.5-104	434.12	95.11	0.511780	-16.74	-15.87
1	1258 A 44-2W 7-9	435.29	95.26	0.511781	-16.71	-15.84
2	1258B 48R-1, 111	435.87	95.34	0.511764	-17.05	-16.18
2	1258B 49R-1, 45	439.20	95.79	0.511822	-15.92	-15.04
2	1258B 49R-3, 31	441.73	96.12	0.511853	-15.31	-14.44
2	1258A 45R 2W 51-53	445.37	96.61	0.511795	-16.44	-15.56
2	1258A 45R-2, 57	445.43	96.62	0.511822	-15.92	-15.04
2	1258A 46R 1W 22-24	448.40	97.02	0.511780	-16.74	-15.85
2	1258A 46R 1W 41-43	448.59	97.04	0.511826	-15.84	-14.96
2	1258A 46R 1W 70-72	448.88	97.08	0.511832	-15.72	-14.84
2	1258A 46R 1W 100-102	449.18	97.12	0.511816	-16.03	-15.15
2	1258A 46R-2, 68	450.22	97.26	0.511859	-15.20	-14.31
2	1258A 46R-4, 33	452.53	97.57	0.511812	-16.11	-15.22
2	1258A 47R-1 ,12	456.04	98.04	0.511873	-14.93	-14.04
2	1258B 56R-2W 23-29	477.07	100.85	0.511959	-13.25	-12.33
2	1258C 27R-2, 0	480.29	101.28	0.511935	-13.71	-12.79
2	1258B. 57CC-15-20	483.47		Base of E. turriseiffelii [1]		

SITE 1260

source	Sample	depth (mcd)	Age	$^{143}Nd/^{144}Nd$	$\varepsilon_{Nd(0)}$	$\varepsilon_{Nd(t)}$
3	1260 A 7-6W 50-52.5	55.60	29.55	0.512013	-12.19	-11.92
3	1260 A 11-2W 50-53	86.92	33.61	0.512036	-11.74	-11.43
3	1260 A 21-2W 20-22	182.29	45.98	0.512004	-12.36	-11.94
3	1260 A 27-3W 51.5-55.5	242.01	53.73	0.512029	-11.87	-11.38
3	1260 B 17R-7 69	257.97	55.80	P/E boundary [1]		
1	1260 A 35-3W 52.5-55.5	319.55	63.79	0.512061	-11.25	-10.67
1	1260A 35R-3, 65-70	319.67	63.80	0.512064	-11.20	-10.61
1	1260A 35R-3, 80-85	319.82	63.82	0.512074	-11.00	-10.42
1	1260 A 35-3W 96-98	319.99	63.84	0.511879	-14.80	
1	1260A 36R-1, 50-55	327.92	64.87	0.511879	-14.81	-14.21
1	1260A 36R-2, 48-53	329.40	65.06	0.511920	-14.01	-13.41
1	1260 A 36-3W 50-52	330.92	65.26	0.511958	-13.26	-12.66
1	1260 A 36R-4, 91-94	332.83	65.50	K/T boundary [1]		
1	1260A 36R-5, 50-55	333.92	65.74	0.511888	-14.63	-14.03
1	1260 A 36-6W 93-94.5	335.85	66.18	0.511900	-14.39	-13.79
1	1260 A 37-1W 23.5-26	336.88	66.41	0.511848	-15.40	-14.80
1	1260 A 37-4W 130-132	342.45	67.65	0.511825	-15.9	-15.24
1	1260A 38R-1 49-52	347.23	68.72	Base. *A. Mayaroensis* [1, 3]		
1	1260A 38R-2 34-40	348.58	68.78	0.511816	-16.0	-15.41
1	1260A 38R-3 41-47	350.15	68.84	0.511770	-16.9	-16.30
2	1260 A 38R 5W 2-4	352.76	68.96	0.511770	-16.9	-16.30
2	1260 A 39R 1W 78	357.12	69.14	0.511788	-16.6	-15.95
2	1260 B 26R 7W 10-12	368.36	69.62	0.511815	-16.0	-15.41
2	1260 A 40-1W 109	369.05	69.65	0.511776	-16.8	-16.18
2	1260 40 3W 104-372	372.00	69.78	0.511801	-16.3	-15.69
2	1260, 40CC, 17-22	377.22		Top. of *U. trifidium*[1]		
2	1260 A 42-2W 77	389.89	70.54	0.511783	-16.7	-16.04
2	1260 A 42-4W 2-4	392.12	70.64	0.511806	-16.2	-15.59
2	1260A 42Rcc 20-22	393.82	89.60	Base of *M. furcatus*[1]		
2	1260 B 31R CCW 3-5	395.00	89.81	0.511866	-15.1	-14.23
2	1260B 32-1W 3-5	398.00	90.35	0.511800	-16.3	-15.52
2	1260 B 32R 1W 24-26	399.00	90.52	0.511741	-17.5	-16.67
2	1260B 32-1W 97-99	399.00	90.52	0.511701	-18.3	-17.45
2	1260B 32-2W 32-34	400.07	90.71	0.511697	-18.4	-17.53
2	1260 B 32R 2W 56-58	400.31	90.76	0.511890	-14.6	-13.76
2	1260B 33 1W 20-33	403.11	91.26	0.511787	-16.6	-15.77
2	1260 B 33R 1W 92-94	403.83	91.39	0.511813	-16.1	-15.25
2	1260 B 33-2W 50-52	404.91	91.58	0.511789	-16.55	-15.72
2	1260B 33 2W 94-96	405.35	91.66	0.511688	-18.5	-17.70
2	1260 B 33-3W 56-58	406.47	91.86	0.511806	-16.22	-15.39

source	Sample	depth (mcd)	Age	$^{143}Nd/^{144}Nd$	$\varepsilon_{Nd(0)}$	$\varepsilon_{Nd(t)}$
2	1260 B 34-2W 7.5-8.5	409.97	92.48	0.511833	-15.70	-14.85
2	1260 B 34-4W 95-97	413.85	93.17	0.511823	-15.89	-15.04
2	1261 B 34-CC 0-5	414.00		Base of *E. eptapetalus*[1]		
2	1260 B 35-1W 70-72	420.54	93.62	0.511944	-13.53	-12.68
2	1260 B 35R 2W 120-121	422.54	93.75	0.511831	-15.7	-14.88
2	1260B 35-3W 41-45	423.28	93.80	0.511873	-14.9	-14.07
2	1260 B 35-4W 5-7	424.36	93.87	0.511840	-15.56	-14.70
2	1260 B 35-4W 30-31.5	424.61	93.88	0.511902	-14.35	-13.49
2	1260B 35-4W 52-54	424.83	93.90	0.511979	-12.9	-12.00
2	1260 B 35R 4W 61-63	424.92	93.90	0.511939	-13.6	-12.77
2	1260 B 35R 4W 70-72	425.02	93.91	0.511969	-13.0	-12.19
2	1260B 35-4W 80-82	425.12	93.92	0.512003	-12.4	-11.53
2	1260 B 35R 4W 90-92	425.22	93.92	0.512062	-11.2	-10.37
2	1260 B 35-4W 98-99	425.29	93.93	0.512067	-11.13	-10.27
2	1260 B 35R 4W 103-104	425.34	93.93	0.512051	-11.4	-10.59
2	1260 B 35R 4W 118-120	425.49	93.94	0.512097	-10.5	-9.69
2	1260 B 35-5W 26-27	426.07	93.98	0.512109	-10.3	-9.46
2	1260 B 35-5W 28-30	426.10	93.98	0.512116	-10.18	-9.32
2	1260 B 35-5W 33-34.5	426.14	93.98	0.512029	-11.87	-11.02
2	1260 B 35R 5W 37-38	426.18	93.99	0.511949	-13.4	-12.58
2	1260B 35-5W 46-47	426.27	93.99	0.511932	-13.8	-12.91
2	1260B 35-5W 55-57	426.36	94.00	0.512100	-10.5	-9.64
				OAE 2 [1,2,4]		
2	1260 B 35-5W 60-62	426.41	94.00	0.512018	-12.1	-11.24
2	1260 B 35-5W 75-76.5	426.56	94.01	0.511804	-16.26	-15.40
2	1260B 35-5W 90-92	426.72	94.02	0.511807	-16.2	-15.35
2	1260 B 35-5W 103.5-105.5	426.85	94.03	0.511812	-16.11	-15.25
2	1260B35-5-120-121	427.01	94.04	0.511792	-16.5	-15.64
2	1260 B 35R 6W 20-22	427.51	94.07	0.511880	-14.8	-13.92
2	1260 B 47-5W 50-52	433.97	94.49	0.511808	-16.19	-15.32
2	1260 B 47-7W 30-32	436.02	94.62	0.511799	-16.36	-15.50
2	1260 A 48-2W 31.5-33	438.91	94.81	0.511860	-15.17	-14.31
2	1260 A 48R 4W 10-22	441.71	94.99	0.511892	-14.5	-13.68
2	1260 A 48-4W 98-100	442.43	95.03	0.512047	-11.52	-10.65
2	1260A 48-6W 30-31	444.57	95.17	0.511867	-15.0	-14.17
2	1260A 49-1W 130-131	447.27	95.34	0.511965	-13.1	-12.26
2	1260 A 49-2W 40-41	447.80	95.38	0.512024	-12.0	-11.11
2	1260A 49-3W 10-12	448.92	95.45	0.511888	-14.6	-13.76
2	1260 A 49-3W 80-82	449.62	95.50	0.511937	-13.7	-12.80
2	1260A 49 4W 50-52	450.82	95.57	0.511937	-13.7	-12.80
2	1260A 49-5W 5-7	451.87	95.64	0.511977	-12.9	-12.02
2	1260A 49-5W 98-100	452.80	95.70	0.511881	-14.8	-13.89
2	1260 A 50-2W 80.5-82	457.99	96.04	0.511936	-13.69	-12.81
2	1260 A 50-6W 70-72	463.88	96.42	0.511914	-14.12	-13.24
2	1260 A 51R 4W 10-11	470.23	96.82	0.511920	-14.0	-13.12
2	1260 A 52-4W 130-132	480.79	97.51	0.511947	-13.5	-12.59

SITE 1261

source	Sample	depth (mcd)	Age	$^{143}Nd/^{144}Nd$	$\varepsilon_{Nd(0)}$	$\varepsilon_{Nd(t)}$
3	1261 A 21-2W 11-14	373.39	40.84	0.512079	-10.90	-11.98
3	1261 A 25-1W 23.5-28.5	410.55	45.54	0.512076	-10.96	-11.70
3	1261 A 25-2W 10-12	411.74	45.69	0.512007	-12.30	-13.03
3	1261 A 27-2W 13-15	431.13	48.14	0.512013	-12.18	-12.74
3	1261 A 29-2W 15.5-16.6	450.34	50.57	0.511984	-12.75	-13.13
3	1261 A 33-2W 14-16	488.44	55.39	0.511995	-12.54	-12.57
3	1261A 33R-4, 128-128	491.69	55.80	P/E boundary [1]		
1	1261 A 35-2W 10-12	507.7	57.82	0.512043	-11.60	-11.45
1	1261 A 37-2W 13-15	526.93	60.26	0.512033	-11.79	-11.47
1	1261 B 2R3-83	538.40	65.50	K/T boundary [1]		
1	1261 B 2-3W 80-86	538.4	65.54	0.511962	-13.18	-13.18
1	1261 B 3-1W 87-93	541.95	66.17	0.511792	-16.50	-16.46
1	1261A 39 1W 40-42	545.00	66.75	0.511799	-16.4	-16.31
1	1261 B 3-3W 96-102	545.04	66.75	0.511766	-17.00	-16.94
1	1261 B 3-4W 47-53	546.05	66.95	0.511767	-16.98	-16.98
1	1261 B 3-5W 40-46	547.48	67.22	0.511771	-16.91	-16.89
1	1261 A 39R CCW 23-25	549.65	67.63	0.511755	-17.2	-17.18
1	1261 B 4-1W 76-82	551	67.88	0.511782	-16.69	-16.64
1	1261 B 4-2W 71-77	552.45	68.16	0.511802	-16.30	-16.24
1	1261 B 4-3W 85-91	554.09	68.47	0.511778	-16.77	-16.69
1	1261 B 4-5W 50-56	556.74	68.97	0.511757	-17.18	-17.07
2	1261 A 40R 3W 10-12	557.26	69.06	0.511713	-18.0	-17.93
2	1261 A, 40R-6, 55-57	562.21		Top. of *U. trifidium*[1]		
2	1261A 41R-1, 0-1	564.71	83.50	Top of KS24 (*D. assymetrica*)[1]		
2	1261 A 41-2W 50-52	566.71	83.95	0.511796	-16.4	-16.41
2	1261 A 43 1W 100-102	585.28	88.10	0.511799	-16.4	-16.17
2	1261 A 43 3W 133-134	588.58	88.84	0.511763	-17.1	-16.84
2	1261 A 43 5W 42-44	590.55	89.28	0.511777	-16.8	-16.55
2	1261 A 44 1W 8-10	594.09	90.07	0.511826	-15.8	-15.57
2	1261 A 44 3W 117-119	597.94	90.93	0.511767	-17.0	-16.68
2	1261 A 44 5W 117-134	600.92	91.60	0.511756	-17.2	-16.87
2	1261A, 45CC 5-7	608.08		Base of *E. eptapetalus*[1]		
2	1261 A 47-2W 90-92	621.59	93.57	0.511872	-14.9	-14.82
2	1261 A 47-2W 142-144	622.1	93.59	0.511790	-16.53	-16.41
2	1261 A 47R 4W 92-94	624.54	93.65	0.511823	-15.9	-15.74
2	1261 A 47R 6W 81-83	627.38	93.73	0.511837	-15.6	-15.44
2	1261 A 47R 6W 131-133	627.88	93.75	0.511820	-16.0	-15.77
2	1261 A 48R 1W 20-22	628.26	93.76	0.511907	-14.3	-14.07
2	1261 A 48R 1W 70-72	628.77	93.77	0.511858	-15.2	-15.02
2	1261 A 48 1W 122-124	629.28	93.79	0.511924	-13.9	-13.73

source	Sample	depth (mcd)	Age	$^{143}Nd/^{144}Nd$	$\varepsilon_{Nd(0)}$	$\varepsilon_{Nd(t)}$
2	1261 A 48R 2W 20-22	629.76	93.80	0.511933	-13.7	-13.55
2	1261 A 48R 2W 70-72	630.26	93.81	0.511954	-13.3	-13.13
2	1261 A 48R 2W 142-144	630.98	93.83	0.511978	-12.9	-12.66
2	1261A 48 3W 43-45	631.49	93.85	0.511931	-13.8	-13.58
2	1261 A 48R 3W 80-82	631.86	93.86	0.511938	-13.6	-13.43
2	1261 A 48R 3W 141-143	632.47	93.87	0.511939	-13.6	-13.41
2	1261 A 48-4W 50-52	633.06	93.89	0.512029	-11.87	-11.64
2	1261 A 48R 4W 141-143	633.97	93.92	0.512159	-9.3	-9.10
2	1261 A 48R 5W 42-44	634.43	93.93	0.512076	-11.0	-10.72
2	1261 A 48-5W 61-63	634.62	93.93	0.512049	-11.48	-11.24
2	1261A 48 5W 81-83	634.82	93.94	0.511898	-14.4	-14.19
2	1261 A 48R 6W 6-8	635.57	93.96	0.511896	-14.5	-14.22
2	1261 A 48R 6W 36-38	635.87	93.97	0.511889	-14.6	-14.35
2	1261 B 13-2W 11-13	635.97	93.97	0.512005	-12.3	-12.09
2	1261 B 13-2W 67-69	636.53	93.99	0.511909	-14.2	-13.96
2	1261 B 13R 2W 97-99	636.83	93.99	0.511948	-13.5	-13.19
2	1260 B 13-2W 116-118	637.03	94.00	OAE 2 [1]		
2	1261 B 13-2W 116-118	637.03	94.00	0.512031	-11.8	-11.58
2	1261 B 13-2W 145-147	637.31	94.01	0.511809	-16.16	-15.90
2	1261 B 13 3W 31-33	637.63	94.02	0.511800	-16.3	-16.08
2	1261 A 49R 1W 127-128	638.54	94.04	0.511797	-16.4	-16.12
2	1261 A 49-4W 120-122	642.95	94.16	0.511795	-16.4	-16.13
2	1261 A 50R 2W 130-132	649.21	94.34	0.511886	-14.7	-14.29

mcd : meter composite depth

Source of data:	Ages references.
1. This study 2. MacLeod et al, 2008 3. Bourbón, 2008.	1. Erbacher et al, 2004 2. MacLeod et al, 2008 3. Huber et al, 2008 4. Jiménez Berrocoso et al, 2009

References

Bourbon, É., 2008. Nd isotopes throughout the North Atlantic in the Late Cretaceous and across the Oceanic Anoxic Event 2: M.S. Thesis. Geological Sciences. Gainesville, University of Florida.

Erbacher, J., Mosher, D.C., Malone, M.J., Berti, D., Bice, K.L., Bostock, H., Brumsack, H.-J., et al., 2004, Proceedings of the Ocean Drilling Program; Demerara Rise; equatorial Cretaceous and Paleogene paleoceanographic transect, western Atlantic. Leg 207 Proceedings of the Ocean Drilling Program, Part A: Initial Reports, Volume 207: United States, Texas A&M University, Ocean Drilling Program : College Station, TX, United States.

Huber, B.T., MacLeod, K.G., and Tur, N.A., 2008. Chronostratigraphic Framework For Upper Campanian-Maastrichtian Sediments On The Blake Nose (Subtropical North Atlantic): Journal of Foraminiferal Research, v. 38, p. 162-182.

Jiménez Berrocoso, A., MacLeod, K.G., Martin, E.E., Bourbon, E., Basak, C., and Isaza-Londoño, C., 2009. Water-mass changes in the western tropical North Atlantic across the Cenomanian (Late Cretaceous) inferred from bioapatite Nd isotopes.

MacLeod, K.G., Martin, E.E., and Blair, S.W., 2008. Nd isotopic excursion across Cretaceous ocean anoxic event 2 (Cenomanian-Turonian) in the tropical North Atlantic: Geology, v. 36, p. 811-814

APPENDIX 3

BERMUDA RISE, BLAKE NOSE AND CAPE VERDE NEODYMIUM ISOTOPE DATA

BERMUDA RISE

source	Sample	depth (mbsf)	Age for $\varepsilon_{Nd(t)}$	$^{143}Nd/^{144}Nd$	$\varepsilon_{Nd(0)}$	$\varepsilon_{Nd(t)}$
2	386 35R 2W 9.5-11	633.60	60.0	0.512079	-10.9	-10.53
2	386 35R 2W 91-94	634.41	60.0	0.512104	-10.4	-10.04
1	386, 35-4, 15	636.63	65.5	*K/T boundary* [5]		
1	386, 35-4, 115	637.50	68.6	FO of *M. mura*[1]		
1	386, 35-5, 48	639.00	69.2	FA of *L. quadratus*[1]		
2	386 36R 1W 113-115	642.63	74.0	0.512209	-8.4	-7.90
				FO of *U. Jankoi* [2]		
2	386 43R 2W 112-113.5	738.92	94.4	0.512269	-7.2	-6.60
				Cenomanian/Turonian OAE2 [3,4]		
2	386 43R 2W 146-147.5	739.26	94.4	0.512269	-7.2	-6.60
2	386 43R 3W 115-117	740.45	94.4	0.512281	-7.0	-6.37
2	386 43R 4W 7-8.5	740.87	97.0	0.512281	-7.0	-6.35
2	386 45R 4W 70-73	770.60	97.0	0.512261	-7.4	-6.74
				Cenomanian/Albian [4]		
2	386 49R 2W 146-148	805.76	97.0	0.512254	-7.5	-6.88
2	386 49R 3W 41-43	806.21	99.0	0.512229	-8.0	-7.35
2	386 50R 1W 71-73	813.01	99.0	0.512222	-8.1	-7.49
2	386 50R 5W 123-125	819.53	99.0	0.512214	-8.3	-7.64
1	387,27R-1W,122-123.5	442.47	60.0	0.512097	-10.55	-10.17
1	387, 27R-1 134-137	443.00	60.0	Early Danian [5]		
1	387, mid core 27	445.00	67.0	*K/T boundary* [5]		
1	387,27R-6W,20-21.5	448.95	67.0	0.512182	-8.90	-8.47
1	387-27 to 28CC	460.00	68.6	FO of *M. mura*[1]		
1	387,29R-2,17-20	471.07	69.0	0.512171	-9.11	-8.69
1	387, 29-2 59	471.49	71.0	FO of *T. trifidius* [1]		
1	387,29R-3W,94-96	473.34	71.0	0.512191	-8.72	-8.27
1	387,29R-4W,68-70	474.58	71.0	0.512213	-8.29	-7.84

mbsfd = meters below sea floor

Source of data:	Ages references.
1. This study 2. Bourbón, 2008	1. Okada and Thierstein, 1979 2. Kuhnt et al, 1992 3. MacLeod et al, 2008 4. Jiménez Berrocoso et al, 2009 5. Norris and Firth, 2002

BLAKE NOSE

source	Sample	depth (mbsf)	Age for $\varepsilon_{Nd(t)}$	$^{143}Nd/^{144}Nd$	$\varepsilon_{Nd(0)}$	$\varepsilon_{Nd(t)}$
1	1050C,2R-1W,70-74	327.80	61.41	0.512188	-8.78	-8.22
1	1050C,4R-1W,69-73	346.99	62.41	0.512144	-9.64	-9.07
1	1050C,4R-6W,61-63	354.40	62.80	Base. *E. Macellus* [1]		
1	1050C 6R 1W 50-56	366.03	63.41	0.51213	-9.91	-9.33
1	1050C,6R-1W,82-86	366.32	63.43	0.512145	-9.62	-9.04
1	1050,9R-1W,65-69	395.15	64.94	0.512212	-8.31	-7.72
1	1050C,9R-5W,62-66	401.12	65.25	0.512201	-8.52	-7.93
1	1050,10R-1W,73-77	404.83	65.44	0.512219	-8.17	-7.58
1	1050C,10R-2W,24-28	405.84	65.50	0.512231	-7.94	-7.34
1	1050C,10R-2W,36	405.93	65.50	K/T Boundary [1]		
1	1050,11R-1W,70-73	409.04	65.74	0.512220	-8.15	-7.55
1	1050C,11R-3,73-75	412.23	65.97	0.512222	-8.11	-7.51
1	1050C,13R-1W,13.5-17.5	423.44	66.78	0.512205	-8.45	-7.84
1	1050C,13R-1W,116-120	424.46	66.86	0.512220	-8.15	-7.54
1	1050C,13R-3W,106-110	427.36	67.07	0.512215	-8.25	-7.64
1	1050C,13R-6W,24-28	431.04	67.33	0.512205	-8.45	-7.83
1	1050C,13R-7W,56-60	432.86	67.47	0.512204	-8.47	-7.85
1	1050C,15R-1W,29-33	442.89	68.19	0.512195	-8.64	-8.02
1	1050C,15R-2W,67-71	444.77	68.33	0.512193	-8.68	-8.06
1	1050C, 15R-6 35-37	450.43	68.72	Base. *A. mayaroensis* [2]		
1	1050C,15R-6,38-42	450.48	68.72	0.512193	-8.68	-8.05
1	1050C,16R-1W,59-63	452.79	69.26	0.512182	-8.90	-8.26
1	1050C,17-1W,80-84	462.60	71.56	0.512191	-8.72	-8.07
1	1050C,18R-2W,85-86	473.75	74.18	0.512158	-9.36	-8.69
1	1050 C 18R 2W 130-132	474.21	74.28	0.5121763		
1	1050C,18R-5W,83-87	478.23	75.23	0.512163	-9.27	-8.58
1	1050C,19R-1,78-82	481.78	76.06	0.512208	-8.39	-7.69
1	1050C,19R-1,126-127	478.90	75.40	Top. *E. eximius* [1]		

source	Sample	depth (mbsf)	Age for εNd(t)	$^{143}Nd/^{144}Nd$	$\varepsilon_{Nd(0)}$	$\varepsilon_{Nd(t)}$
2	1050C 20R 1W 30-36	490.93	85.56	0.512179	-8.95	-8.17
2	1050 C 20R 4W 120-121	495.60	89.52	0.512320	-6.20	-5.39
2	1050 C 20R 5W 40-42	497.02	90.72	0.512317	-6.26	-5.43
2	1050 C 21R 1W 20-21	500.40	93.58	0.512332	-5.97	-5.11
2	1050 C 21R 1W 42-43	500.62	93.76	0.512342	-5.77	-4.92
2	1050 C 21R 1W 47-48	500.67	93.81	0.512332	-5.97	-5.11
		500.88	94.00	OAE 2 [3]		
2	1050 C 21R 1W 68-69	500.88	94.00	0.5123373	-5.87	-5.01
2	1050 C 21R 1W 72-73	500.91	94.00	0.512325	-6.11	-5.25
2	1050 C 21R 1W 105-108	501.26	94.02	0.5123323	-5.96	-5.10
2	1050 C 21R 7W 45-46	508.75	94.51	0.512311	-6.38	-5.52
2	1050 C 22R 1W 46-50	510.28	94.61	0.512308	-6.44	-5.57
2	1050 C 23R 4W 60-64	524.52	95.54	0.512295	-6.69	-5.82
2	1050 C 23R 6W 126-129	528.17	95.78	0.512359	-5.44	-4.57
2	1050 C 25R 1W 82-85	539.53	96.52	0.512354	-5.54	-4.66
2	1050 C 26R 1W 53-56	548.94	97.13	0.512308	-6.44	-5.55
2	1050 C 26R 4W 140-142	554.31	97.48	0.512337	-5.87	-4.98
2	1050 C 27R 1W 73-76	558.74	97.77	0.512365	-5.33	-4.43
2	1050C 27R 2W 100-106	560.53	97.89	0.512349	-5.64	-4.74
2	1050 C 28R 1W 70-73	568.31	98.40	0.512355	-5.52	-4.62
		577.40	98.99	Top. *R. irrefularis* [1]		
2	1050C 29R 2W 100-106	579.73	99.14	0.512334	-5.93	-5.02
2	1050 C 31R 1W 132-134	597.73	100.32	0.512359	-5.44	-4.53
2	1050C 31R 2W 100-106	598.93	100.40	0.512298	-6.63	-5.72
2	1050C 31R 2W 100-106	598.93	100.40	0.512337	-5.87	-4.95

mbsfd = meters below sea floor
Ages calculated based on Huber et al (2008) age model

Source of data:	Ages references.
1. This study 2. MacLeod et al, 2008	1. Norris et al, 1998 2. Huber et al, 2008 3. MacLeod et al, 2008

CAPE VERDE

source	Sample	depth (mbsf)	Age for $\varepsilon_{Nd(t)}$	$^{143}Nd/^{144}Nd$	$\varepsilon_{Nd(0)}$	$\varepsilon_{Nd(t)}$
1				Rads. Top of P. striata =/- 50 [4]		
1	367,14R-3W,11-14	381.61	60	0.512143	-9.66	-9.15
1	367,14R-3W,125-127	382.75	60	0.512126	-9.99	-9.48
1	367,14R-4W,63-65	383.63	60	0.512104	-10.42	-9.91
2	367 14-4W 100-104	384.02	60	0.512071	-11.05	-10.54
1		378.5	60	poorly defined base of NP12 [1]		
1		474.93	67	C. *gigantea* present in highest core 15 [2,3]		
1	367,15R-2W,17-20	475.17	67	0.511909	-14.22	-13.65
1	367,15R-3W,84-88	477.34	67	0.511936	-13.69	-13.13
1				LO of *Uvigerinammina jankoi* [2,3]		
1	367,15R-4W,117-119	479.17	67	0.511884	-14.71	-14.14
1	367,15R-5W,87-89	480.37	76.5	0.51195	-13.42	-12.77
2	367 16-2W 100-102.5	542.51	76.5	0.512000	-12.44	-11.79
1	367,16R-3W,61-65	543.61	76.5	0.512039	-11.68	-11.04
1	367,16R-5W,61-64	546.61	76.5	0.512102	-10.46	-9.81
3	367 16R 6W 36-	547.87	76.5			
1		548	76.5	Presence of *Uvigerinammina jankoi* [2,3]		
3	367 17R 1W 121-124	617.21	88.95	0.512164	-9.1	-8.49
3	367 17R 4W 137-139	621.87	88.95	0.512119	-9.9	-9.37
				Cenomanian-Turonian [5]		
3	367 18R 1W 63-69	636.63	94.4	0.512158	-9.2	-8.56
2	367 18-1W 90-104	636.91	94.4	0.512202	-8.50	-7.70
3	367 18R 1W 117-124	637.17	94.4	0.512255	-7.3	-6.67
2	367 18-1W 125-132	637.3	94.4	0.512208	-8.38	-7.58
3	367 18R 2W 5-7	637.55	94.4	0.512226	-7.9	-7.24
3	367 18R 2W 71-73	638.21	94.4	0.512149	-9.4	-8.74
3	367 18R 3W 20-22.5	639.20	94.4	0.512186	-8.6	-8.02
2	367 18R 3W 20-22	639.21	94.4	0.5121950	-8.64	-7.84
3	367 18R 4W 23-26	640.73	94.4	0.512170	-9.0	-8.33
				Cenomanian-Albian [6]		
2	367 18R 4W 23-26	640.74	97	0.5121790	-8.95	-8.13
3	367 18R 4W 88-91	641.38	97	0.512155	-9.2	-8.60
2	367 18-4W 87-90	641.49	97	0.5121640	-9.25	-8.42
2	367 19-2W 5-10	646.08	97	0.512109	-10.31	-9.49
3	367 19R 3W 24-27	647.74	97	0.512137	-9.6	-8.95
3	367 20R 2W 24-27	691.24	97	0.512117	-10.0	-9.34
3	367 20R 3W 125-128	693.75	97	0.512214	-8.1	-7.45
3	367 20R 4W 47-50	694.47	97	0.512163	-9.1	-8.44
3	367 20R 4W 96-100	694.96	97	0.512093	-10.5	-9.81

mbsf: meters below sea floor

Source of data:
1. This study
2. Bourbón, 2008
3. Jiménez Berrocoso et al, 2009

Ages references.
1. Cépek, 1978
2. Houlborn et al, 1999
3. Kuhnt et al, 1992
4. Lancelat and Seibold, 1977
5. Jiménez Berrocoso et al, 2009
6. Bourbón, 2008.

References

Bourbon, É., 2008. Nd isotopes throughout the North Atlantic in the Late Cretaceous and across the Oceanic Anoxic Event 2 : M.S. Thesis. Geological Sciences. Gainesville, University of Florida.

Cepek, P., 1978. Mesozoic calcareous nannoplankton of the eastern North Atlantic, Leg. 41: Initial Reports of the Deep Sea Drilling Project 41, p. 667-688.

Holbourn, A., Kuhnt, W., El Albani, A., Ly, A., Gomez, R., and Herbin, J.P., 1999. Palaeoenvironments and palaeobiogeography of the Late Cretaceous Casamance transect (Senegal, NW Africa): Distribution patterns of benthic foraminifera, organic carbon and terrigenous flux: Neues Jahrbuch fur Geologie und Palaontologie - Abhandlungen, v. 212, p. 335-377.

Huber, B.T., MacLeod, K.G., and Tur, N.A., 2008. Chronostratigraphic Framework For Upper Campanian-Maastrichtian Sediments On The Blake Nose (Subtropical North Atlantic): Journal of Foraminiferal Research, v. 38, p. 162-182.

Jiménez Berrocoso, A., MacLeod, K.G., Martin, E.E., Bourbon, E., Basak, C., and Isaza-Londoño, C., 2009. Water-mass changes in the western tropical North Atlantic across the Cenomanian (Late Cretaceous) inferred from bioapatite Nd isotopes.

Kuhnt, W., Geroch, S., Kaminski, M.A., Moullade, M., and Neagu, T., 1992. Upper cretaceous abyssal claystones in the North Atlantic and Western Tethys: current status of biostratigraphical correlation using agglutinated foraminifers and palaeoceanographic events: Cretaceous Research, v. 13, p. 467-478.

Lancelot, Y., and Seibold, E., 1977. Site 367: Cape Verde Basin: Init. Rep. DSDP, v. 41, p. 163-232.

MacLeod, K.G., Martin, E.E., and Blair, S.W., 2008. Nd isotopic excursion across Cretaceous ocean anoxic event 2 (Cenomanian-Turonian) in the tropical North Atlantic: Geology, v. 36, p. 811-814.

Norris, R.D., Kroon, D., Klaus, A., and et al., 1998. Proceedings of the Ocean drilling program, initial reports, 171B, Ocean Drilling program, College Station, TX.

Norris, R.D., and Firth, J.V., 2002. Mass wasting of Atlantic continental margins following the Chicxulub impact event: Catastrophic Events and Mass Extinctions: Impacts and Beyond, v. 356, p. 79-95.

Okada, H., and Thierstein, H.R., 1979. Calcareous nannoplankton-Leg 43, Deep Sea Drilling Project: Initial Reports of the Deep Sea Drilling Project, v. 43, p. 507-573.

Tucholke, B.E., 1979. (DSDP) Site 386: fracture valley sedimentation on the Central Bermuda Rise: Initial reports of the Deep Sea Drilling Project, Leg 43, Istanbul, Turkey to Norfolk, Virginia, 1975, (Scripps Institution of Oceanography; UK distributirs IPOD Committee, NERC, Swindon), p. 195-322.

VITA

Ph.D. in Geology, 2009, University of Missouri

Advisor: Dr. Kenneth G. MacLeod

Dissertation topic: Late Maastrichtian paleoclimatology, paleoceanography, and foraminifera paleobiology.

M.S. in Geology, 2004, University of Missouri

Advisor: Dr. Kenneth G. MacLeod

Thesis: Late Maastrichtian paleoclimatology and the paleobiology of Racemiguembelina fructicosa, Contusotruncana contusa and Rugoglobigerina rugosa inferred from single specimen δ13C and δ18O data.

B.S. in Geology and Mines, 2001, Universidad de Caldas (Manizales), Colombia

Advisor: Dr. Fernando Sanchez

Thesis: Macro-geotechnical analysis of the western slope of Pácora river and micro-geotechnical analysis of the road Aguadas – Pácora.

Upon receiving her PhD in Geology during the summer of 2009, Carolina plans to begin work as an Exploration Geologist at Royal Dutch Shell in Houston, Texas. She will also be getting married in late 2010 to Dr. Scott Lepley.